WOOD AND FIBER SCIENCE

The Sustainable Natural Materials Journal

Volume 54, Number 1_2022 *(ISSN 0735-6161)*

Open Access

JOURNAL OF THE

SWST – International Society of Wood Science and Technology

There are three classes of membership (electronic only) in the Society: Members – dues $150; Retired Members – dues $75; Student Members – dues $50. We also have membership category for individuals from Emerging Countries where individual members pay $30, individual students pay $10; Emerging Group of 10 pay $290, and Student Groups of 10 pay $90. Institutions and individuals who are not members pay $300 per volume (electronic only). Applications for membership and information about the Society may be obtained from the Executive Director, Society of Wood Science and Technology, P.O. Box 6155, Monona, WI 53716-6155 or found at the website http://wwww.swst.org.

Site licenses are also available with a charge of:

- $300/yr for single online membership, access by password and email
- $500/yr for institutional subscribers with 2–10 IP addresses
- $750/yr for institutional subscribers with 11–50 IP addresses
- $1000/yr for institutional subscribers with 51–100 IP addresses
- $1500/yr for institution subscribers with 101–200 IP addresses
- $2000/yr for institutions subscribers with over 200 IP addresses.

New subscriptions begin with the first issue of a new volume. All subscriptions are to be ordered through the Executive Director, Society of Wood Science and Technology.

The Executive Director, at the Business Office shown below, should be notified 30 days in advance of a change of email address.

Business Office: Society of Wood Science and Technology, P.O. Box 6155, Monona, WI 53716-6155.
Editorial Office: Susan LeVan-Green, sue.levangreen@gmail.com

EXPERIMENTAL MODAL ANALYSIS OF A PALM TREE LOG UNDER RADIAL VIBRATIONAL EXCITATION[1]

*Djamel Ouis**
Associate Professor
of Architectural Engineering
King Fahd University of Petroleum & Minerals
Dhahran, Saudi Arabia
E-mail: djamel@kfupm.edu.sa

(Received June 2021)

Abstract. Trees may be subject to rot-inducing agents that degrade the strength of the material making their trunk, and decrease the quality of their crop. Several techniques, both nondestructive and destructive, are available for assessing the extent of damage caused by rot in a tree trunk. The present work presents the results of a preliminary study conducted on a palm tree trunk for isolating a specific mode from its response to a vibrational excitation, namely the so-called "ovalling" mode. The latter is cross-sectional and in a circular cylinder, and manifests itself relatively locally, ie has little dependence on the lateral extension of the cylinder. An experimental modal analysis is made on a piece of a date palm tree trunk when set into vibration through a radial mechanical excitation, and the response is collected at points along a circumference on the trunk. The value of the resonance frequency of the ovalling mode was found to be somehow variable, probably resulting from some coupling phenomena between various modes of vibration due to the inhomogeneity, anisotropy, and fiber-like structure of the trunk wood. As rot usually affects markedly the strength of the trunk wood, the frequency of the ovalling mode, which depends on the strength of the material, can be used for estimating the severity of rot attack in the trunk. A numerical simulation is also made to a cylinder as a simplified representation of a tree trunk.

Keywords: Palm tree, modal analysis, vibration, cross-sectional mode, rot detection, nondestructive testing.

INTRODUCTION

In countries with hot climate, palm trees are an important part of the landscape. Date palm trees in the hot Middle Eastern areas, as well as oil and coconut palm trees in the more temperate and humid climates by the Equator tropic are also important sources of revenue for their fruit or the oil extracted from them. Trees in general are vulnerable to attack by pests that weaken the trunk after some time of activity in it. Rot-infected trees standing in city parks and streets may constitute potential hazards to passersby, and the trees in plantations require constant control of their health status. The reliance on a fast and efficient monitoring procedure becomes therefore necessary to decide on the felling and clearing of a tree from the site. The use of the technique, if successful, will not be restricted to use in palm trees, but will encompass any kind of trees while standing, or to logs and wooden utility poles.

The present study has for its main goal to investigate the health condition of a tree trunk through simply striking it by a hammer blow and then recording and analyzing the response to that excitation. The nondestructive technique that will be developed for date palm trees is expected to cover other tree species as well. Hence once the vibrational behavior of the tree stem is known, and the resonant mode of vibration of interest identified, along with its frequency for each tree species, it is possible to establish a "soundness chart" for determining the extent of rot attack in the stem. Such a chart expresses the proper frequency of the vibration mode as a function of the geometrical characteristics of the stem, such as its width and length.

REVIEW OF LITERATURE ON TREES

Rot attacks almost all tree species and often spreads from the roots up to the trunk of the tree.

* Corresponding author

It is the result of attack by certain species of fungi, and the consequent colonization of the tree stem leads to decay by which the mass of the wood is reduced and its strength is weakened. Visual inspection of the tree, core sample-taking from the trunk, and the measurement of resistance to drill are a few of the commonly accepted methods used in forestry and urban trees' inspection for the detection of decay in trees. The former is rather based on subjective interpretation of external signs, which often makes it an unreliable method (Wagener and Davidson 1954). The second method, which consists of taking core samples from the tree trunk by means of an increment borer, is also found to be somehow unreliable in predicting the percentage of decayed trees in a forest stand. Its unreliability becomes even more accentuated when the location of rot is off the pith, the center axis of the trunk, and in which case hitting a decayed area becomes less likely when taking the core sample. Moreover, it has been found that the success in finding decay is lower when the core sample is taken at breast height than at a lower height near ground level (Stenlid and Wästerlund 1986). A tree may live with the wounds caused by the increment borer; the destructive nature of the method may increase the susceptibility to rot.

Nondestructive detection methods are based on various different technologies and have been suggested during the last few decades. Many of these methods are based on acoustical techniques and function on scanning the interior cross section of the tree trunk through setting it to an impulse excitation and then establishing an image through processing the data collected from an array of sensors attached to the surface of the tree trunk (Rust 2000; Deflorio et al 2008). This is a more elaborate way of implementing earlier and simpler vibrational techniques where a single sensor is used for measuring the time of flight of the mechanical pulse induced in the tree trunk. A stress wave is thus generated by, for instance, a hammer strike, and calculations of the speed of wave propagation permits to determine the stiffness of the material as expressed in terms of the Modulus of Elasticity, MOE (wood is a highly anisotropic material, and more specifically a tree trunk exhibits radial anisotropy, and the determination of the strength properties of the material is highly dependent on the direction of wave propagation within the material). The extent of the zone of rot attack and the degree of its severity in the tree trunk may be established through comparing the measured speed of wave propagation, or the MOE, depending on to what extent the values of these parameters fall below a species-dependent threshold (Mattheck and Bethge 1993).

In this work, the modes of vibration of a piece cut transversally from the trunk of a date palm tree are investigated. The purpose of this preliminary investigation is to list the few lowest modes of vibration, both in shape and frequency, when a tree trunk is excited by a radial excitation. The study, which is of a pilot character, is limited to the few lowest vibration modes for the sole reason that these are the most important ones when it comes to examine the response of a tree trunk to mechanical excitation. Moreover, as a tree trunk behaves as a complex mechanical system (because of the various kinds of modes that the trunk may exhibit in its response to a mechanical excitation), and the response of modes is most pronounced for the lowest ones and tends to decrease for modes of higher order. For instance, it is known from studies carried on wooden beams that rot, as well as other structural defects, reduce the stiffness of the material as quantified by the value of its MOE. As a consequence it is found that the frequency of resonance, or eigenfrequency, of the flexural modes is also diminished, however, without too appreciably affecting the shape of these bending modes (Yang et al 2002; Choi et al 2007).

MATERIALS AND METHODS

The purpose from the present experimental study is to conduct an investigation into the various vibrational modes of interest in a palm tree trunk. Hence, a log was cut from the trunk of a sound palm tree and is in the first set of experiments set upon thin supports at about the nodes of the first flexural mode of vibration. In the second set of experiments, the log is hinged with its axis in the

vertical direction, to study the characteristics of the circumferential expansion modes of vibrations. A broadband signal is then fed into a shaker attached to the middle of the log and the response of the log to the excitation is recorded by an accelerometer. This latter is displaced stepwise over the whole cylindrical area of the log. The frequency and vibrational shape of the excited mode are thus determined from the analysis of the frequency response of the log at each of the positions considered.

Materials

A series of measurements were conducted on a log that was cut from the trunk of a date palm tree. The experiments conducted on the log were divided into two series, one series being where the log was laid horizontally on two supports and the other series with the log maintained standing and held at its two ends by sharp metallic rods.

The palm log was almost cylindrical in shape as the flaring was negligible along its axial direction, 110 cm of length and with an average perimeter of 143 cm, making an average diameter of 45.5 cm. Prior to making measurements, the log was wrapped with a thin plastic film, on which were glued equidistant tape strips along the axis, and other equidistant strips on its circumference. The mesh thus obtained was composed of cells of square shape, with an average size of 14×14 cm^2. The axial strips were lettered in order from A to P, starting from the uppermost position on the log and moving around it, while the circumferential ones were numbered from 1 to 11, starting from the uppermost edge surface of the log and moving toward the bottom. Pictures over the measurement setups are shown in Fig 1, with details over the vertical setup in Fig 2. An illustration of the vertical setup with the connections of the measurement equipment is also shown in Fig 3. The setup makes, in total, 176 measurement points, evenly distributed on the surface of the log and that will be used for mapping the vibration amplitude on the surface of the log.

Experimental Modal Analysis, EMA

Experimental Modal Analysis, EMA (or modal testing), has grown steadily in popularity since the advent of the digital Fast Fourier Transform, FFT, spectrum analysis technique in the mid-1970s. It has become a widely accepted tool that is used in structural engineering and material sciences for the nondestructive evaluation of mechanical properties of materials and structures. The principle of using EMA is built about setting a structure into vibration through submitting it to a short impact and then study the response of the structure for determining its proper, or natural, modes of vibration (Schwarz and Richardson 1999).

An essential concept in EMA is that of the Frequency Response Function, or Frequency Transfer Function, and the measurement of which helps isolating the natural dynamic properties of the mechanical structure under investigation. The latter is a complex function and determines the relationship, expressed as a function of frequency, between excitation and response (or input and output), between two points on the structure under study.

Experimental Setup

The measurements on the log for the purpose of its modal analysis were conducted in the standing position. For the log in the horizontal setup, it was laid on the supports so that the boundary conditions were intended to satisfy approximately those of the first bending mode, that is to say, that the log was set on two wedge-like supports at a distance of one-sixth of its length from either of its ends. These are the positions of the nodes of this specific mode, and setting the supports at these nodes does not affect the flexural deflections of the log. A Brüel and Kjær, B&K, electrodynamic mini-shaker, model 4810, was then coupled to a steel rod, also usually called *stinger* in modal analysis parlance, to be connected to the vibrating cone of the shaker. The stinger, oriented in the radial direction of the log, was in its turn attached to a metallic plate in its turn screwed onto the log at its midst.

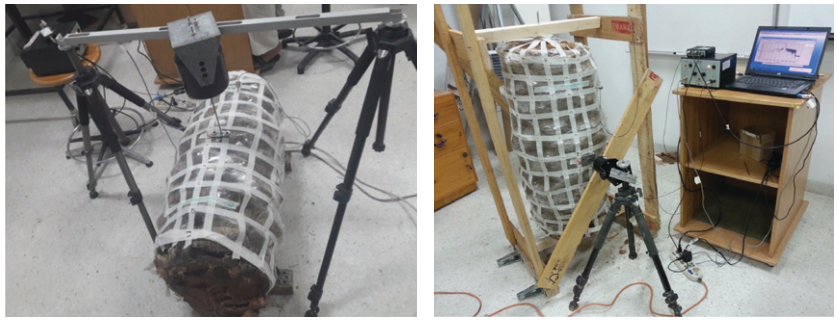

Figure 1. Pictures over the experimental measurement setup on the palm tree log. (a) Log on horizontal setup. (b) Log on vertical setup.

The vibration sensor consisted of a uniaxial piezoelectric charge accelerometer of type B&K 4381 with a sensitivity of 10 pC/ms^{-2} and a working frequency range from 0.1 Hz to 4800 Hz. To enable easy and fast displacement of the vibration sensor from a measurement position on the log to the next one, a needle-like screw 2.5 cm in length was attached to its base. The signal from the accelerometer was then fed into a B&K charge amplifier model B&K 2626 with the appropriate sensitivity calibration and signal amplification, and was maintained for the whole series of measurement positions so as to avoid inconvenient later adjustments of measurement data. This was accomplished through a prior reading of the response at a presumed position where the weakest response signal was expected to be recorded (at the most remote position on the log from the point of signal excitation, which is at the rim of the log and diametrically opposed to the excitation position), and another reading at a measurement position where the signal was the most pronounced, ie nearest to the position of input of excitation signal. The charge amplifier was then set at a level with an acceptable signal-to-noise ratio at the weakest signal record, but at the same time without overloading the input to the amplifier at the position of the strongest signal. The measured signal was then conveyed to the input of a signal processor for the necessary cross-correlation operation to be executed with the signal that gave rise to it.

Measurement Technique

The quantity of interest that was measured is the impulse response, IR, which is acquired through submitting the test specimen to a chirp consisting

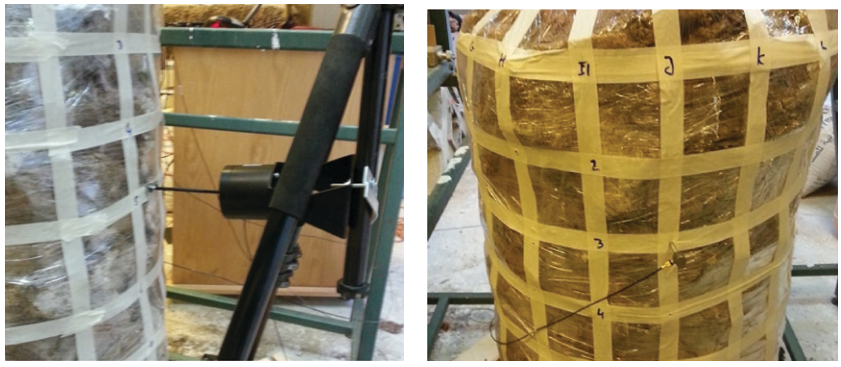

Figure 2. Pictures over details of the experimental measurement setup on the palm tree log. Left: Attachment of shaker, for force excitation. Right: Attachment of accelerometer, for response signal recording.

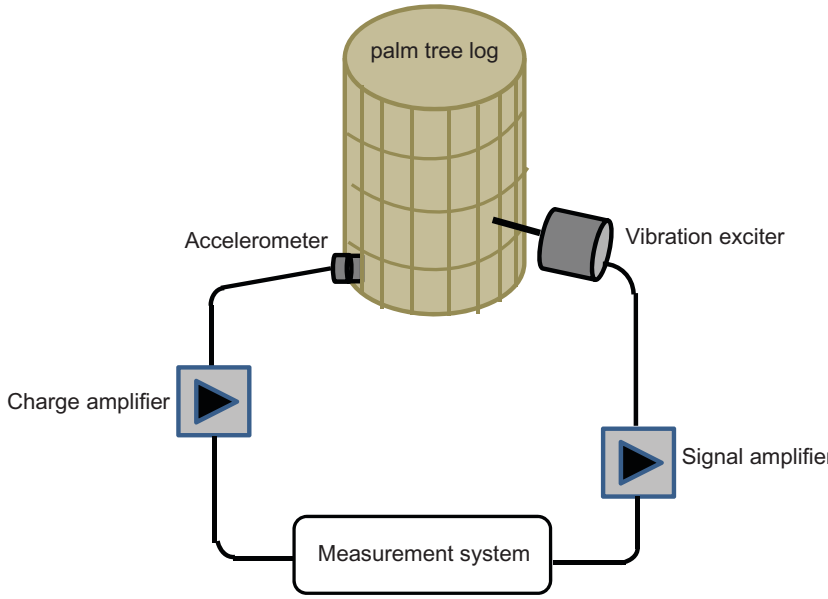

Figure 3. Schematic experimental set-up for measurements of the distribution of vibration amplitude on the log of the date palm tree set in vertical orientation.

of a sine sweep signal (this kind of excitation has shown superior reliability than the broadband random signal excitation, as it ensures, among others, higher immunity against distortion; Müller and Massarani 2001). In the actual measurement system the frequency sweep is set in the range 20-20,000 Hz and the sampling rate to 44,100 Hz prior to the FFT operation. For an FFT size of 8192 this gives a frequency resolution of 5.4 Hz for the frequency spectrum, or equivalently a time resolution of 0.19 s for the IR. The IR is thus obtained through executing a cross-correlation operation between the response recorded by the vibration sensor and the excitation signal. This measurement technique also spares the trouble of measuring the transfer function between the response signal and the excitation signal, and instead focuses on evaluating the FFT, of the impulse response at the measurement point.

A schematic representation over this measurement procedure is illustrated in Fig 4, and more details may be read in Kuttruff (2010). This measurement procedure has lately been incorporated in the room-acoustical and simulation software ODEON software, which originally was designed for room acoustical simulations and calculations. For an appropriate level of the excitation signal above that of the background noise, and as the excitation signal is perfectly repeatable, the response result is also expected to be repeatable, hence avoiding the need for executing several measurements and then evaluating their average.

RESULTS

A typical signal trace of the IR, and its frequency counterpart, the transfer function, as recorded at measurement position P07 on the log are shown in Fig 5. The purpose from an antecedent measurement carried on the log on the horizontal mounting setup was to identify the approximate frequencies of the major natural vibration modes. This was conducted prior to the major measurement series at all measurement positions on the log. In the plot on the right-hand side of Fig 5, one can differentiate the peaks of some of the most important modes of vibration in the curve of

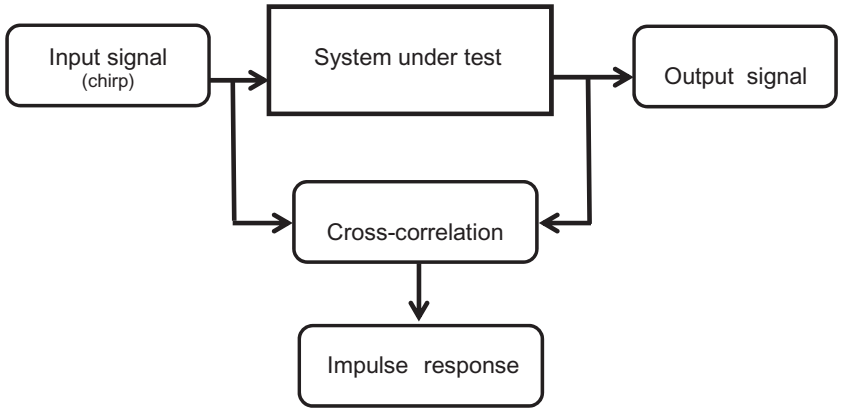

Figure 4. Illustration of the general principle behind the measurement procedure used for acquiring the impulse response of a system.

the amplitude as a function of the frequency. The first mode of vibration at around 45 Hz, depicted as "m," is the mode of whole-body motion of the log, and which is at the resonance frequency of the spring-mass system composed of the log and the vibrating part of the shaker. The presence of this mode was made even more obvious when the log was set into vibration by the stronger shaker. The second mode, "b1," in the range 180-210 Hz is the first bending mode, and the next one, "b2," is the second bending mode with, theoretically, a frequency 2.55 that of the first bending mode, ie around 470 Hz. The next peak is that of the third bending mode, "b3," with a frequency 5.44 that of the first one, ie around 900 Hz. It looks as if this mode vibrates at its most pronounced response at this measurement position, and its amplitude overrides that of the other two lower bending modes. Next, the peak denoted as "o" on the frequency plot, has been investigated in the frequency responses of the measurement positions, and is found to be, to a high degree of confidence, the "ovalling" mode. However, its frequency is found to shift within the frequency range 1050-1600 Hz depending on the position of the sensor on the log. For some positions it did not exhibit lucid existence through a well-marked peak, like the one in Fig 5. More specifically, these positions of lesser display of the ovalling mode, were those positioned remotely far from the plane normal to the axis of action of the excitation signal, at a distance of approximately more than 30 cm along the axis of the log. An explanation of this position-dependent behavior of the modal amplitude and frequency of this cross-sectional mode is probably attributed to some

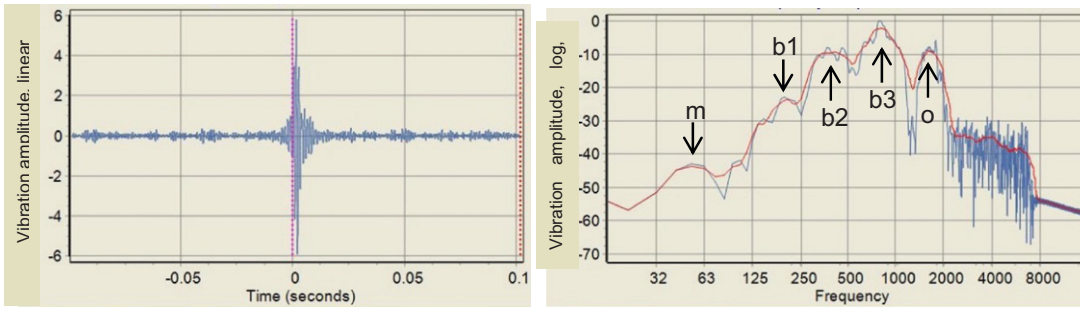

Figure 5. Left: Impulse response recorded at position P07 on the log. Right: Amplitude of the transfer function, ie the transform of the impulse response in the frequency domain.

coupling between this mode and the bending ones, and where a substantial part of the vibratory energy may be exchanged between the modes. The best performance of the ovalling mode was found on the circumference normal to the trunk's axis and containing the point of application of the excitation force. The manifestation of this mode showed a higher dampening of the vibration amplitude the farther away from the position of the excitation. The most plausible explanation to this behavior may be attributed to the inner fibrous structure of the trunk favoring the absorption of propagating vibratory energy through friction between contiguously packed fibers, which is believed to increase with increasing moisture content. Figure 6 depicts the linear vibration amplitude as recorded on the surface of the log on this circumferential line (measurements at positions 14 and 26 were not possible, hence unreliable, due to their falling in a deep trough, and the values of the vibration amplitude on the graph were simply extrapolated from those of positions on either of their sides). Polar plots, on both a linear and a logarithimic scale, are presented in Figure 7. The attenuation of the vibration amplitude of the ovalling mode, as depending on the lateral distance from the plane of application of the excitation signal, is illustrated in the curve plot of Fig 8. The measurement positions were taken on the line parallel to the axis of the log at 90° from the excitation position and on either side of the plane of its application. At a distance about 30 cm from the plane of application of the excitation force, where the amplitude of vibration is maximum, the ovalling mode was scarcely observable. Its vibration amplitude was over 30 dB lower, ie less than ca. one-thirtieth of its highest value at the point of vibration excitation.

The graph in Fig 9 is a plot of the amplitude of vibration along a circumference of the log for the first bending mode at the frequency range between 180 Hz and 210 Hz, where it is seen the weak response on the lateral positions of the log. Measurements were conducted on the palm trunk at a lateral position mid-distance from the middle of the trunk toward its edge. Figure 10 presents polar plots of the amplitude of this first bending mode of vibration.

DISCUSSION

The modes of vibration that can be set into motion in the palm tree log may have various characters, and these can be arranged into the bending, cross-sectional, torsional, and longitudinal classes. Knowledge of the behavior, shape, and frequency of these modes will serve as a benchmark for a subsequent study concerned with establishing the degree of influence of rot on the physical and geometrical attributes of these

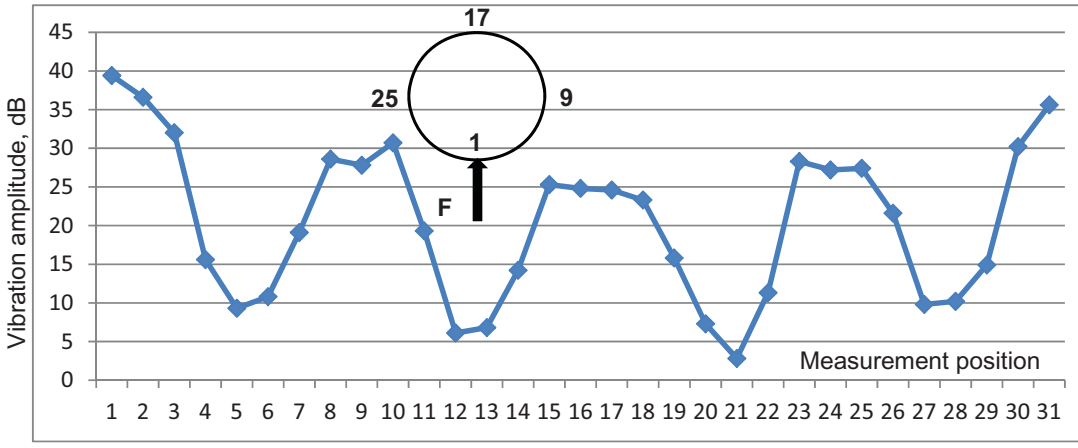

Figure 6. Vibration pattern along a circumference on the log for ovalling mode "o" at average frequency 1300 Hz. Linear amplitude.

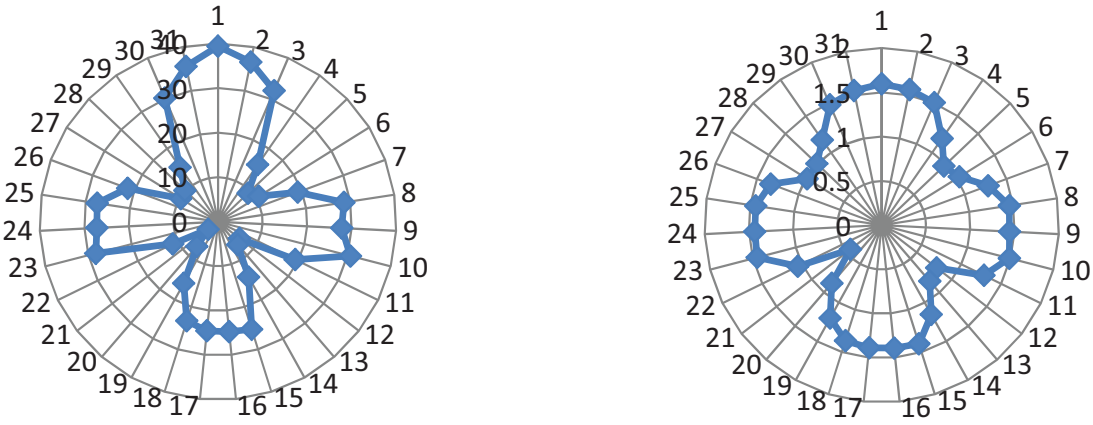

Figure 7. Polar plot over the vibration amplitude data pattern of Fig 6. Left: Linear scale. Right: Logarithmic scale.

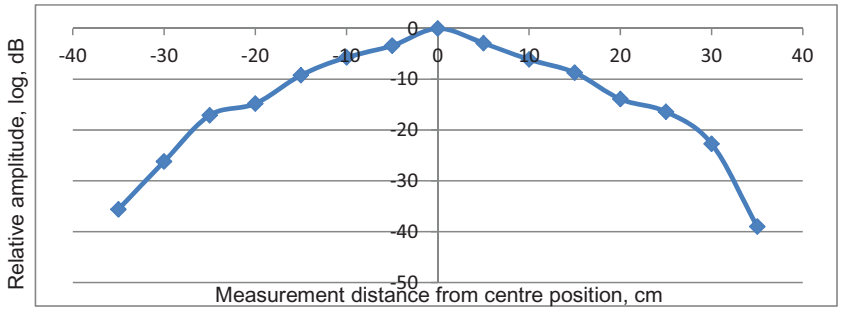

Figure 8. Relative vibration amplitude of the ovalling mode, in dB, as function of the lateral distance, in cm, from the point of application of the excitation force.

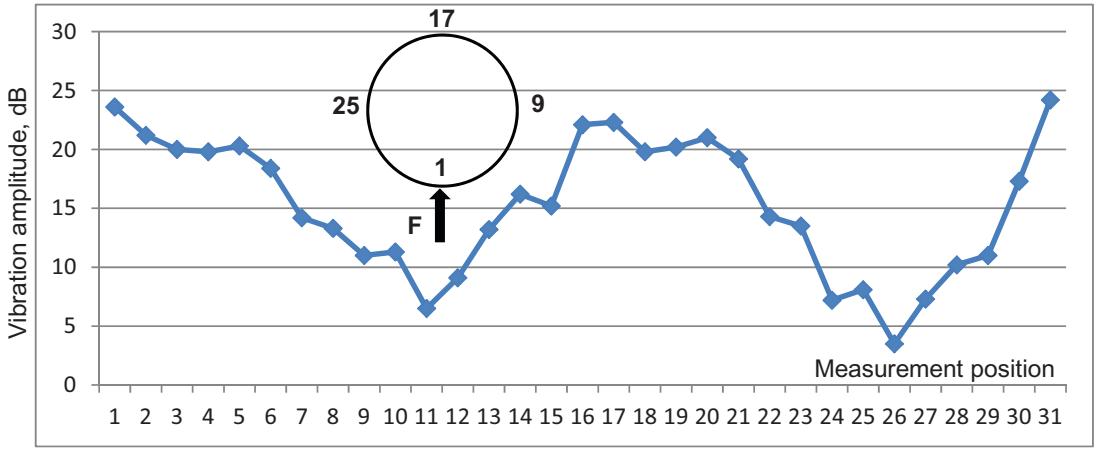

Figure 9. Vibration pattern along a circumference on the log for bending mode b1 at average frequency 190 Hz.

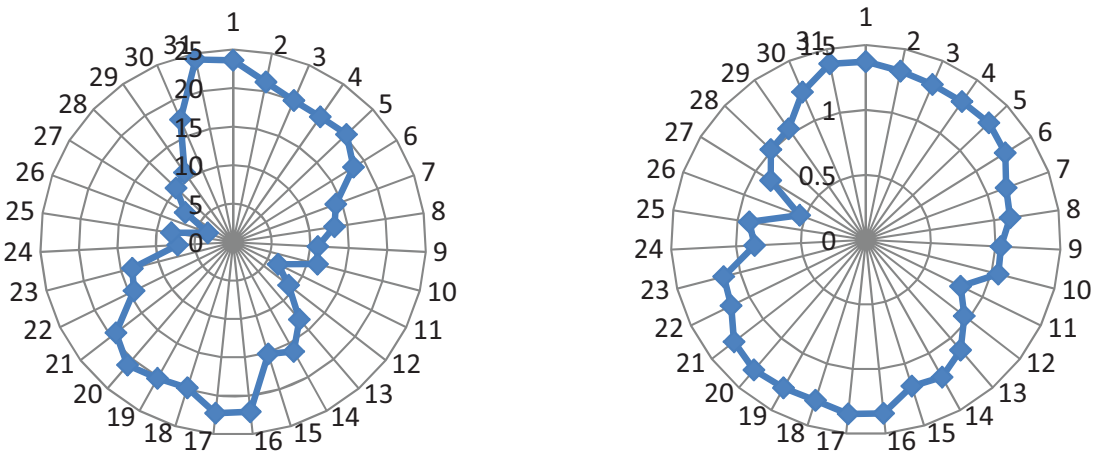

Figure 10. Polar plot over the vibration amplitude data pattern of Fig 9 for the first bending mode. Left: Linear scale. Right: Logarithmic scale.

modes. The excitation of these vibration modes depends primarily on the application position in the log of the force exciting source, the electrodynamic shaker, and on the orientation of the excitation force. For the purposes of this study the torsional and the longitudinal modes were excluded through attaching the rod fixed to the vibrating part of the shaker radially on the surface of the log and at mid-distance from its extremities. The choice of the position of the excitation force is also important inasmuch as the vibrational modes responding with their maximum amplitude will be those with such that an antinode line crosses the point of application of the excitation force. The surface jaggedness in the present experimental specimen hindered for some measurement points to be conducted at their prescribed position. The log also had some flaws on it and this caused disturbances for some measurements as it is known that flaws and delaminations are material defects that can cause modal coupling, not only enhancing the response of some modes and reducing that of others, but they even can generate new modes of vibration for the simple reason that their presence causes a change in the boundary conditions of the vibrational modes (Shen and Grady 1992).

The natural frequencies of a bar with large slenderness (ratio of length to width) of solid material with MoE, E and density, ρ, and under flexural motion with free-free boundary conditions is expressed as (the approximation is often referred to as the Euler-Bernoulli, Cremer and Heckl 1988):

$$f_{f-f} = \frac{\pi}{8}\sqrt{\frac{B}{m}}\frac{(2n-1)^2}{l^2} \tag{1}$$

n being the number of nodes of the mode, and $B = EI$, the bending stiffness of the bar with I its sectional moment of inertia, which for a filled circular cylinder with radius a is expressed as:

$$I = \pi\frac{a^4}{2} \tag{2}$$

In Eq (1) m is the mass per unit length of the rod in kg/m; it is expressed as $m = \pi\rho Z a^2$. The values of the natural frequencies of vibration for a bar of general dimensions are not expressible in as a simple explicit form as in Eq (1), but are instead determined through a nondirect procedure starting from the value of the slenderness of the bar and a frequency parameter. A system of equations is then established for the boundary conditions of the displacements of the beam's particles. From the latter the coefficients of the series' development leads to the values of the natural frequencies from setting the determinant of the

system of equations as equal to zero (Hutchinson 1980; Hutchinson 1981). The classical approximations underestimate the displacement and overestimate the natural frequencies of vibration as compared with results from more elaborated theories (starting from Timoshenko's in 1921; Sayyad 2011).

If we consider the first bending mode of a slender cylindrical beam, Eq (1) can be rearranged, with $n = 2$, as:

$$f_{f-f,1} = \frac{9\pi a}{8l^2}\sqrt{\frac{E}{2\rho}} \quad (3)$$

There are no exact available published data concerning the value of the MoE for the wood constituting the stem of date palm trees as opposed to those of other palm species. It is also important to mention that for trees, in general, the mechanical and strength properties of wood processed from their trunks depends on several parameters. These are not only limited to external growing conditions, like climatic and the chemical composition and water content properties of the soil on which the trees stand, but even on the part of the stem from which wood material is sawn. Regarding palm trees and due to the remarkable height, their size can reach up to 20-40 m, the MoE is found to be of distinctly higher values at the periphery of the stem and at its base. This mechanical characteristic enables these tall trees to withstand high strain constraints under windy conditions (Rich 1987; Gibson 2012). Using Eq (3) for the first bending resonance frequency $f_{f\text{-}f,1} = 170$ Hz gives a value for the MoE of $E = 63$ MPa (using a value of 490 kg·m^{-3} for its density as calculated from its weighing and measuring its volume). This value is noticeably low for softwood species (Douglas fir, Norway spruce, or oak), widely used as building materials, and which usually have values in the range 1-10 GPa, but it is also low as compared for lately reported MoE values of palms in the range 0.3-1.0 GPa (Rich 1987). Although these values apply for palm species other than the date. Because there were no visual signs of decay in the heart or near the periphery of the log under study, it is concluded that this low MoE value, and if not what is expected from a date palm tree, may only be attributed to an aged palm tree from which the log was most probably cut, and which is supported by the large cross-sectional size, Ø 45 cm, of the test specimen. Moreover, it should be emphasized here that so far theoretical treatment concerns a slender beam, ie a beam whose length exceeds about 10 times its average cross-sectional size, and therefore a more elaborate approach is to be considered if a more accurate analysis is to be applied to present palm log. A further correction to be added to the analysis of thick beams is that of mass adding at the ends of the beam and which has for essential consequence to decrease the value of the resonance frequency of the vibration mode. This fact leads to an overestimate of the MOE, therefore the more qualitative than quantitative character of the present analysis.

The resonance frequency f_{cs} of the extensional vibrational modes is inversely proportional to the circumference C of the cylinder and directly dependent on the strength of the material filling the cylinder, especially on the propagation speed of shear waves v_s, ie $f_{cs} \approx xC^{-1}v_s$, x being a dimensionless factor proportional to the Poisson ratio of the material (Axmon et al 2002).

This pilot study is an incentive for the future, a more comprehensive and larger scale study needs to be conducted on the stem of standing palm trees. A recent publication by the author has shed some light on a method for extracting the ovalling mode from the frequency response of a palm tree trunk in response to a mechanical stress excitation. The method builds on using a combination of two similar vibration sensors attached to the trunk at two diametrically opposed positions and then to recording and adding their response (in phase) to the mechanical excitation induced radially at midway distance between the sensors (Ouis 2020). The tree specimen considered in that study was a California fan palm (*Washingtonia filifera*), and the results showed the possibility to determine the strength of the wood material at different heights above the ground from measuring the natural frequency of the ovalling mode as a function of the circumference of the trunk.

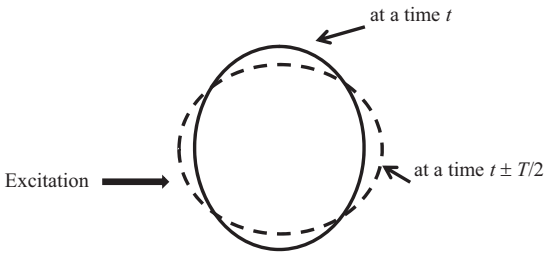

Figure 11. Illustration of the "ovalling" mode for a cylinder excited radially. T is the period of vibration of the mode, or $T = 1/f_o$, f_o being its frequency.

The resonance frequency for a filled cylinder is proportional to the speed of wave propagation in the material, which in turn is proportional to the square root of the MOE. Hence a degradation of the strength of the cylinder material will result in a reduction of the value of the frequency of the ovalling mode, the vibration of which is illustrated in Figure 11. The aim of the present investigation is to serve as an initiator to a study at a larger scale to be conducted on standing date palm trees of various sizes and planted on different stands to establish a possible correlation between the characteristics of the ovalling mode and the severity of rot attack in the tree stem.

Numerical calculations were conducted using mechanical and computational simulation Finite Element Analysis–based software. Two software, namely COMSOL Multiphysics and ANSYS, were used for predicting the shape and frequency of the ovalling mode of vibration on a cylinder with geometrical and physical attributes similar to those of the log used in this experimental study. A first computation with a cylinder made of isotropic material showed that for a value of MoE equal to 60 MPa, the frequency f_{ov} of the ovalling mode was obtained at 353 Hz. Including anisotropy in the material, specifically considering orthogonal isotropy between the radial and the axial directions, showed very minor effect on the value of f_{ov}; with a Poisson ratio taken as 0.3, an

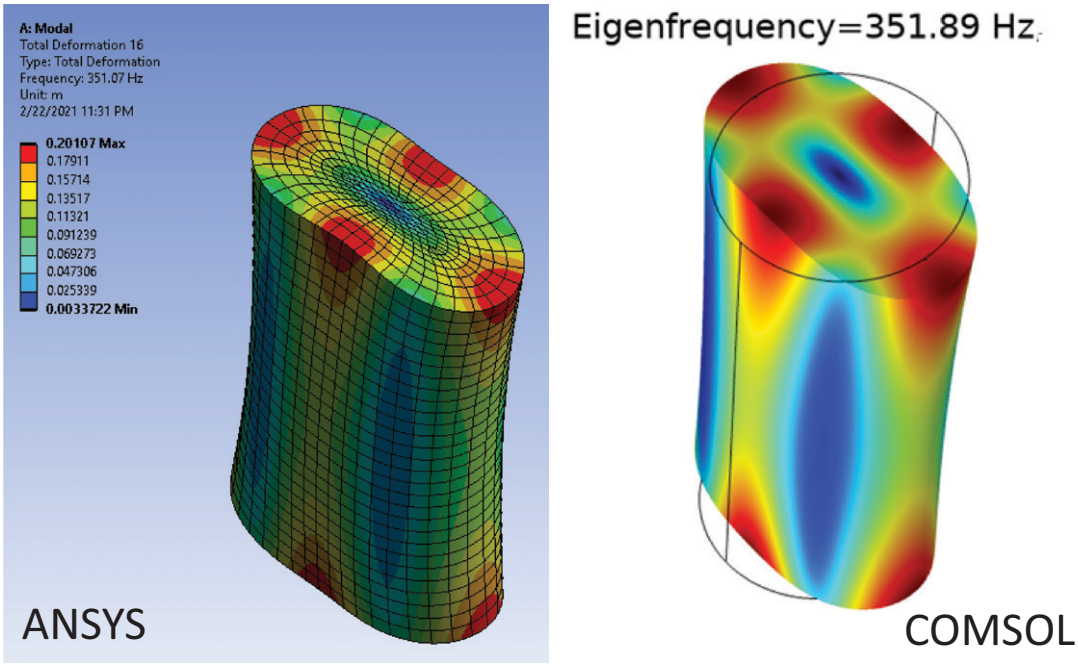

Figure 12. Numerical simulation and calculation of the vibration pattern and the frequency f_{ov} of the ovalling mode in a free solid cylinder made of material with orthogonal isotropy. Length $l = 1.10$ m, diameter $d = 0.45$ m, material density $\rho = 490$ kg/m^3 and material stiffness MoE = 60 MPa. In both simulations the natural frequency of the mode was found $f_{ov} \approx 352$ Hz. Left: Using ANSYS. Right: using COMSOL Multiphysics.

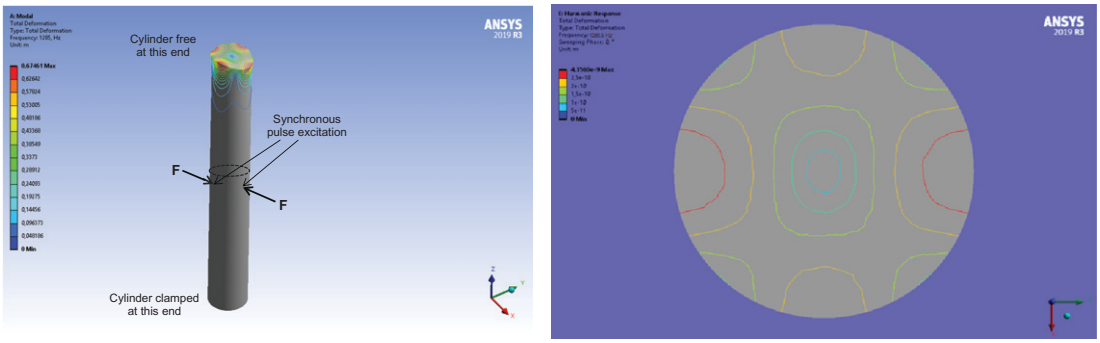

Figure 13. Left: Numerical simulation of the ovalling mode in a clamped-free solid isotropic cylinder subject to a pair of synchronous identical radial force pulses applied to its midst. Overall motion of the cylinder. Cylinder characteristics: height $h = 3.00$ m, diameter $d = 0.45$ m, material density $\rho = 490$ kg/m^3 and material MoE = 750 MPa. Right: Details over the stress distribution on the cross section of the cylinder at a distance of 15.0 cm above the point of application of the excitation forces. Resonance frequency of the ovalling mode $f_{ov} = 1285$ Hz.

increase factor of 10 for the axial/tangential MOE resulted in a relative decrease of the f_{ov} by only 0.1%. (for palm trees' wood, the value of the MOE along the grain may be as high as 20 times that of the MOE value in the transverse direction). Figure 12 presents the results of calculations for this cylinder.

Assigning a value of 750 MPa for the tangential MOE resulted in a value of 1285 Hz for f_{ov} and this was taken for simulating, as a last investigation, the behavior of a filled cylinder with finite size and that was clamped, ie with no motion, at one end and free of motion at the other end (roughly representing the trunk of a standing tree). Its length was taken as 3.00 m for limiting the load and time of computations. The excitation of the cylinder was accomplished through the simultaneous application at midheight location on the cylinder of two similar force pulses radially opposed in direction and acting on two diametrically positions on the cylinder, Fig 13 (left). In the time domain, each of these force pulses was a half-sine shaped, with a maximum magnitude of 1.0×10^4 N, and a duration of 0.15 ms. The purpose of exciting the cylinder by two oppositely in-phase radial forces is to enhance the response of the ovalling mode (as well as that of all even cross-sectional modes). Figure 13 (left) illustrates the overall vibration of the cylinder, whereas on the right-hand side of the figure is shown the deformation of its cross-sectional surface at a distance of 15.0 cm above the plane of application of the excitation forces (dotted line).

CONCLUSIONS AND FUTURE WORK

The objective from the investigation conducted in this study was to identify the vibrational modes that are excited in a palm tree trunk subject to a radial mechanical excitation and to study their attributes in terms of shape, frequency, and damping characteristics. Special emphasis was placed on the cross-sectional expansion "ovalling" mode, the vibration of which is considered as local as it is less affected by the axial extent of the tree trunk. From knowledge of the vibrational behavior and frequency of this particular mode, and which depends on the cross-size of the palm tree trunk, it may be possible to establish a correlation between the severity of rot attack in the trunk and the frequency of the ovalling mode.

ACKNOWLEDGMENTS

The author is much indebted to the Deanship of Scientific Research, DSR, at the King Fahd University of Petroleum & Minerals, KFUPM, for financing this research project, under project code IN141050 at the author's joining the

University. The submission of the final report to the research project has unwishfully been delayed due to asynchronous availability of the test specimens and the measurement equipment. The latter has been provided through a loan from the Mechanical Engineering department at KFUPM, and for which Professor Y. Khulief is gratefully acknowledged.

REFERENCES

Axmon J, Hansson M, Sornmo L (2002) Modal analysis of living spruce using a combined Prony and DFT multichannel method for detection of internal decay. Mech Syst Signal Process 16:561-584.

Choi FC, Li L, Samali B, Crews K (2007) Application of modal-based damage-detection method to locate and evaluate damage in timber beams. J Wood Sci 53: 394-400.

Cremer L, Heckl M (1988) Structure borne sound, 2nd edition. Springer Verlag, Berlin, Germany. https://books.google.com.sa/books?hl=en&lr=&id=5rPrCAAAQBAJ&oi=fnd&pg=PR14&dq=Structure+Borne+Sound&ots=cF_UxLKgOm&sig=8MsqpiZNC9F7E0Z4MB2HJeQedJo&redir_esc=y#v=onepage&q=Structure%20Borne%20Sound&f=false.

Deflorio G, Fink S, Schwarze F (2008) Detection of incipient decay in tree stems with sonic tomography after wounding and fungal inoculation. Wood Sci Technol 42:117-132.

Gibson LJ (2012) The hierarchical structure and mechanics of plant materials. J R Soc Interface 9:2749-2766.

Hutchinson JR (1980) Vibrations of solid cylinders. J Appl Mech 47:901-907.

Hutchinson JR (1981) Transverse vibrations of beams, exact versus approximate solutions. J Appl Mech 48: 923-928.

Kuttruff H (2010) Room acoustics, 5th edition. Elsevier Applied Science, London, United Kingdom.

Mattheck CG, Bethge KA (1993) Detection of decay in trees with the Metriguard stress wave timer. J Arboric 19:374-378.

Müller S, Massarani P (2001) Transfer-function measurement with sweeps. J Audio Eng Soc 49:443-471.

Ouis D (2020) Monitoring of a cross-sectional vibrational mode in the trunk of a palm tree. Arboric Urban For 46(4):307-318.

Rich PM (1987) Developmental anatomy of the stem of *Welfia geogii*, *Iriartea gigantea* and other arborescent palms: Implications for mechanical support. Am J Bot 74:792-802.

Rust S (2000) A new tomographic device for the nondestructive testing of trees. Pages 233-237 *in* Proc 12th International Symposium on Nondestructive Testing of Wood, University of Western Hungary, Sopron, Hungary.

Sayyad AS (2011) Comparison of various refined beam theories for the bending and free vibration analysis of thick beams. Appl Comput Mech 5:217-230.

Schwarz BJ, Richardson MH (1999) Experimental modal analysis, CSI Reliability Week, Orlando, FL.

Shen MH, Grady JE (1992) Free vibrations of delaminated beams. AIAA J 30:1361-1370.

Wagener WW, Davidson RW (1954) Heart rots in living trees. Bot Rev 20:61-134.

Yang X, Ishimaru Y, Iida I (2002) Application of modal analysis by transfer function to nondestructive testing of wood I: Determination of localized defects in wood by the shape of the flexural vibration wave. J Wood Sci 48:140-144.

MOMENT RESISTANCE PERFORMANCE OF LARCH LAMINATED TIMBER BEAM-COLUMN JOINTS REINFORCED WITH CFRP[1]

Dong-Hyeon Kim
Master's Student
E-mail: wrudoing0202@naver.com

Seung-Yeoup Baek
Master's Student
E-mail: bso1936@naver.com

Seok-Hoon Yu
Master's Student
Department of Forest Biomaterials Engineering
Chuncheon, Republic of Korea
E-mail: bibunm1ss@hanmail.net

Yo-Jin Song
Researcher
Institute of Forest Science
Kangwon National University
1 Gangwondaehakgil
Chuncheon-Si 24341, Republic of Korea
E-mail: syj85@kangwon.ac.kr

In-Hwan Lee
Research Fellow
Wood Engineering Divison Forest Products and Industry Department
National Institude of Forest Science
57 Hoegi-ro, Dongdaemun-gu, Seoul 02455, Republic of Korea
E-mail: ih1990@korea.kr

*Soon-Il Hong**
Professor
Department of Forest Biomaterials Engineering
Kangwon National University
1 Gangwondaehakgil
Chuncheon-Si 24341, Republic of Korea
E-mail: hongsi@kangwon.ac.kr

(Received August 2021)

Abstract. Laminated timber is a wood composite made by multiple-layering of small-square timber. Laminated timber was produced as a substitute for glulam or large-section timbers. Existing studies have shown that laminated timber has potential as a structural member, but experiments on joints for using laminated timber as a structure are insufficient. Slotted-in steel plates type joint are commonly used among various types of joints for timber owing to their outstanding strength and stiffness. However, they are vulnerable to cyclic loads such as earthquakes, and to brittle fractures due to the bearing deformation of the wood given the large difference in stiffness between the wood and the joint composed of metal fasteners and steel plate. Since brittle

* Corresponding author

fractures cause a large decrease in joint capacity, many studies are being conducted to solve this problem. Among them, carbon fiber-reinforced plastic (CFRP) is used as reinforcing material due to its excellent strength characteristics, but experiments on the performance of column-beam joints reinforced with CFRP joints are insufficient. Therefore, this study evaluates the moment capacity according to CFRP reinforcement ratio of the drift pin larch beam-column joint with slotted-in steel plates of larch laminated timber. The main strength characteristics and seismic performance of the joints were calculated using the elasto-plastic model. There was almost no difference in strength between the control specimens and the joints composed of glulams. The strength gain of the joints of the larch laminated timber was greater when glulam and laminated timber were reinforced with CFRP of the same volume ratio compared with CFRP reinforcement. Unlike the specimens wrapped in CFRP in the previous study, the moment of resistance specimens reinforced with CFRP were improved without any reduction in yield strength and ductility ratio, and it was confirmed that the failure mode was improved. Through the experimental results, it was confirmed that the internal reinforcement method of CFRP contributes to the performance improvement of the joint.

Keywords: Laminated timber, timber dowel-type joints, reinforcement, elasto-plastic analysis, failure mode, ductility.

INTRODUCTION

In modern heavy wood structures, a frame composed of large-section columns and beams generally supports the load, and large-section timber or glulam are used as structural members. However, in the case of large-dimensional member, drying stress occurs in the timber due to the difference in MC between the surface and inner layers during drying, leading to the easy occurrence of drying defects. Based on the thinning method that is used in low value-added industries in Korea such as chip production, larch small-square timber can be fabricated into a wood material similar to large-section member by creating laminated timber through multilayering. However, in order for laminated timber to be used as a structural member, it is necessary to review the strength performance compared with other members such as glulam. According to a previous study, Lee et al (2019) evaluated the bending performance of laminated timber manufactured by bonding two small-square timbers to use as a heavy timber structural member with laminated timber and various reinforcements. As a result of the experiment, the laminated timbers showed sufficient potential as structural members compared with glulams. However, the joints must be considered in addition to the structural members as main factors for the design of a building. The joint is an important factor when designing a heavy timber structure using larch laminated timber. This is because it can determine the overall strength and performance, but is considered a highly vulnerable area in extreme situations like earthquakes (Huang and Chang 2017). When a seismic load occurs on a heavy wood structure with a drift pin larch beam-column joint with slotted-in steel plates, bending moment acts. When a load exceeding tension perpendicular to grain and longitudinal shear strengths of timber, which is a particularly vulnerable point in wood, is applied, brittle failure occurs at the joint, and there is a risk of collapse of the structure (LAM et al 2008). Therefore, many studies have been conducted to suppress brittle fractures. Various reinforcement methods are implemented to solve the problems in existing joints for wood. Among them, carbon fiber-reinforced plastic (CFRP) has been widely used as a reinforcing material for wooden building members owing to its excellent strength capacity and fire resistance. Xiong et al (2017) applied a horizontal cyclic load after wrapping the CFRP around the joint to improve the lateral resistance performance of the timber beam and post structure. As a result of the experiment, the reinforcement of CFRP around the joint showed a tendency to increase the maximum strength capacity of the joint and suppress the brittle fracture. Yang et al (2019) confirmed the superior performance of CFRP by conducting cyclic tests on joints with multiple reinforcement methods for preventing the loss of joint capacity due to structural damage during earthquakes. However, Xiong et al (2017) showed disadvantages of the reinforcement method, that wrapping CFRP lowered the yield moment and ductility ratio and had

poor aesthetics. In the experiment of Yang et al (2019), the yield strength increased, but the ductility ratio decreased in some specimens. To check the effect of CFRP insertion reinforcement on the performance of wood joints, Lee (2021) conducted the bearing strength test on larch square timber inserted and reinforced with different CFRP reinforcement ratios. Additionally, the tensile shear capacity of the single-bolt joint, which was reinforced by inserting and bonding CFRP with a slit within the member by changing reinforcement positions, was examined. The bearing strength experiment confirmed that the wood bearing strength increased with the increase in the CFRP reinforcement ratio. Additionally, through the tensile-type shear strength test, it was confirmed that the insertion of CFRP reinforcement improved the maximum shear strength and yield shear strength, and there was no significant difference in bonding strength according to the insertion reinforcement position. Previous studies focused on evaluating laminated timber as a structural component or joints with reinforcement wrapped around the external joint or with insertion reinforcements. Even with insertion reinforcement, it focused on the evaluation of the joint strength of a single bolt joint. There have been few studies on the joint behavior of structures with insertion of CFRP reinforcement. In this study, cyclic tests were carried out to confirm the moment of resistance capacity according to CFRP reinforcement ratio of beam-column joints with slotted-in steel plates of larch laminated timber.

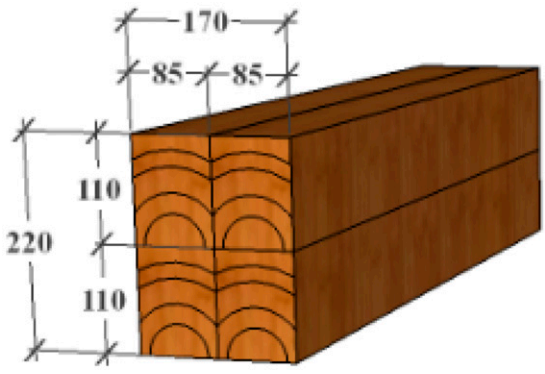

Figure 1. Production process of larch laminated timber specimens.

MATERIALS AND METHODS

Specimen production

Larch laminated timber was manufactured by multi-layering Larix Kaemferi Carr small square timber, as shown in Figure 1. The modulus of elasticity of each member used to prepare the specimen was 10 GPa, the average moisture content was 16 ± 0.9 % and the average air-dried gravity was 0.52 ± 0.03 (adding coefficient of variation data for the listed sample properties). The modulus of elasticity of each member was measured using a non-destructive method by the natural frequency of the longitudinal vibration. Phenol-resorcinol-formaldehyde (PRF) adhesive was used for adhesion by applying 400 g/m^2 of the adhesive on one side with 1.0 MPa pressure (Lee et al 2019). Pre-drilling for slit and drift pin insertion in laminated timber CFRP reinforcement and steel plate insertion was precision machined with a Computer Numerical Control (CNC) precutting machine (K2i 1259, Hundegger). Eight fastener holes with a diameter of 16 mm were pre-drilled in the column-beam joint to prepare the larch laminated timer specimen for the moment of resistance test. The edge distance and end-distance of the joint and row spacing between the fasteners were designed as 3.5 D (DL diameter of the drift pin, 16 mm). The SS275 drift pin, 16 mm in diameter and 170 mm in length (based on the KS D 3503 standard), was used as a beam-column joint fastener. The slotted-in steel plate was used as the joint, and the inserted SS275 steel was 440 mm × 220 mm and 8 mm thick, a rolled steel also based on the KS D 3503. For each steel plate, 16 holes with a diameter of 17 mm were pre-drilled for the drift pin group pattern of the column-beam joint (Figure 2a). The center of the control specimen was slit to a thickness of 10 mm and a depth of 225 mm to insert a steel plate. Subsequently, the steel plate was inserted to prepare a specimen for the moment of resistance test. For Type-A and Type-B specimens, a slit with a thickness of 13 mm and a depth of 225

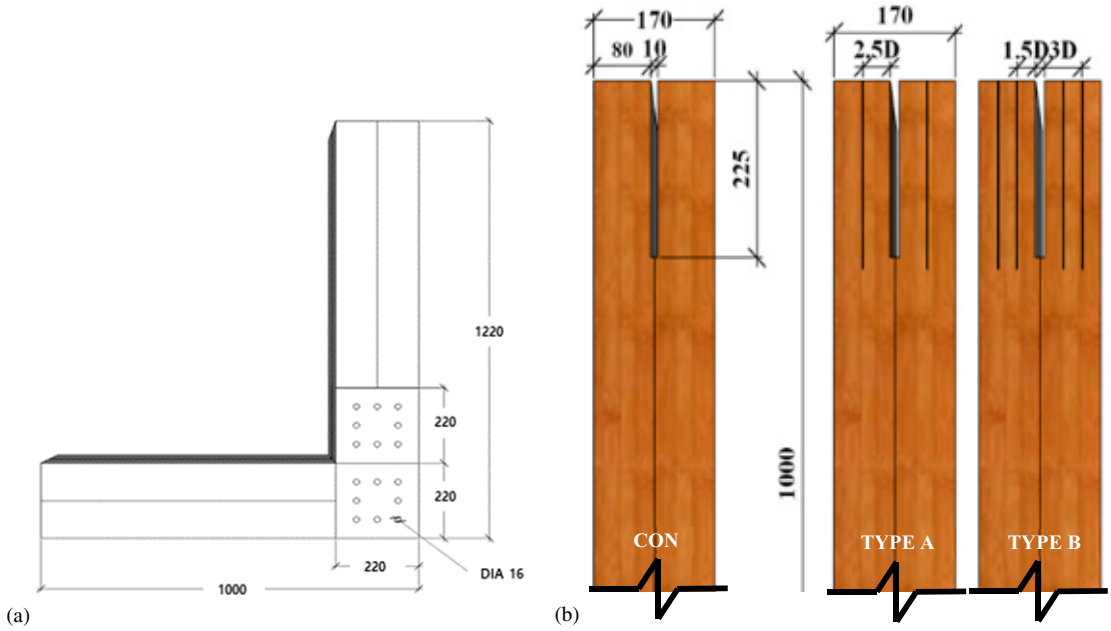

Figure 2. Schematic diagram of moment resistance specimens: (a) shape of moment resistance specimens and (b) strengthening schemes.

mm was machined in the center for reinforcement. The Type-A and Type-B moment of resistance specimens were reinforced with 1.4 mm thick carbon fiber reinforced plastic (CFRP) at the column-beam joint. The epoxy adhesive was used for joining the timber and CFRP. The Type-A specimen was prepared by inserting and joining plate-type CFRP with a thickness of 1.4 mm at 2.5D (D: diameter of drift pin, 16 mm) left and right from both sides of the steel plate slit and the slit as the starting point (volume ratio of the joint reinforced with CFRP: 3.6%). The Type-B specimen was prepared by inserting and joining the plate-type CFRP at 1.5D and 3D from both sides of the steel plate slit and the slit on the left and right (volume ratio of the joint reinforced with CFRP: 5.4%). A total of nine specimens were prepared, three for each type of moment of resistance specimens (Figure 2b).

Test Methods

Loading cell (TCL-100KNB, Tokyo Sokki Kenkyjo) with 100 kN capacity was used for the cyclic test. The moment of resistance specimens was rotated 90 degree before the test for the ease of load application of the load cell. To fix the moment of resistance specimens, the bottom part of column member was fixed onto the stopper using 12 mm bolts. Then, a cyclic load was applied from the upper right corner of the moment of resistance specimen.

A total of six 50 mm Tokyo Sokki Kenkyujo displacement transducers were used to measure the deformation caused by the moment increase of the column-beam joint of the moment of resistance specimen (Fig 3a). A data logger (TDS-302, Tokyo Sokki Kenkyujo) and a computer data acquisition system were used to identify the displacement of each displacement transducer according to changing load. Transducers were installed as shown in Fig 3a to measure the deformation according to the increase in the moment at the column-beam joint of the moment of resistance specimens. Transducer 1 was installed to measure the horizontal displacement on the opposite side of the beam, at which the load was applied. Transducers 2 and 3 were attached to the beam (D2 and D3 positioned at the center of the

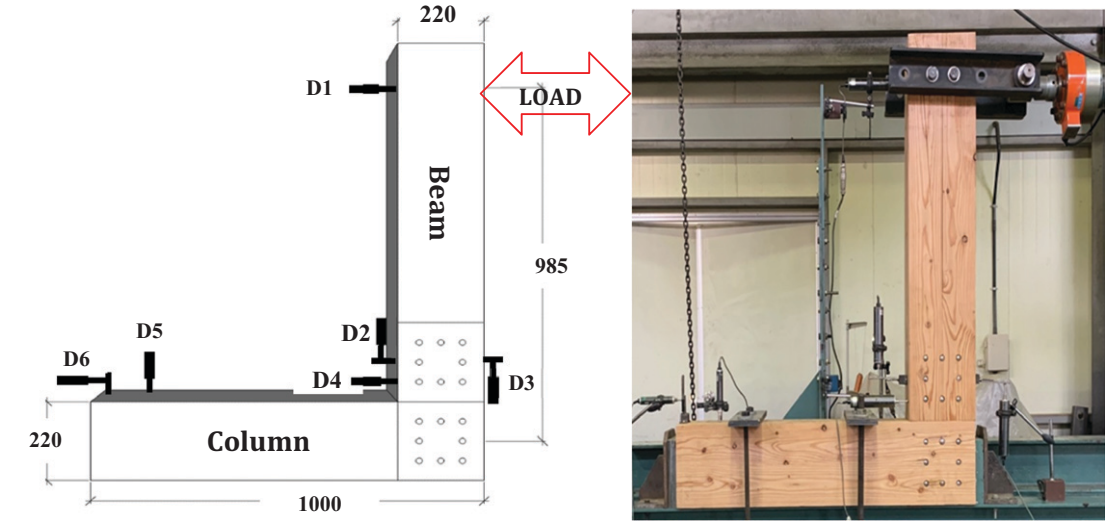

Figure 3. Test set-up for moment resistance performance test (Lee et al 2017): (a) measurement of joint rotation (schematic drawing) and (b) photograph of moment resistance specimens.

eight drift pins on the beam) and transducers 2 and 3 were installed to measure the vertical displacement. Displacement transducers 4, 5, and 6 were fixed to the lower part of the column member of the specimen with a stopper to correct occurring deformations other than joint moment deformation due to cyclic loads. The moment value was calculated with the distance from the center of rotation of the column member to the point where the horizontal force was applied (h: 985 mm) and the load applied from the load cell.

The loading protocol of the cyclic test was based on the standards of the AIJ (Architectural Institute of Japan), and the positive and negative cycles, corresponding to the rotation angles of ±1/600, ±1/450, ±1/300, ±1/200, ±1/150, ±1/100, ±1/75, and ±1/50 rad, were applied three times. The test was terminated when the load was reduced to 80% of the maximum load in the positive direction (Fig 4). Details of loading procedure for each cycle are shown in Table 1. The loading speed was set at 40 mm/min. The rotation angle (φ)

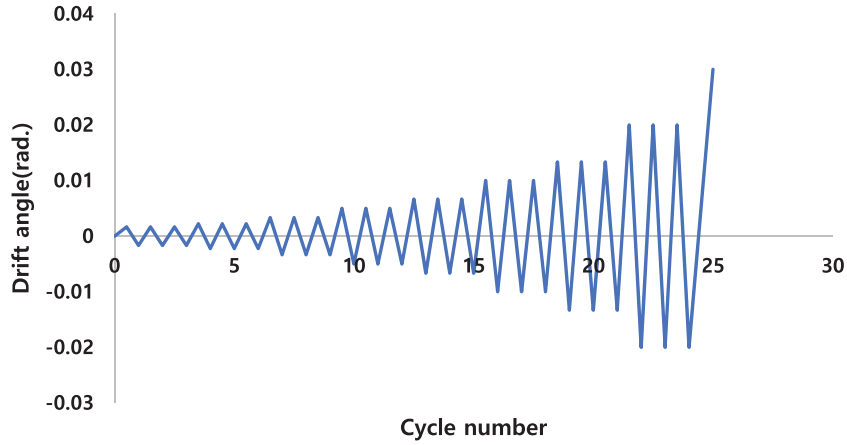

Figure 4. Loading protocol according to Architectural Institute of Japan.

Table 1. Horizontal displacement according to drift angle.

Drift angle (rad.)	Horizontal displacement (mm)	Cycle number
1/600	1.64	3
1/450	2.18	3
1/300	3.27	3
1/200	4.93	3
1/150	6.57	3
1/100	9.85	3
1/75	13.14	3
1/50	19.7	3
Failure		1

φ = Rotation angle between column and beam members; H_1 = Horizontal displacement of transducer 1; H_3 = Horizontal displacement of transducer 3; h = Distance from the center of rotation to the point where the horizontal force is applied (985 mm).

between the column and beam member was calculated by Eq 1.

$$\varphi = \tan^{-1}\left[\frac{H_1 - H_3}{h}\right] \quad \text{(Eq 1)}$$

Calculation Method of Strength Properties of Joints by Elasto-Plastic Model (Bilinear Method)

The strength characteristics of the joint were calculated using the elasto-plastic model (bilinear method) according to AIJ (Park et al 2014). The bilinear curve was originally designed for concrete and steel systems. It is assumed that the area under the test curve is the same as the area under the bilinear curve by two straight lines, and this method the behavior of the structure that separates the elastic and plastic regions (Muñoz et al 2008) (Fig 5). The envelope curves were obtained from a moment-rotation angle curve. The M_{max} (maximum moment), θ_{max} (maximum rotation angle), M_y (yield moment capacity), θ_y (yield rotation angle), R (rotational stiffness), M_u (ultimate moment), θ_u (ultimate moment rotation cycle), θ_v (elasto-plastic model's yield point rotation angle), and μ (ductility ratio) were calculated after the envelope curves were obtained from the moment-rotation angle curve (Lee et al 2017; Beak and Iimura 2009).

RESULTS AND DISCUSSION

Evaluation of Joint Capacity

Maximum Moment and Failure mode. The moment-rotation relations were established from the load-displacement data recorded during the cyclic tests. The maximum moment was calculated from the maximum load when the forward

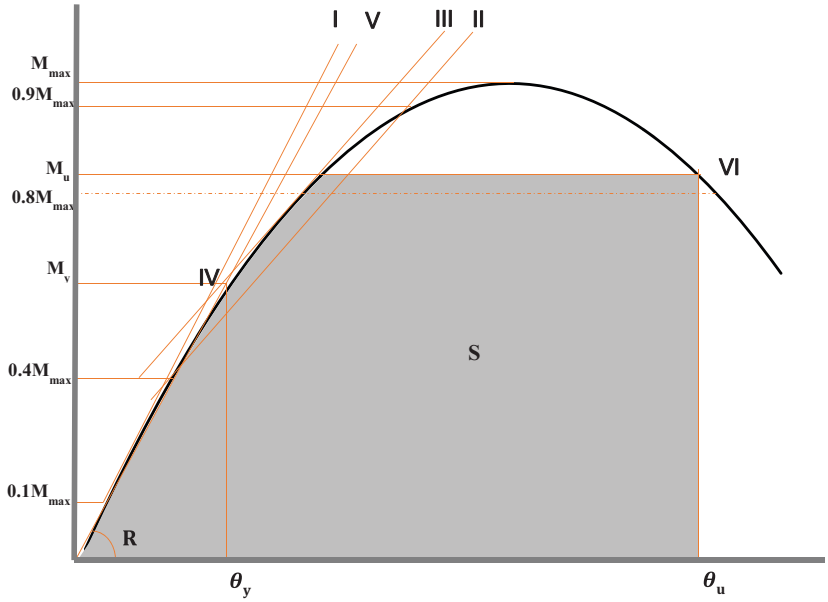

Figure 5. Estimation method for the joint capacity (Lee et al 2017).

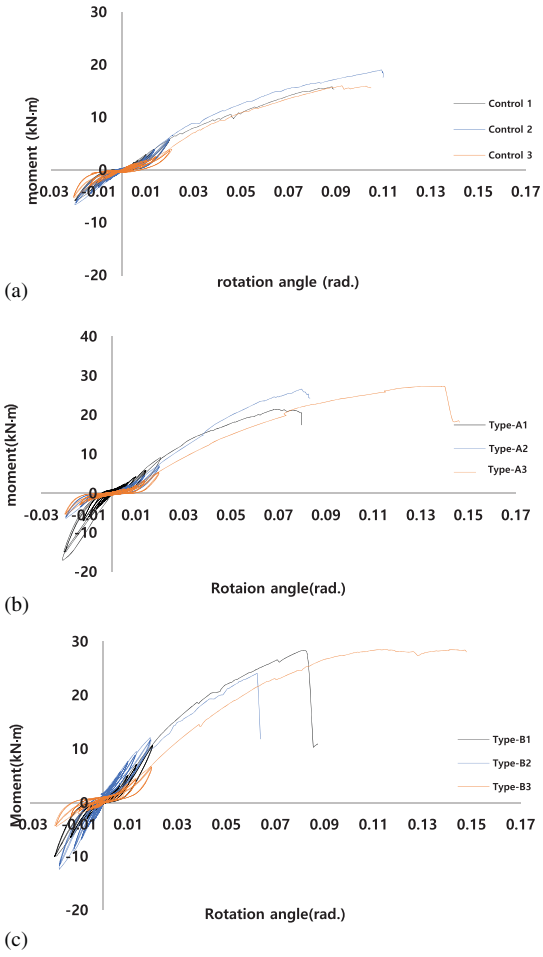

Figure 6. Moment-rotation angle curves: (a) control—non-reinforced joint, (b) Type-A—carbon fiber-reinforced plastic (CFRP) reinforcement volume ratio 3.6%, and (c) Type-B—CFRP reinforcement volume ratio 5.4%.

horizontal force was applied after repeating the positive and negative cycles three times. Figure 6 shows the moment-rotation angle curves of each specimen according to the cyclic test standard. The average maximum moment of the control specimen was 16.9 kN·m. When compared with the beam-column joint with slotted-in steel plates using glulam by Lee et al (2017) and Jung et al (2016), the applicability of the laminated timber joint was confirmed. Generally, when an external force is applied to the drift pin joint with slotted-in plates, the surface of the wood is pressed by the drift pin, causing deformation. Deformation by such bearing significantly affects the strength and rigidity of the joint. The bearing strength refers to the yield strength per unit area when the wood is pressed by fasteners such as drift pins. For the control specimen, as the column member rotated by the horizontal force, the bearing was generated in wood, which had relatively weak bearing strength compared with the steel plate and drift pin, causing cleavage cracks in the end distance direction. As the load gradually increased, the cleavage cracks increased along the drift pin row of the column member. The rotation of the column member then generated the bearing, resulting in a secondary fracture (Fig 7a). According to Gehloff et al (2010) and Yang et al (2019), splitting failure occurred in the column-beam joint of the unreinforced moment of resistance specimen in the cyclic tests, which was also observed in the control specimen in this study. Type-A and Type-B specimens reinforced with CFRP exhibited higher maximum moments than the control specimens. The average maximum moment of the Type-A (volume ratio of the joint reinforced with CFRP: 3.6%) was 24.6 kN·m, which was improved by 46% compared with that of the control specimen. All Type-A specimens tended to suppress the splitting failure in the beam members owing to the reinforcing effect of the CFRP. In the Type-A1 specimen, cleavage cracks generated from the cross-section of the column member gradually increased along the drift pin row until the test was terminated, resulting in splitting failure after 0.07 rad, and the Type-A2 specimen exhibited a similar failure mode (Fig 7b). In Type-A3, cleavage cracks occurred, but the cleavage cracks did not increase, and splitting failure occurred after 0.14 rad. (Fig 7c).

The maximum moment of the Type-B (volume ratio: 5.4%) specimen was 27.3 kN·m, which was improved by 62% compared with that of the control specimen. In the Type-B1 specimen, the net tension failure occurred in the beam member (Fig 7d). When the structure rotated, the beam member may have received a tensile force, leading to a failure in the direction perpendicular to grain of

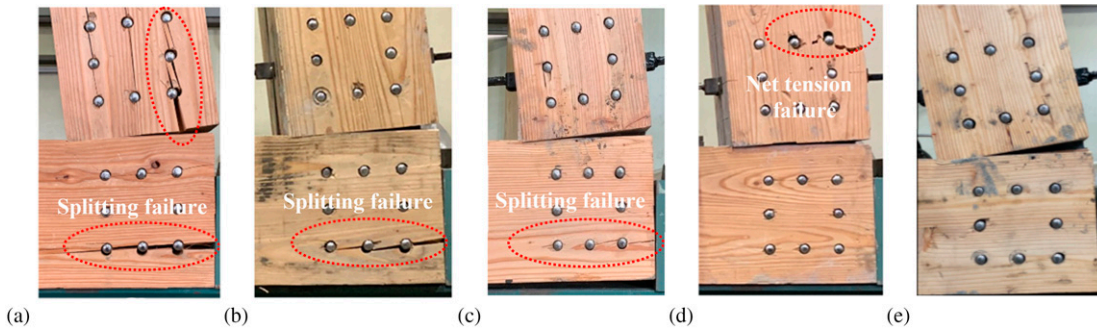

Figure 7. Failure mode of moment resistance joint specimens after test: (a) general failure mode of control specimens, (b) Type-A1, A2 specimens, (c) Type-A3 specimen, (d) Type-B1 specimen, and (e) Type-B3 specimen.

the beam member. The Type-B2 specimen exhibited splitting failure after 0.08 rad, and the failure was similar to that of the Type-A specimen. The Type-B3 specimen may have exhibited sufficient ductility because the CFRP reinforced at the joint suppressed the brittle failure of the member (Fig 7e). Thus, the CFRP suppressed the splitting failure by improving the joint capacity of the column-beam joint, showing a similar trend to the studies by Xiong et al (2017) and Yang et al (2019). Furthermore, as the reinforcement ratio of the CFRP increased, the joint capacity and ductility were improved, and the failure was suppressed in the end distance direction.

Cyclic Stiffness. When each cycle (1/600 rad. ~1/50 rad.) was repeated three times according to the cyclic test standard, high stiffness was observed in the first cycle for each cycle. However, as the cycle was repeated, the bearing was generated on the surface of the wood by the drift pin, resulting in a gap between the drift pin and wood. This gap was continuously widened as the cycle was repeated, causing a decrease in stiffness; a brittle failure may occur. When a brittle failure occurred in wood, the stiffness was significantly decreased. Figure 8 shows the cyclic stiffness for the first cycle of each cycle of the control, Type-A, and Type-B specimens. The cyclic

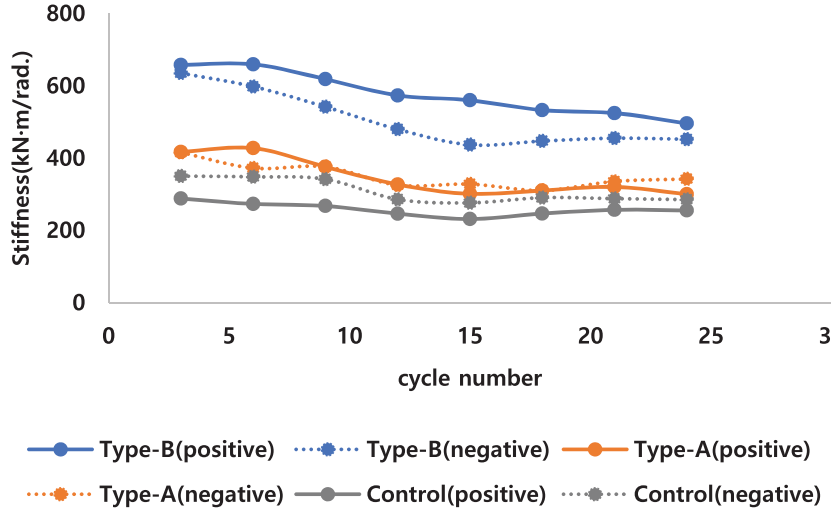

Figure 8. Stiffness variation according to the rotation angle.

stiffness, used to evaluate the stiffness degradation experienced by specimens, is calculated for each cycle as the slope of the line connecting the origin with the two points of loading corresponding to the maximum positive and negative displacements (Poletti et al 2016). Although the stiffness decreased with cyclic loading of all specimens, splitting did not appear until 1/50 rad. In this study, the stiffness tended to decrease as the test was repeated. The cyclic stiffness of the control specimen was 262.4 kN·m/rad. The Type-A and Type-B specimens showed superior cyclic stiffness than the control specimen in all sections, which were improved by 30% and 89%, respectively, compared with that of the control specimen.

Elasto-plastic analysis. When the joint is subjected to repeated loads such as earthquakes, stiffness, which is a characteristic in the elastic region, is important, but the behavior after passing the yield point is also important (Gehloff et al 2010). The ductility indicates how much deformation a structure can undergo without breakage (strength loss),and is an important evaluation index of seismic performance. Ductility is crucial in design as the ductile behavior of structures increases the ability to absorb energy if the structures exhibit ductile behaviors. The ductility is largely divided into displacement ductility and energy ductility, and in general, ductility ratio means the degree of displacement ductility. Ductility ratio was calculated through the elasto-plastic model (Table 2).

In this experiment, the ductility ratio refers to the ultimate moment angle divided by the yield moment rotation angle of the elasto-plastic model. For the reinforcement of the column-beam joint, Lam et al (2008) reinforced the self-tapping screw to improve the joint capacity and ductility of the dowel-type column-beam joint with slotted-in steel plates. They determined that the maximum moment and yield moment were improved by 75% and 22%, respectively, compared with that of the nonreinforced joint. Compared with the reinforcement method of Yang et al (2019) and Xiong et al (2017), the insertion reinforcement effect was slightly improved. In this study, the Type-A and Type-B specimens reinforced with CFRP exhibited superior strength and stiffness than the control specimen. The yield moment of the control specimen was 9.3 kN·m, the ultimate moment was 15.86 kN·m, and the ductility ratio was 2.13. The Type-A specimen showed an improved yield moment by 43% and cyclic stiffness by 58% compared with the control specimen, and the ductility factor was approximately 7% higher.

Table 2. Elasto-plastic results of the moment specimen joints.

	Control	Type-A	Type-B
M_y (kN·m)	9.3 (13.2)	13.4 (13.3)	13.7 (17.0)
θ_y (rad.)	0.037	0.034	0.028
R (kN·m/rad.)	255.6	403.9	507.3
$M_{\max}$ (kN·m)	16.9 (14.7)	24.6 (15.8)	27.3 (8.0)
θ_{max} (rad.)	0.097	0.092	0.086
M_u (kN·m)	15.86	21.68	22.57
θ_u (rad.)	0.13	0.125	0.117
θ_v (rad.)	0.061	0.055	0.047
μ	2.13	2.27	2.48

The Type-B specimen showed the highest joint capacity, and the yield moment was not significantly different from that of the Type-A specimen. However, the cyclic stiffness and ductility rate were 98% and 17% higher than those of the control specimen, respectively. Through this, it was confirmed that the yield moment and ductility ratio were improved as the reinforcement ratio of CFRP increased.

CONCLUSION

#1. Laminated timber is a wood composite made by multiple-layering of small-square timber. Unreinforced laminated timber moment of resistance specimen showed similar moment of resistance performance and failure mode as glulam specimen, which confirmed the potential use of laminated timber structures.

#2. The improvement in the bearing strength of the wood in the moment of resistance specimen was achieved through the insertion of CFRP reinforcement. This effect restrained the generation of a change in bearing from a large stiffness difference between the wood and metal fastener, which

restrained splitting. Accordingly, high stiffness and the maximum moment capacity were gained.

#3. The reinforcement effects of CFRP were observed in the initial elastic region and the plastic region. The CFRP dispersed the stress concentration at the junction, increasing the ductility ratio. Higher ductility was observed with the increase in the CFRP reinforcement ratio.

ACKNOWLEDGMENTS

This study was conducted as a basic research project supported by the Korea Research Foundation with funding from the Korean Ministry of Education in 2016 (Grant No. R1D1A1B01011163).

REFERENCES

Beak HS, Iimura Y (2009) Development of moment resisting joints using threaded steel shaft and drift pin. J Archit Inst Korea Struct Constr 25(8):61-69.

Gehloff M, Closen M, Lam F (2010). Reduced edge distances in bolted timber moment connections with perpendicular to grain reinforcements. *In* Proceedings, World Conference on Timber Engineering, Vol. 201.

Huang H, Chang WS (2017) Seismic resilience timber connection—adoption of shape memory alloy tubes as dowels. Struct Contr Health Monit 24(10):e1980.

Jung HJ, Song YJ, Lee IH, Hong SI (2016) Moment resistance performance evaluation of larch glulam joints using GFRP-reinforced laminated plate and GFRP rod. J Korean Wood Sci Technol 44(1):40-47.

Lam F, Schulte-Wrede M, Yao CC, Gu JJ (2008) Moment resistance of bolted timber connections with perpendicular to grain reinforcements. *In* Proceedings, 10th World Conference on Timber Engineering (WCTE).

Lee IH, Song YJ, Hong SI (2017) Evaluation of moment resistance of rigid frame with glued joint. J Korean Wood Sci Technol 45(1):28-35.

Lee IH, Song YJ, Hong SI (2021) Tensile shear strength of steel plate-reinforced larch timber as affected by further reinforcement of the wood with carbon fiber reinforced polymer (CFRP). BioResources 16(3):5106.

Lee IH, Song YJ, Song DB, Hong SI (2019) Results of delamination tests of FRP-and steel-plate-reinforced Larix composite timber. J Korean Wood Sci Technol 47(5):655-662.

Muñoz W, Mohammad M, Salenikovich A, Quenneville P (2008) Determination of yield point and ductility of timber assemblies: in search for a harmonised approach. Engineered Wood Products Association.

Park CY, Kim H, Eom CD, Kim GC, Lee JJ (2014) Effect of lintel on horizontal load-carrying capacity in post-beam structure. J Wood Sci 60(1):30-38.

Poletti E, Vasconcelos G, Branco JM, Koukouviki AM (2016) Performance evaluation of traditional timber joints under cyclic loading and their influence on the seismic response of timber frame structures. Constr Build Mater 127:321-334.

Xiong H, Liu Y, Yao Y, Li B (2017) Experimental study on the lateral resistance of reinforced glued-laminated timber post and beam structures. J Asian Archit Build Eng 16(2):379-385.

Yang JQ, Smith ST, Wang Z (2019) Seismic behaviour of fibre-reinforced-polymer-and steel-strengthened timber connections. Adv Struct Eng 22(2):502-518.

DEVELOPMENT OF A MODIFIED STANDARD TERMITE TEST FOR MASS TIMBER PRODUCTS[1]

*Tamara S. F. A. França**†*

Assistant Professor
E-mail: tsf97@msstate.edu

C. Elizabeth Stokes

Associate Professor
Department of Sustainable Bioproducts
Mississippi State University
Mississippi State, MS 39762-9820
E-mail: ces8@msstate.edu

Juliet D. Tang

Research Forest Products Technologist
USDA Forest Service
Forest Products Laboratory
Starkville, MS 39762-9820
E-mail: julietdtang@fs.fed.us

(Received August 2021)

Abstract. US manufacturers are looking to expand the use of cross-laminated timber (CLT) panels into the North American market, including states located in the southeast where termites are important pests. However, there is no current assessment method for determining CLT vulnerability to the highly destructive native termites found in many states across the United States. The impact of damage by these termites is of particularly high interest in areas with suitable climate to their proliferation, such as the southeastern United States. This study evaluated durability of CLT panels and developed a laboratory assay to test susceptibility of this product to termites. Untreated CLT suffered mass losses of up to 5.8% in testing with an average visual rating of 7.2, indicating a moderate to severe attack with 10-30% of the cross section of the product affected by termite intrusion. Recommendations were developed for the inclusion of modifications presented in standardized testing protocols and will be presented to standards organizations. The proposed method may also be applied to evaluate termite resistance of other mass lumber products such as laminated veneer lumber and Glulam.

Keywords: Cross-laminated timber, subterranean termites, laboratory assay, wood durability.

INTRODUCTION

Cross-laminated timber (CLT) has gained attention from the "green" building movement as a renewable prefabricated panel material with excellent thermal insulation, sound insulation, and fire restriction qualities (Laguarda-Mallo and Espinoza 2014). Other advantages include the ease of handling on-site and considerably lower weights than precast concrete. These characteristics make CLT panels ideal for rapid construction of modular buildings, including apartment/condominium structures (Van de Kuilen et al 2011; Smyth 2018).

Construction of numerous single and multilevel buildings in Europe and North America has provided real-world examples of the uses and benefits of CLT products. As investors are always searching for new markets, manufacturers have looked toward expanding the use of this product into the North American market, including the southeastern United States (Grasser 2015). As the adoption of CLT construction expands, so does the need for research focused on specific regional hazards or conditions.

Seismic design factors, R-factor, elastic properties, responses to fire, structural properties, and some

* Corresponding author
† SWST member

strength properties have been examined for CLT (Steiger et al 2008; Frangi et al 2009; Ceccotti et al 2010; Gulzow et al 2011; Popovski and Karacabeyli 2012; Pei et al 2013; Shen et al 2013; Gavric et al 2014; He et al 2020). Durability of panels has been examined regarding the delamination and bonding pressure, with increased bonding pressure resulting in lower incidence of delamination (Lim et al 2020). Durability studies with decay fungi have established that CLT left untreated and unprotected from water intrusion is susceptible to deterioration (Singh et al 2019). In addition, others have investigated the durability of CLT against weathering and wood-decaying fungi (Cappellazzi et al 2020; Sinha et al 2020; Bobadilha et al 2021). However, the extent to which termites may damage CLT in use is still under investigation (Mankowski et al 2018; Oliveira et al 2018).

Subterranean termites are found in most of the United States but are most common in the southern states. The warm and moist environment of the southern United States is the preferable climate for subterranean termites, increasing the chances of termite infestation in wood structures. The continental United States has four hazard zones for the risk of termite infestation, which are based on climate (Peterson et al 2006), and this risk must be taken into account when expanding CLT building to the southern region of the United States. The economic impact of termite damage in wood products in the United States is estimated at $1 billion to $7 billion when repair costs are included (Rust and Su 2012).

Wang et al (2018) summarized the main biological risks related to the use of mass timber. The risk of termite attack should be considered especially now that CLT buildings are being placed in areas of increased termite hazard. However, only preliminary studies have been conducted to evaluate the resistance of CLT to termite attack in laboratory assays (Stokes et al 2017; França et al 2018a, 2018b). Testing wood products for susceptibility to termite attack is standardized by the American Wood Protection Association (AWPA) standard method E1-17 (AWPA 2020) and by the American Society for Testing and Materials (ASTM) standard method D3345 (ASTM 2017). However, neither method offers parameters to accommodate the increased volume of CLT as a material. Although CLT can be tested at many dimensions, based on the preferences of the researcher, this study aims only to provide a starting point for assessing termite attack on commercially available CLT product, with number of lamina and overall thickness as commonly applied in low to midrise construction. At the same time, testing CLT at the specimen size recommended in the standard tests is not feasible, as it would not take into account the volume or multiple layers of material within CLT.

AWPA E1 calls for 400 individual termites per test container, with no more than 10% soldiers (AWPA 2020). Matching the increased scale of the test piece would require approximately 27,000 termites for each container. Since that would require collection of a termite population of nearly 675,000 individuals for a test with five treatments and five replicates, this scale is not feasible. Therefore, data to support a modified testing method is needed while still attempting to follow an existing protocol (Hassan and Morrell 2021).

Expanding the range of use for mass timber products throughout the United States requires research into the product's resistance to specific regional hazards. In addition, because CLT is a new product to the United States, there is also a need to develop new methods to measure termite damage, and to be sure that traditional testing methods are still applicable. However, modifications are necessary to accommodate the larger CLT dimensions, and the procedures should be repeatable and reliable. The objectives of this study were to 1) evaluate the resistance of untreated CLT to termite damage and 2) provide a baseline of adjusted methodology for testing CLT panels exposed to termites under laboratory conditions.

MATERIALS AND METHODS

Test Preparation

AWPA E1-17 (AWPA 2020) was used as a basis for this study with modifications to the sample and container size, amount of sand and water

substrate, number of termites, and test duration. CLT samples were prepared from sections of 3-ply spruce/pine/fir CLT panels obtained from a western US commercial manufacturer. To minimize the variability present in the material, samples within a test were taken from the same large block providing each test with samples in all treatments that had similar properties. For this test, panels were cut to 10 cm × 10 cm × 2.5 cm (length × width × thickness). This sample size was chosen to demonstrate CLT in its full thickness as shown in Fig 1. When placed in the test containers, the widest face of the CLT sample was placed in contact with the sand surface in the test containers.

Native subterranean termites (species of *Reticulitermes*) were collected from logs found in the Sam D. Hamilton National Wildlife Refuge, Mississippi. For each phase of testing, termites were collected from one population and used within 2 wk of collection. Termites were separated from woody debris by the cleaning methods recommended in AWPA E1-17 (AWPA 2020) and maintained temporarily on dampened coarse paper towel in covered containers.

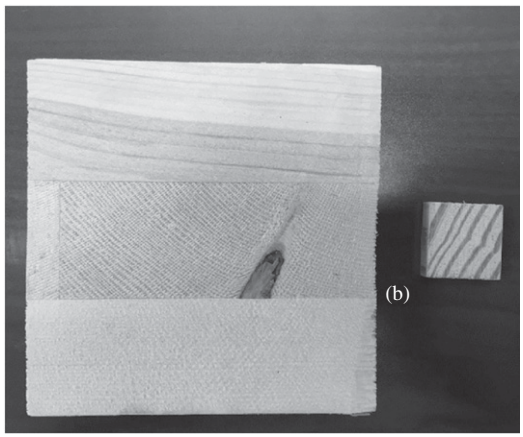

(a)

Figure 1. Comparison between cross-laminated timber (CLT) and standard test samples: (a) CLT test block face with dimensions of 10 cm × 10 cm × 2.5 cm (length × width × thickness); (b) American Wood Protection Association (AWPA) E1-17 with sample size of 2.5 cm × 2.5 cm × 0.6 cm (radial × tangential × longitudinal).

Prior to this series of tests, preliminary tests were conducted to select an appropriate container size, and 4-L clear polycarbonate containers with a tight-fitting lid were selected. A $1/4''$ hole for air exchange was drilled in each lid. These holes were then plugged with sterile cotton. Before starting the test, samples were oven-dried at 60°C to a constant weight. Five replicate CLT samples were used for each set of conditions. Following testing, blocks were again oven-dried at the same temperature to a constant mass to determine mass change. The variables evaluated in this test series included 1) variation of number of termites, 2) amount of sand substrate and water, and 3) duration of test. For each test phase, replicate control containers were also prepared without the presence of termites, to assess the impact of the test conditions on the CLT samples. For every variable tested, a total of five replicates were used and one container per replicate. Each test container received the same soldier:worker ratio (not to exceed 10% soldiers) specified in the AWPA E1-17 (AWPA 2020) standard.

Variable 1: Termite number variation test. Termites were separated from the wood as described earlier. Groups of 400, 600, 800, and 1000 termites were each counted three times and weighed. The average weight was calculated. Termites were added to test containers based on weight, which created some variation in the actual number of termites per container. All containers were prepared with 1500 g sand and 180 mL sterile distilled water and exposed for 4 wk, but each treatment received a different number of termites. The first group received the number of termites stipulated by AWPA E1 (AWPA 2020), which is 400 termites (approximately 1 g), and the other containers received 600, 800, or 1000 termites (1.8, 2.4, and 3 g, respectively).

Variable 2: Substrate variation test. The amount of sand and water recommended by AWPA E1-17 is 150 g and 27 mL, respectively (AWPA 2020). In the chosen 4-L container, this amount of water and sand could not provide enough sand substrate and moisture for termite survival. Four variations were selected for comparison in this second phase of testing: 375, 750, 1125, and 1500 g of sand with

proportional increases of water (45, 90, 135, and 180 mL, respectively). For this phase of testing, the number of termites was kept constant at 1000 termites (3 g) in each container, and the test duration was 4 wk.

Variable 3: Variation in duration of test. In the third phase of testing, containers were prepared using the amount of sand (1125 g) water (135 mL), and termites (1000 termites) determined from phases 1 and 2, and three test periods were compared (4, 8, and 12 wk). The recommended length of testing in AWPA E1-17 is 4 wk (AWPA 2020). This phase of testing was included to examine whether the larger test container and larger wood specimen would allow the termite population to remain healthy and active for longer than the standard test period, and whether a longer test period would result in increased damage to the CLT test samples. This test was designed to identify the significant differences between durations of exposure for the visual rating and mass loss variables.

Analysis of Tested Material

Test containers were incubated in a dark room at 21°C and 64% RH. Containers were inspected weekly throughout each phase of testing for signs of mold or secondary fungal contamination, and to verify that the termite populations were active. At the end of each test phase, CLT samples were removed and photographed. Living termites were carefully knocked out of the blocks and counted using an aspirator to collect the individuals. Test samples were then cleaned of mud tubes and debris and oven-dried under the same conditions as the pretest (60°C to a constant weight). Samples were photographed and each sample was examined and visually rated using the AWPA E1-17 (AWPA 2020) visual ratings (Table 1).

Images taken from tested materials were grouped into a single reference image, presented here in Fig 2. These images are presented here to clarify positioning and surface exposure and serve as guidelines for future research. CLT specimens from test series shown in Fig 2 include the following: termite number variation test, sand-adjacent face (a) and nonadjacent face (b); sand variation test, sand-adjacent face (c) and nonadjacent face (d); time variation test, sand-adjacent face (e) and nonadjacent face (f). Figure 3 demonstrates the damage observed on multiple sides of CLT samples from the termite number variation test, indicating an active, foraging termite population. CLT images shown in Fig 3 include the narrow faces of a single specimen, with the top and bottom of the original panel (a and c), and the cut edges (b and d).

Table 1. Visual rating system according to AWPA Standard E1-17 (AWPA 2020).

Visual rating classification	Rating
Sound	10
Trace, surface nibbles permitted	9.5
Slight attack, up to 3% of cross-sectional area affected	9
Moderate attack 3-10% of cross-sectional area affected	8
Moderate/severe attack, penetration, 10-30%, of cross-sectional area affected	7
Severe attack, 30-50% of cross-sectional area affected	6
Very severe attack, 50-75% of cross-sectional area affected	4
Failure	0

AWPA, American Wood Protection Association.

Statistical Analysis

Statistical Analysis System Version 9.4 (SAS Institute, Cary, NC) was used to analyze the differences in termite number, substrate level, and duration on response variables. Assumptions of normality and homogeneity of variance (HOV) were tested on raw data using the Shapiro–Wilk test and Levene's test, respectively. The threshold for significance for all tests was set at $\alpha = 0.05$. If assumptions were met, one-way analysis of variance (ANOVA) was performed using PROC GLM and then mean comparison was done with LSMEANS. If assumptions were not met, logarithmic transformation was used to normalize the data. For visual rating data and data that could not be normalized, Kruskal–Wallis H test, a nonparametric equivalent of one-way ANOVA, was performed. If the effect being analyzed proved to be significant at $\alpha = 0.05$, then mean rank separation was done using a Wilcoxon rank pairwise test adjusted by the Bonferroni correction.

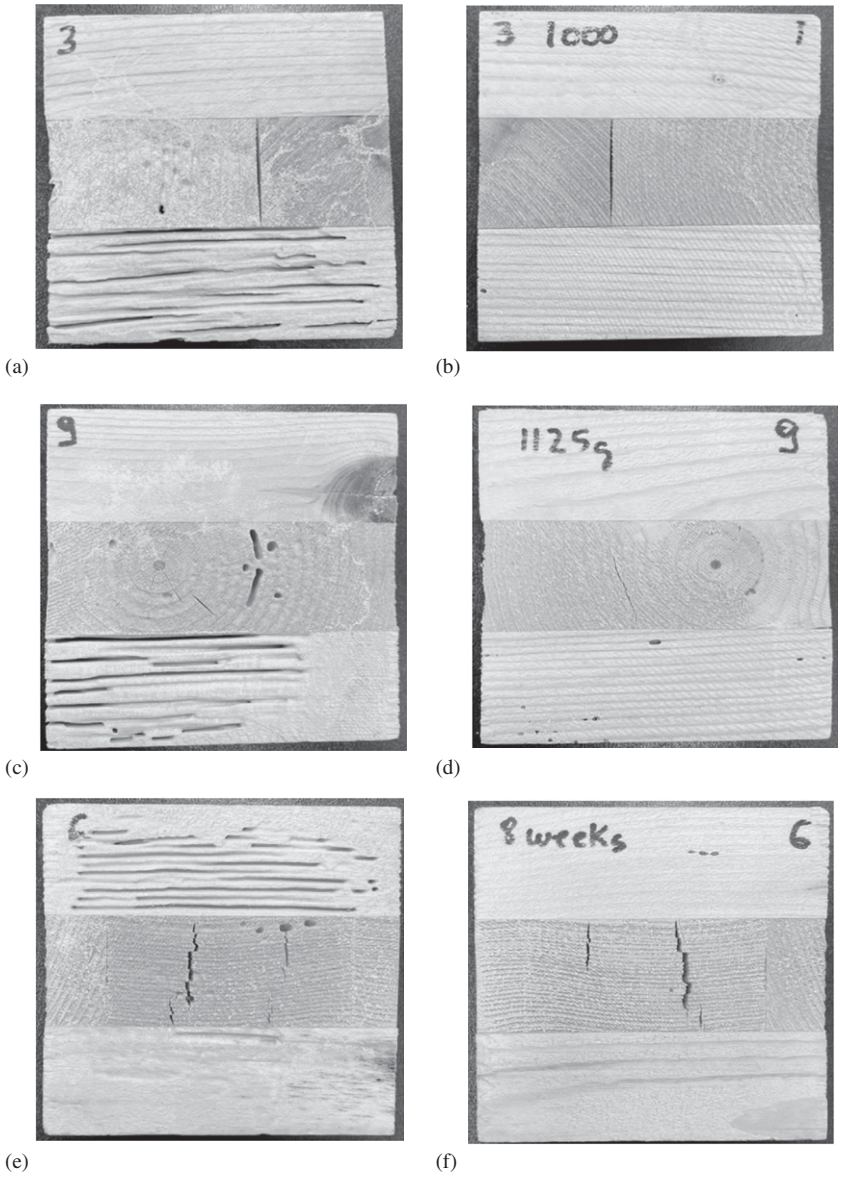

(a) (b) (c) (d) (e) (f)

Figure 2. Cross-laminated timber (CLT) specimens from tests series: termite number variation test, sand-adjacent face (a) and nonadjacent face (b); sand variation test, sand-adjacent face (c) and nonadjacent face (d); time variation test, sand-adjacent face (e) and nonadjacent face (f).

RESULTS AND DISCUSSION

Variable 1: Termite Number Variation Test

Table 2 summarizes mass loss, visual rating, and termite mortality. The data set for mass loss on phase 1 passed normality and HOV tests, so a one-way ANOVA was used to compare the effect of number of termites on mass loss. The average mass loss of samples exposed to 1000 termites per container (1.7%) was significantly higher than the other treatments. There was no statistical difference between the samples exposed to 800 and

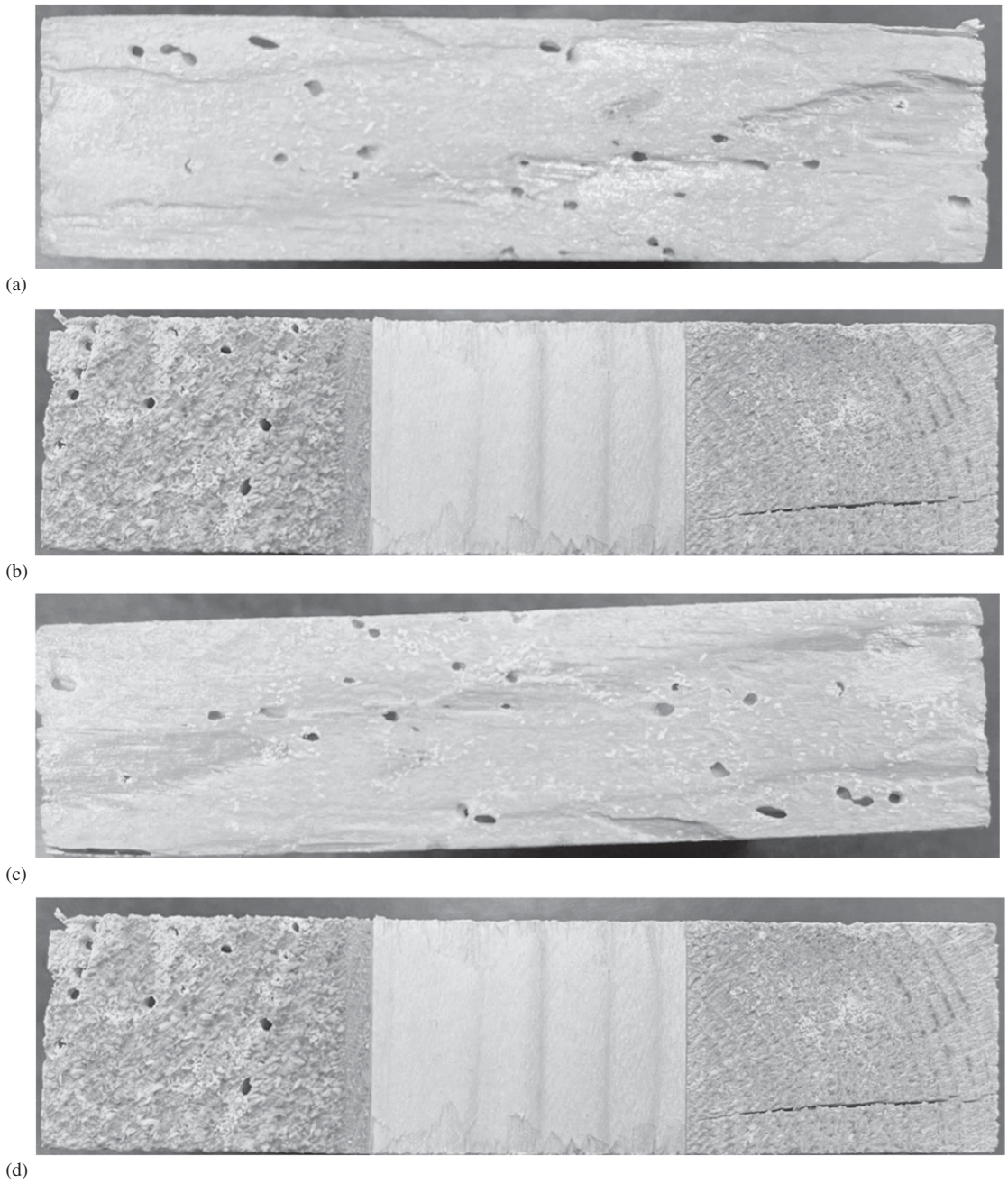

Figure 3. Example of termite damage on all sides of cross-laminated timber (CLT) samples from the test to evaluate termite number: with the top and bottom of the original panel (a and c), and the cut edges (b and d).

600 termites per container (1.0% and 0.9%, respectively). Blocks exposed to 400 termites showed a significantly lower mass loss (0.5%) compared with the other treatments. Damage in wood material is often determined by observing mass loss, for which the samples should be oven-dried to a constant mass. The AWPA E1-17 recommendation for drying is 40°C in a forced-draft oven for

Table 2. The effect of termite number on mean and percent coefficient of variation (in parenthesis) of mass loss, visual rating, and termite mortality.[a]

Number of termites	Mass loss[b] (%)	Visual rating[b] (AWPA E1)	Termite mortality (%)
1000	1.7a (15.8)	6.3d (3.9)	0.0 (0.0)
800	1.0b (19.0)	7.2c (3.4)	0.0 (0.0)
600	0.9b (10.6)	7.1c (2.8)	0.0 (0.0)
400	0.5c (43.8)	8.0b (2.8)	0.0 (0.0)
No Termite Control	−0.4d (−25.8)	10.0a (0.0)	N/A

AWPA, American Wood Protection Association.

[a] Test containers were evaluated at 4 wk and contained 1500 g sand and 180 mL of water.

[b] A significant difference among mean values in a column is indicated when no lowercase letters are shared ($\alpha = 0.05$).

solid wood materials and 40°C or 103°C for wood plastic composites (AWPA 2020). After working with CLT specimens during this series of tests, it was found that the CLT posttest specimens could not be dried at 40°C in a reasonable amount of time. Therefore, the recommended oven-drying temperature was increased to 60°C ± 2 for all tests. This temperature allowed CLT samples to dry in a reasonable time but was not high enough to damage samples resulting in cracks, checks, or delamination.

CLT samples exposed to 1000 termites per container received a significantly lower visual rating (6.3) compared with the other treatments (Table 2). According to the AWPA E1-17 visual rating, this attack is classified as severe attack with 30-50% of cross-sectional area affected (AWPA 2020). Blocks exposed to 800 or 600 termites received visual ratings of 7.2 and 7.1, respectively. This damage is classified as moderate attack with 10-30% of cross-sectional area affected. CLT blocks exposed to 400 termites received an average grade of 8.0 and the damage was classified as moderate attack with 3-10% of the cross-sectional area affected. There was no observed mortality in the tested conditions.

Variable 2: Substrate Variation Test

After transforming percent mass loss data using $\log_{10}$, assumptions of normality and HOV were satisfied (Table 3). One-way ANOVA showed that the effect of treatment was significant. A total of 1000 termites per container (approximately 3 g) produced the highest mass loss percentage in phase 1. Wood specimens in containers prepared with 1125 g and 750 g of sand had 2.4% and 2.1% mass loss, respectively, which was statistically higher than containers with 375 g (1.5%) but was not significantly different from containers with 1500 g (1.9%). Containers with 1125 g showed the

Table 3. The effect of amount of sand on mean and percent coefficient of variation (in parenthesis) of mass loss, visual rating, and termite mortality.[a]

Amount of sand (g)	Mass loss[b] (%)	Visual rating[b] (AWPA E1)	Termite mortality (%)
1500	1.9ab (25.4)	8.0b (6.9)	0.0 (0.0)
1125	2.4a (7.2)	7.5b (5.5)	0.0 (0.0)
750	2.1a (12.0)	7.5b (6.0)	0.0 (0.0)
375	1.5b (30.6)	7.8b (5.1)	0.0 (0.0)
1500_C[1]	0.6c (39.9)	10.0a (0.0)	N/A
1125 C[1]	0.6c (36.2)	10.0a (0.0)	N/A
750 C[1]	0.7c (19.5)	10.0a (0.0)	N/A
375_C[1]	0.7c (22.0)	10.0a (0.0)	N/A

AWPA, American Wood Protection Association.

[1] Control = no termites, otherwise containers had about 1000 termites and were evaluated at 4 wk.

[a] Test containers were evaluated at 4 wk and tested with 1000 termites per container.

[b] A significant difference among mean values in a column is indicated when no lowercase letters are shared ($\alpha = 0.05$).

lowest coefficient of variation (CV) among all sand levels tested.

Test blocks in containers with 1500 g of sand received higher average visual ratings (8.0) and were classified as having moderate attack, with 3-10% of the cross-sectional area affected (Table 3). However, no significant differences were observed between sand levels for visual ratings. Containers with 1125, 750, and 375 g of sand (7.5, 7.5, and 7.8 visual rating, respectively) were classified as severe attack, with 10-30% of cross-sectional area affected. No termite mortality was observed in this phase of testing. Even though no significant differences were observed between the three different sand levels (1500, 1125, 750 g of sand), 1125 g of sand was used in the third phase of testing.

Variable 3: Variation in Duration of Test

The variation in exposure duration is presented in Table 4. Since mass loss data in phase 3 were not normal and did not pass HOV even after transformation, differences in time duration were tested using the Kruskal–Wallis H test. Treatment was significant and a Wilcoxon multiple comparisons test was performed. Containers exposed to termite infestation for 12 or 8 wk had significantly higher mass losses (5.8% and 5.2%, respectively) than those exposed for only 4 wk (3.6%). No termite mortality occurred on wood in containers exposed for 4 and 8 wk; however, a high termite mortality (68.6%) was observed in containers exposed for 12 wk.

Although no statistically significant differences were observed in mass loss data between test samples exposed for 12 and 8 wk, the 8-wk duration had other advantages: 1) it was shorter, thereby providing a faster turnaround time for test results, 2) it produced lower CV values (4.2% vs 20.7% for 12 wk), and 3) it showed much lower termite mortality (0% vs 68.6% for 12 wk).

Table 4 also shows the companion visual rating data for exposure duration. Containers exposed for 4 and 8 wk had significantly higher mean visual ratings (7.4 and 7.0, respectively) compared with containers exposed for 12 wk (5.6). Containers exposed for 4 and 8 wk had termite damage classified as moderate/severe attack with penetration and 10-30% of the cross-sectional area affected. Containers exposed for 12 wk had severe attack with 30-50% of the cross-sectional area affected.

The results suggest that adjustments should be made to the existing standard tests to provide a basis for lab-scale testing of CLT, or that this material requires such different handling that a new standard should be developed. AWPA E1-17 (AWPA 2020) was selected as the basis for this test design since this standard is commonly used to evaluate the resistance of solid and composite wood products to subterranean termites. AWPA E1, however, was originally developed for wood products of a uniform composition, for which a small sample size is viable. CLT panels are a massive and heterogeneous product that should be tested at a size representative of use conditions. Table 5 describes the conditions from this series of testing that were

Table 4. The effect of exposure time on mean and percent coefficient of variation (in parenthesis) of mass loss, visual rating, and termite mortality.[a]

Treatment (weeks)	Mass loss[b] (%)	Visual rating[b] (AWPA E1)	Termite mortality (%)
4	3.6b (3.9)	7.4b (6.6)	0.0 (0.0)
8	5.2a (4.2)	7.0b (0.0)	0.0 (0.0)
12	5.8a (20.7)	5.6c (14.3)	68.6 (58.0)
4_C[1]	2.0c (6.5)	10.0a (0.0)	N/A
8_C[1]	1.6d (6.1)	10.0a (0.0)	N/A
12_C[1]	2.1c (5.8)	10.0a (0.0)	N/A

AWPA, American Wood Protection Association.

[1] Control = no termites, otherwise containers had 3 g or about 1000 termites and 1125 g sand.

[a] Test containers had 1000 termites and contained 1125 g sand and 135 mL of water.

[b] A significant difference among mean values in a column is indicated when no lowercase letters are shared ($\alpha = 0.05$).

Table 5. Recommended modifications to the AWPA Standard E1-17 test method for evaluating termite damage to CLT material.

Testing conditions	AWPA standard	Modifications for CLT samples
Oven-drying temperature	40°C ± 2 or 103°C ± 2	60°C ± 2
Wood sample size	2.5 cm × 2.5 cm × 0.6 cm	10 cm × 10 cm × 2.5 cm
Test container	80 mm × 100 mm glass screw-top jars	4-L food-safe container
Sand and water	150 g/27 mL	1125 g/135 mL
Number of termites	400	1000
Test duration	4 wk	Up to 8 wk

AWPA, American Wood Protection Association; CLT, cross-laminated timber.

determined to be suitable for the evaluation of termite damage on CLT at the bench scale.

When considering mass loss of CLT in an AWPA E1 style test, and the mass losses typically derived from testing solid wood in this test, a trend in the end results has been observed. With solid wood specimens of pine, spruce, and fir using standard test dimensions, values obtained in other studies were 40%, 23%, and 25%, respectively (Arango et al 2006; Kose and Tylor 2012; França et al 2016). In the AWPA E1 modified test presented here, with CLT at larger dimensions than the standard sample, the greatest mass loss achieved was 5.8%. Mass loss results from standard solid wood tests are much higher than the values obtained in this study, possibly due to the larger sample size used, or perhaps due to the laminate characteristic of CLT.

It is clear, however, that testing CLT in this manner should not be directly correlated to solid wood tests conducted at standard sample dimensions. Due to these differences and the lack of laboratory-scale testing of CLT products to date, it is unclear whether mass loss over time is a true indicator of change in CLT due to termite feeding behavior. It is also unclear whether mass loss is a true indicator of MC in CLT, as wood layers and glue lines exist at different moisture contents and may have distinct variations in drying. Perhaps, application of more precise technologies to measure volume loss and moisture changes should be combined with mass loss for better evaluation of termite damage on CLT samples.

For example, Arango et al (2016) evaluated the resistance of laser marking on wood to termite attack. Samples of solid southern pine wood and plywood samples measuring 75 mm × 37 mm × 9 mm were marked with a laser and the laser-marked surface was exposed to termites. In this study, termite damage to the longitudinal wood face, marked by a laser, was evaluated using percent surface attack as analyzed by ImageJ software rather than by mass loss. The larger scale of the samples required a change in evaluation methods. França et al (2019) used ImageJ to determine percent cross-sectional area affected on CLT samples subjected to termite attack. Percent cross-sectional area affected by termite feeding, in conjunction with mass loss and visual rating, resulted in a more accurate determination of overall termite damage in CLT than mass loss alone was able to describe.

This study outlines guidance for the laboratory-scale testing of CLT. These recommendations are meant to serve as a beginning for further testing of CLT and other mass timber products, each with their own characteristics that must be considered. In addition, test protocols for CLT exposure to termites under laboratory conditions should continue to be refined from the starting point provided here with comparison of other variables such as MC of wood, MC of adhesive, thickness of glue line, wood density, and wood grain orientation included.

CONCLUSIONS

A termite assay was developed for testing 3-ply CLT, a product that is heterogeneous in composition. This methodology can be used as a starting point for the development of standardized procedures to asses termite damage on CLT panels.

The evaluation of appropriate conditions to compare the number of termites, amount of substrate and moisture, and duration of testing was completed. Adjustments to test conditions are presented as a comparison with standard test conditions in Table 5. Further testing is underway, and additional testing is recommended to continue the examination of all variables that may influence testing, such as adhesive thickness and type, MC, preservative treatment of wood lamina, and wood species included in CLT.

ACKNOWLEDGMENTS

The authors acknowledge the support from USDA Forest Service Forest Products Laboratory (FPL) in Madison, WI, as a major contributor of technical assistance, advice, and guidance to this research. This paper was approved as journal article SB 1042 of the Forest & Wildlife Research Center, Mississippi State University.

REFERENCES

Arango RA, Green F, Hintz K, Lebow PK, Miller RB (2006) Natural durability of tropical and native woods against termite damage by *Reticulitermes flavipes* (Kollar). Int Biodeterior Biodegradation 57(3):146-150.

Arango RA, Woodward BM, Lebow ST (2016) Evaluating the effects of post dip-treatment laser marking on resistance to feeding by subterranean termites. *In* Proc IRG Annual Meeting (ISSN 2000-8953), The International Research Group on Wood Protection, 19-22 July 2016, Lisbon, Portugal; IRG/WP 16-10854; Section 1 Biology.

American Society for Testing and Materials (ASTM) (2017) D 3345-17: Standard test method for laboratory evaluation of solid wood for resistance to termites, American Society for Testing and Material International, West Conshohocken, PA.

American Wood Protection Association (AWPA) (2020) E1-17: Laboratory methods for evaluating the termite resistance of wood-based materials. American Wood Protection Association Book of standards. American Wood Protection Association, Birmingham, AL.

Bobadilha GS, Stokes CE, Kirker G, Ahmed SA, Ohno KM, Lopes DJV (2021) Effect of exterior wood coatings on the durability of cross-laminated timber against mold and decay fungi. BioResources 15(4):8420-8433.

Cappellazzi J, Konkler MJ, Sinha A, Morrell JJ (2020) Potential for decay in mass timber elements: A review of the risks and identifying possible solutions. Wood Mater Sci Eng 15(6):351-360.

Ceccotti A, Sandhaas C, Yasumura M (2010) Seismic behavior of multistory cross-laminated timber buildings. *In* Proc International Convention of Society of Wood Science and Technology, Geneva, Switzerland CSA S-16. Design of Steel Structures. Ottawa, Canada: Canadian Standards Association.

França TSFA, França FJN, Arango RA, Woodward BM, Arantes MDC (2016) Natural resistance of plantation grown African mahogany (*Khaya ivorensis* and *Khaya senegalensis*) from Brazil to wood-rot fungi and subterranean termites. Int Biodeterior Biodegradation 107:88-91.

França TSFA, Stokes CE, Tang JD (2018a) Durability of cross laminated timber against termite damage. *In* Proc 61st international convention of society of wood science and technology and Japan wood research society. Monona, WI: Society for Wood Science and Technology. 10 pp.

França TSFA, Stokes CE, Tang JD (2018b) Evaluation of cross-laminated timber resistance to termite attack. *In* Proc American Wood Protection Association Annual Meeting, 22-24 April 2018, Seattle, WA. 114:266-271.

França TSFA, Stokes CE, Tang JD, Arango RA (2019) Utility of image software in quantification of termite damage on cross-laminated timber (CLT). *In* Proc 21st International Nondestructive Testing and Evaluation of Wood Symposium, 24-27 September 2019, Freiburg, Baden-Württemberg, Germany. General Technical Report FPL-GTR-272. Madison, WI: U.S. Department of Agriculture, Forest Service, Forest Products Laboratory. pp. 643-649.

Frangi A, Fontana M, Hugi E, Jübstl R (2009) Experimental analysis of cross-laminated timber panels in fire. Fire Saf J 44(8):1078-1087.

Gavric I, Fragiacomo M, Popovski M, Ceccotti A (2014) Behavior of cross-laminated timber panels under cyclic loads. Pages 689-702 *in* S Aicher, HW Reinhardt, H Garrecht, eds. Materials and joints in timber structures. The Netherlands: Springer.

Grasser KK (2015) Development of cross laminated timber in the United States of America. MS thesis, University of Tennessee, Knoxville, TN. 115 pp.

Gulzow A, Richter K, Steiger R (2011) Influence of wood moisture content on bending and shear stiffness of cross laminated timber panels. Holz Roh-und Werkst 69(2): 193-197.

Hassan B, Morrell JJ (2021) Termite testing methods: A global review. J Test Eval 49(6):20200455.

He M, Sun X, Li Z, Feng W (2020) Bending, shear, and compressive properties of three- and five-layer cross-laminated timber fabricated with black spruce. J Wood Sci 66(38):1-17.

Kose C, Tylor AM (2012) Evaluation of mold and termite resistance of included sapwood in eastern redcedar. Wood Fiber Sci 44(3):319-324.

Laguarda-Mallo M, Espinoza O (2014) Outlook for cross-laminated timber in the United States. BioResources 9(4): 7427-7443.

Lim H, Tripathi S, Tang JD (2020) Bonding performance of adhesive systems for cross laminated timber treated with micronized copper azole type C (MCA-C). Constr Build Mater 232:1-10.

Mankowski M, Shelton TG, Kirker G, Morrell J (2018) Ongoing field evaluation of Douglas-fir cross laminated timber in a ground proximity protected test in Mississippi. *In* Proc 114th American Wood Protection Association Annual Meeting, 22-24 April 2018, Seattle, WA. pp. 132-137.

Oliveira GL, Oliveira FL, Brazolin S (2018) Wood preservation for preventing biodeterioration of cross laminated timber (CLT) panels assembled in tropical locations. Procedia Structural Integrity 11:242-249.

Pei S, Van de Lindt JW, Popovski M (2013) Approximate R-factor for cross-laminated timber walls in multistory buildings. J Archit Eng 19(4):245-255.

Peterson C, Wagner TL, Mulrooney JE, Shelton TG (2006) Subterranean termites—their prevention and control in building. Home and Garden Bulletin 64. U.S. Department of Agriculture, Forest Service, Forest Products Laboratory, Starkville, MS. 38 pp.

Popovski M, Karacabeyli E (2012) Seismic behaviour of cross-laminated timber structures. Pages 335-344 *in* P Quenneville, ed. Proc World Conference on Timber Engineering, 16-19 July 2012, Auckland, New Zealand.

Rust MK, Su NY (2012) Managing social insects of urban importance. Annu Rev Entomol 57:355-375.

SAS Institute (2013) SAS® software, version 9.4. Cary, NC: The SAS Institute Inc.

Shen Y, Schneider J, Tesfamariam S, Stiemer SF, Mu Z (2013) Hysteresis behavior of bracket connection in cross-laminated-timber shear walls. Constr Build Mater 48:980-991.

Singh T, Page D, Simpson I (2019) Manufactured structural timber building materials and their durability. Construction Structural Timber Building Materials and Their Durability 217:84-92.

Sinha A, Udele K, Cappellazzi J, Morrell JJ (2020) A method to characterize biological degradation of mass timber connections. Wood Fiber Sci 52(4):419-430.

Smyth M (2018) Cross laminated timber for residential construction. MS thesis, KTH Royal Institute of Technology, Stockholm, Sweden. p. 95.

Steiger R, Gülzow A, Gsel LD (2008) Non-destructive evaluation of elastic material properties of cross-laminated timber (CLT). Pages 29-30 *in* WF Gard and JWG van deKuilen, eds. Proc International Conference COST E53, 29-30 October 2008, Delft, The Netherlands.

Stokes CE, Tang JD, Shmulsky R (2017) Potential impact of subterranean termites on cross-laminated timber (CLT) in the Southeastern U.S. *In* Proc American Wood Protection Association Annual Meeting, 09-11 April 2018, Las Vegas, NV. 113:214-219.

Van de Kuilen JWG, Ceccotti A, Xia Z, He M (2011) Very tall wooden buildings with cross laminated timber. Procedia Eng 14:1621-1628.

Wang JY, Stirling R, Morris PI, Taylor A, Lloyd J, Kirker G, Lebow S, Mankowski M, Barnes HM, Morrell JJ (2018) Durability of mass timber structures: A review of the biological risks. Wood Fiber Sci 50(Special Issue):110-127.

CHARACTERIZATION OF THERMOMECHANICAL PULP MADE FROM PINE TREES INFECTED WITH NEMATODES[1]

Chul-Hwan Kim
Professor
E-mail: jameskim@gnu.ac.kr

*Jin-Hwa Park**
Graduate Student
E-mail: wlsghk2332@naver.com

Min-Seok Lee
Graduate Student
E-mail: symara9@naver.com

Chang-Yeong Lee
Graduate Student
E-mail: wsx630523@naver.com

Jeong-Heon Ryu
Graduate Student
E-mail: aof05@naver.com

Jin-Hong Park
Student
Department of Forest Products
IALS, Gyeongsang National University
Jinju, 52828, Korea
E-mail: skyeowl12@naver.com

(Received September 2021)

Abstract. Pine wilt is a lethal disease caused by the nematode *Bursaphelenchus xylophilus*. It causes tree death by blocking water and nutrient uptake in pine trees. Pine trees infected by these nematodes are used as fertilizer or fuel for thermal power plants, but their utilization is still only about 37%. To increase the utilization of the infected trees, this study investigated whether the shredded wood chips prepared from them could be used as raw materials for manufacturing thermomechanical pulp (TMP) and chemithermomechanical pulp (CTMP). TMP and CTMP prepared from the infected pine chips showed fewer pitch contents and better strength properties than those made from domestic pine. After refining, the infected chip could reduce the sacrifice of fiber length more than the normal chip, and there was no remarkable difference between the two chips in terms of optical properties.

Keywords: Pine wilt, nematode disease, thermomechanical pulp, chemithermomechanical pulp, pulp strength.

INTRODUCTION

Pine wilt leads to a dramatic disease that typically kills infected pine trees within a few weeks to a few months. The causal pathogen is known to be a thread-like nematode, *Bursaphelenchus xylophilus* that blocks the passage of water and nutrients and consequently kills the pine tree (Lee 2021). Also, when the infected pine trees die, the insect vectors move to other trees, so it is necessary to

* Corresponding author

cut down all surrounding trees to prevent the spread of the wilt worms (Rajotte 2017). A relationship between pine nematode and pine wilt disease was first reported by Japanese forest researchers (Mota and Vieira 2008). Pine wilt disease was evident only in East Asian countries in the early days following its discovery. However, it is currently occurring mainly in East Asia, North America, and Western Europe; Australia and South America are classified as areas at risk of pine wilt disease (Ikegami and Jenkins 2018).

It is difficult to use nematode-damaged pine because it must be fumigated, heat-treated, or chipped to kill the pine nematode or its vectors (Moon 2007; Donald et al 2016). Damaged trees are crushed and supplied as fuel for combined heat and power plants, or used as fertilizer after composting (Kim 2015). The tree loss due to pine wilt disease reaches 10^6 m^3 annually, which has become a serious disaster for the coniferous forest ecosystem (Chen et al 2021).

The pulp and paper industry, which consumes more than 40% of the world's industrial wood, is considered to harm the environment (World Wildlife Fund 2021). As of 2020, the wood self-sufficiency rate in Korea is about 16%, of which the self-sufficiency rate of wood for pulp production is 9% including pine and oak trees, which was 2125×10^3 m^3. In particular, the amount of pine trees obtained through nematode control and logging operations in areas affected by forest fires is 1873×10^3 m^3 and most of these pines are usually used for fuel.

There are various demands for domestic pine trees for different purposes. And as a major source of raw material for mechanical pulp in Korea, there has been shortage in its supply (Lee et al 2016b). Currently, there is one company in Korea that manufactures about 67,000 tons of thermomechanical pulp (TMP) annually using domestic pine. Considering the yield of TMP, more than 70,000 tons of pine logs are needed every year.

In Korea, the area of pine forests continues to decrease due to infection by wilt worms, climate change, and forest transition. As it is becoming increasingly difficult to secure raw materials for TMP, it is now necessary to use not only pine trees obtained from regular forestry management activities but also those harvested from wilt disease-affected areas.

The use of the nematode-damaged pine trees in the pulp and paper mills will be relatively free from raw material competition and environmental impacts, and the virtuous cycle of resources will lead to sustainable cyclical economic development and value enhancement.

Paper is manufactured by using pulps prepared through a mechanical or chemical pulping process for wood chips, either separately or by mixing them according to the final uses. TMP is a method of mechanical pulping in which pressurized steam is applied to raise the temperature of the wood to soften the lignin, whereas chemithermomechanical pulp (CTMP) also uses alkaline chemicals such as NaOH and Na_2SO_3 during the pulping process to soften wood chips and then refines them to produce pulp with high yields while reducing energy consumption and severe fiber damage (Fiber lab 2013). These mechanical pulps have higher yields than chemical pulps and have the advantage of reducing pulp manufacturing costs (Sundholm 1999; Illikainen 2008; Lee et al 2016b; Lee et al 2016c). During the manufacturing process of TMP, high-pressure steam treatment at 90-140°C and mechanical grinding treatment such as refining are applied to pine chips manufactured from wilt-damaged trees. It is possible to kill nematodes under such harsh manufacturing conditions, so it will be possible to dispel the concern about the spread of these nematodes to the surroundings by the vector in the infected pine chips.

In this study, TMP and CTMP were prepared from *Pinus densiflora* obtained from forest regions damaged by wilt nematodes, and the properties of TMP and CTMP made from normal pine chips were compared with evaluate the suitability of nematode-infected pines as raw materials for TMP and CTMP.

MATERIALS AND METHODS

Raw Material

For the preparation of TMP and CTMP, pine chips manufactured at Jeseoksan Mountain in Geoje-si, Gyeongnam Province, were used. In this area, more than 60% of pine trees were infected with the wilt nematodes, and after clear-cutting, they were chipped at the site (refer to Fig 1). The control chips were provided by Jeonju Paper Co.

Pretreatment of Wood Chips

Before manufacturing TMP and CTMP, the wood chips were washed with water to remove contaminants and impurities. The washed wood chips were impregnated at 40°C for about 12 h and then placed in an autoclave (DS-PAC 40, Lab house Co., Pocheon, Korea) and steam-treated at 90°C for 30 min. To further soften the preheated wood chips, a laboratory digester (Duko, Daejeon, Korea) was used to heat them at a liquid-to-wood ratio of 4:1 and 120°C for 60 min.

To manufacture CTMP, NaOH and Na_2SO_3 were further added to the digester at 3% based on the oven-dried weight of the wood chips representatively. Na_2SO_3 used in the CTMP process was impregnated during pretreatment to soften the chip, and NaOH maintained pH 9-10. This pretreatment caused less destructive separation of fibers, with long fiber and a much lower shive content. The pretreated TMP and CTMP raw materials were refined under the same.

Refining

As shown in Fig 2, the pretreatment wood chips were fed into a single disk refiner (KOS1, Kimhae, Korea) and refined several times at 1500 rpm until there was little change in freeness. Stock throughput was measured through the amount of the stock discharged during refining, and the pulp production efficiency was compared with the power consumption. After refining, a small bundle of wood fibers (shives) was removed using the Sommerville Screen (DM-850, Daeil Machinery Co., Daejeon, Korea) fitted with slots of a width of 0.15 mm and a length of 45 mm. The percentage of shives to TMP and CTMP remaining on the slot plate was calculated as follows:

$$\text{Shives content}(\%) = \frac{\text{Dried fiber weight left on screen (g)}}{\text{Dried fiber weight (g) before screening}} \times 100 \quad (1)$$

After removing shives, the pulps were further refined using a valley beater (DM-822, Daeil Machinery Co., Daejeon, Korea) up to the target freeness, which was 150 mL CSF according to ISO 5264-1.

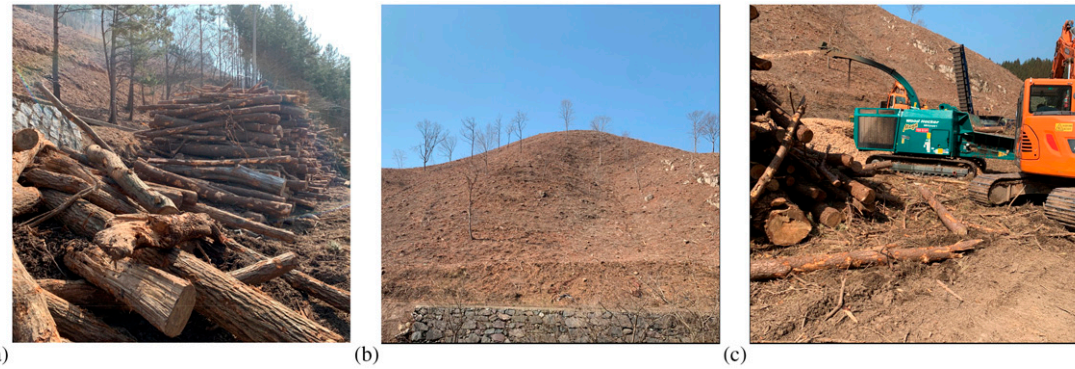

(a) (b) (c)

Figure 1. (a) Piles of cut pine trees infected with the wilt nematodes, (b) pine wilt disease-disturbed forest after clear-cutting, and (c) chipping of the infected pine trees.

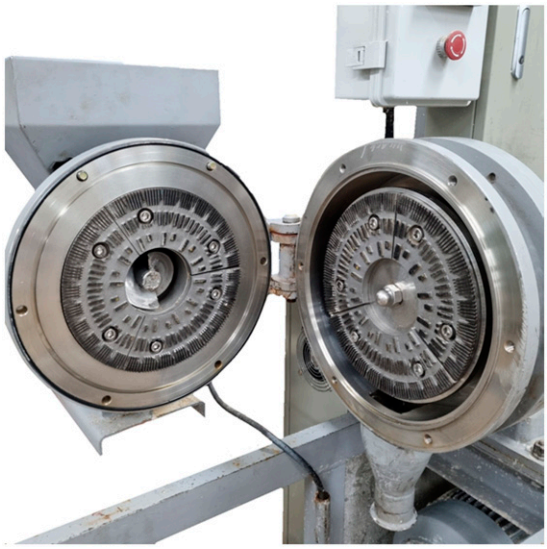

Figure 2. Single disk refiner fitted with thermomechanical pulp (TMP) plate.

Measurement of TMP and CTMP Properties

A fiber quality analyzer (FQA-360, Optest Equipment Inc., Hawkesbury, Canada) was used to measure the mean fiber length and fines contents. For the measurement of physical and optical properties of pulps, handsheets with 60 g/m^2 were produced. Tensile strength and tear strength were measured based on ISO 1924-1 and ISO 1974, respectively. Brightness and opacity were measured using the Elepho Spectrophotometer (Lorentzen & Wettre, Kista, Sweden).

Pitch Analysis

To analyze the pitch in TMP and CTMP, the analysis method applied by Nam et al was used (2015a). Sudan IV dye was used to selectively stain the hydrophobic pitch in TMP. Images of the selectively stained pitches were acquired using a stereomicroscope (Olympus BX51TF, Tokyo, Japan). Pitch analysis was performed using image analysis software (Axiovision, Carl Zeiss, Oberkochen, Germany).

RESULTS AND DISCUSSION

Chemical Characteristics of Infected Wood Chips

Table 1 compares the chemical properties of the control chips and the pine chips produced in the wilt disease-disturbed region. The infected chips had more cellulose and ash, and less lignin than the control chips, although their hemicellulose and extractives contents were similar.

Shives Content

Shives are fiber bundles that are not separated into individual fibers during the mechanical pulping process and can cause paper quality and productivity problems. In making paper using mechanical pulps, shives can lead to machine breaks, coater scratches, pick-out, and poor print quality (Pulmac International 2020). Unfortunately, refining during the TMP process does not break down all of the wood chips into individual fibers.

Figure 3 is a graph comparing the shive contents of TMP and CTMP prepared under the same conditions using normal and infected chips. In both TMP and CTMP, there was almost no difference in the content of shives according to the type of raw material. It is considered that the nematodes simply block the passage of moisture and have little effect on the structure of the pine tree itself. Therefore, this means that the presence of pine wilt disease rarely affects the formation of shives.

Fewer shives were detected in the CTMP samples than in the TMP samples due to the lignin

Table 1. Chemical characteristics of pine chips.

	Cellulose (%)	Extractives (%)	Hemicellulose (%)	Lignin (%)	Ash (%)
Wood chip	48.21 ± 3.62	5.95 ± 1.39	21.70 ± 1.29	23.85 ± 3.72	0.29 ± 0.12
Infected chip	53.89 ± 0.29	4.36 ± 0.27	20.29 ± 0.11	20.90 ± 0.14	0.56 ± 0.04

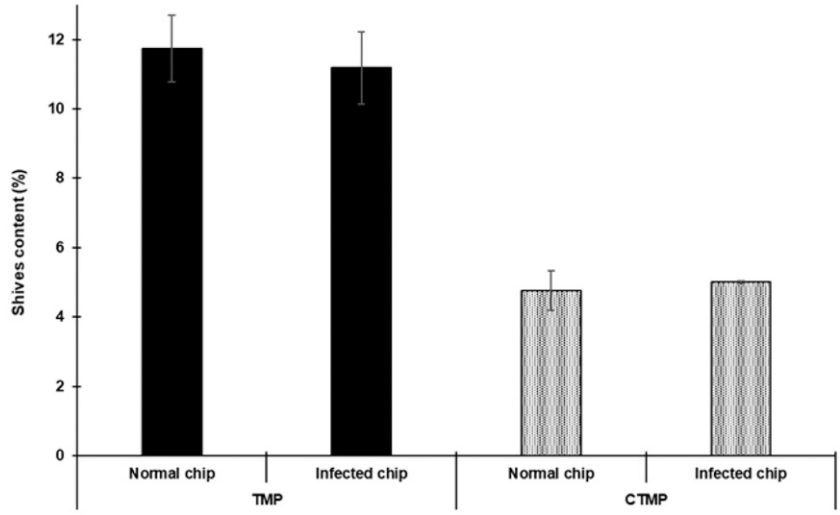

Figure 3. Shives contents of thermomechanical pulp (TMP) and chemithermomechanical pulp (CTMP) manufactured from the normal chip and the infected chip.

softening effect of alkaline chemicals such as NaOH and Na_2SO_3 (Lee et al 2016a).

Pitch Analysis

Pitch and stickies problems are the most common issues in mechanical pulping and papermaking (Guéra et al 2005). The pitch formed in the papermaking process directly affects the end products, such as reduced productivity and sheet break, and also shortens the lifespan of wire or felts, refiners, and other processing equipment (Hoekstra et al 2009). Therefore, it is preferable to avoid including tacky materials in the raw material as much as possible.

Figure 4 shows the number and area of pitches per unit area in TMP and CTMP manufactured from two different raw materials. TMP and CTMP prepared from the infected wood chips showed 27.7% and 9.5% fewer pitches per unit area, and 39.0% and 44.4% smaller pitch areas, respectively, than the normal chips. Lipophilic extractives containing pitches are known to cause problems in pulp and paper mills, mainly in the form of deposits and specks. As shown in Table 1, more contents of extractives were detected in the normal chips than in the infected chips, and it was considered that more pitches and a larger area of pitches were quantified in the TMP and CTMP prepared from the normal chips. The pitch content of softwoods varies depending on the species, age, and region, but there is no direct relationship between the wilt-damaged trees and the pitch content. Nevertheless, it was confirmed that the infected trees used in this study contributed to some extent in alleviating the pitch problem in the manufacturing process of TMP and CTMP.

Stock Throughput

Figure 5 is a graph comparing the stock throughput (g/s) and the refining time consumed up to the target freeness (150 mL CSF) when TMP and CTMP were manufactured using the two types of pine chips. In both TMP and CTMP, the amount of pulp discharged within a certain period of time was greater in the infected chips than in the normal ones. As shown in Table 1, the infected chips contained a lower amount of lignin than the normal chips, and thus were considered to be more easily refined, resulting in greater throughput. There is no direct relationship between the wilt nematodes and the lignin content, and it is known that the lignin content varies depending on the environment in which the infected tree grew.

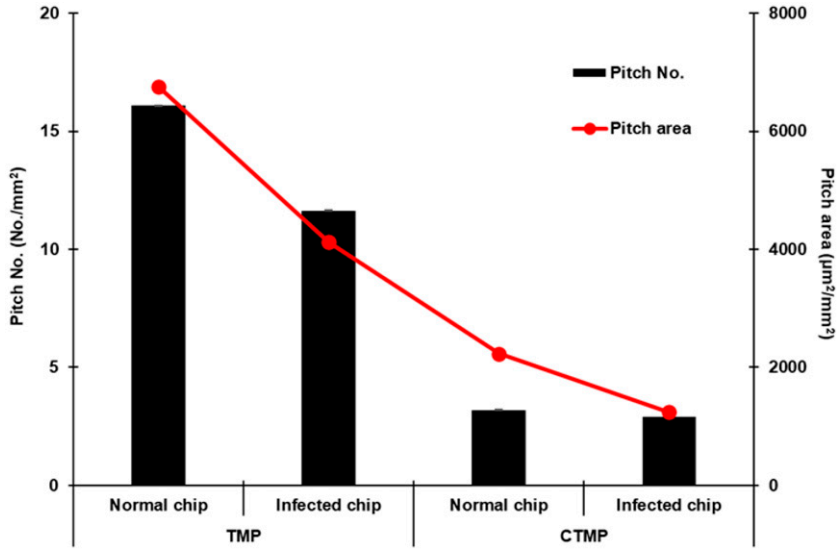

Figure 4. The number and area in a unit area in thermomechanical pulp (TMP) and chemithermomechanical pulp (CTMP) manufactured from the normal chip and the infected chip.

The more lignin the wood chips have, the more slowly the softening occurs. As a result, the swelling of the wood tissue is also slower, requiring more time for refining (Eriksson et al 1991).

Fiber Properties

Figure 6 is a graph comparing the mean fiber length and fines contents of TMP and CTMP prepared from normal and infected chips. Before refining, the infected chips had shorter mean fiber lengths than the normal chips. However, the infected chips after refining, had longer mean fiber lengths and fewer fines than the normal chips. TMP made with the infected chips had 12.7% longer fiber length and 6.7% fewer fines than TMP made using normal chips. CTMP made with the infected chips had 21% longer mean

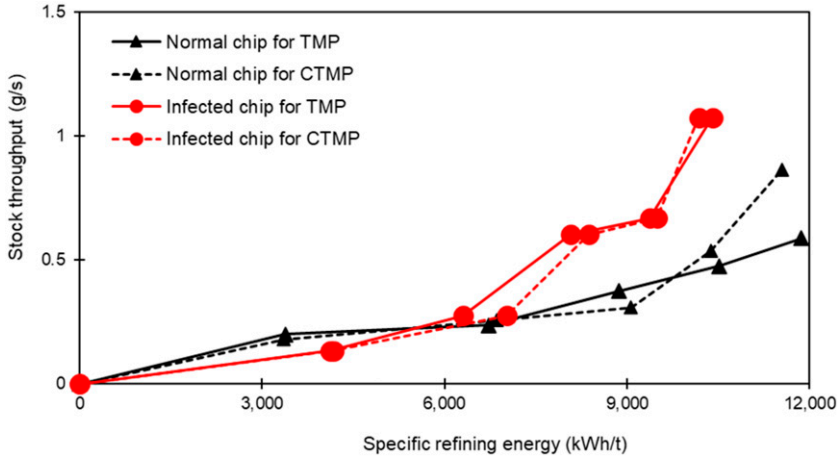

Figure 5. Stock throughput during refining of thermomechanical pulp (TMP) and chemithermomechanical pulp (CTMP) manufactured from the normal chip and the infected chip.

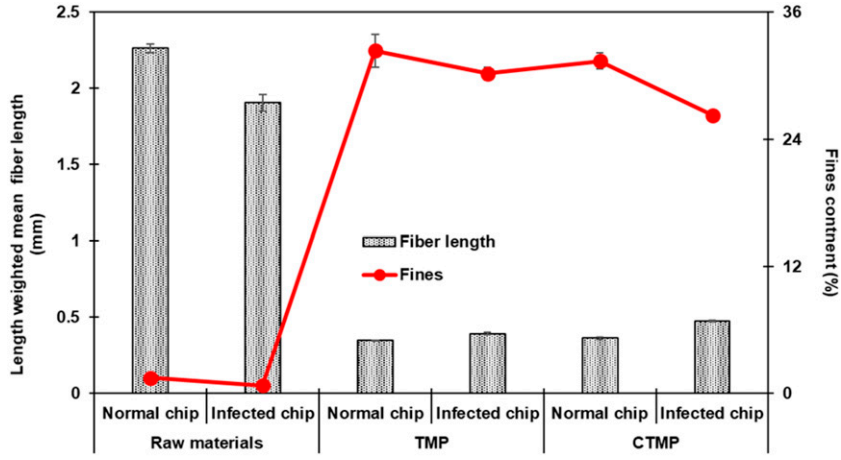

Figure 6. Mean fiber length and fines content of thermomechanical pulp (TMP) and chemithermomechanical pulp (CTMP) manufactured from the normal chip and the infected chip.

fiber length and 13% fewer fines than CTMP made with normal chips. The normal chips with longer fiber length during the manufacturing process of TMP and CTMP seemed to be refined more coarsely than the infected chips, resulting in shorter fiber lengths and more fines.

Fiber coarseness is an index that can indicate fiber flexibility, and if the coarseness is low, the tensile strength is improved due to the high flexibility of the thin-walled fiber (Nordström and Hermansson 2018). Figure 7 is a graph comparing fiber coarseness of TMP and CTMP made with the normal and infected chips. Fiber coarseness of TMP manufactured from the infected chip was 11.5% lower than that from the normal chip. Fiber coarseness of CTMP manufactured with the infected chip was 13.6% lower than that with the normal chips.

In conclusion, it was confirmed that the infected chips from TMP and CTMP could reduce the fiber length loss and contribute to the production of fibers with low coarseness.

Strength Properties

Figures 8 and 9 show the tensile strength and tear strength of TMP and CTMP manufactured from two different raw materials. TMP prepared with infected chips showed 12.7% and 2.6% higher tensile and tear strength, respectively, than TMP prepared with normal chips. CTMP made with

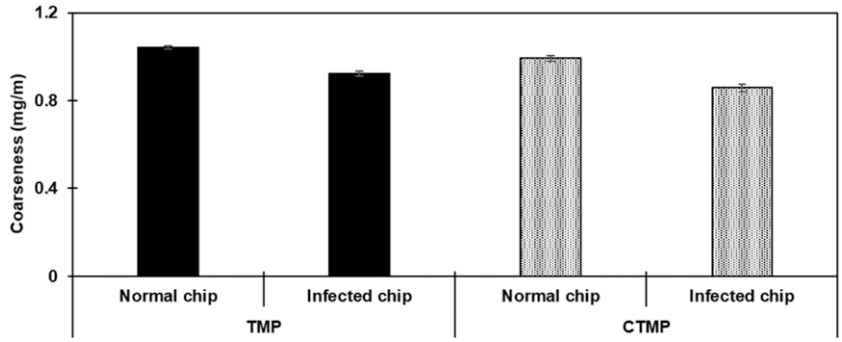

Figure 7. Coarseness of thermomechanical pulp (TMP) and chemithermomechanical pulp (CTMP) manufactured from the normal chip and the infected chip.

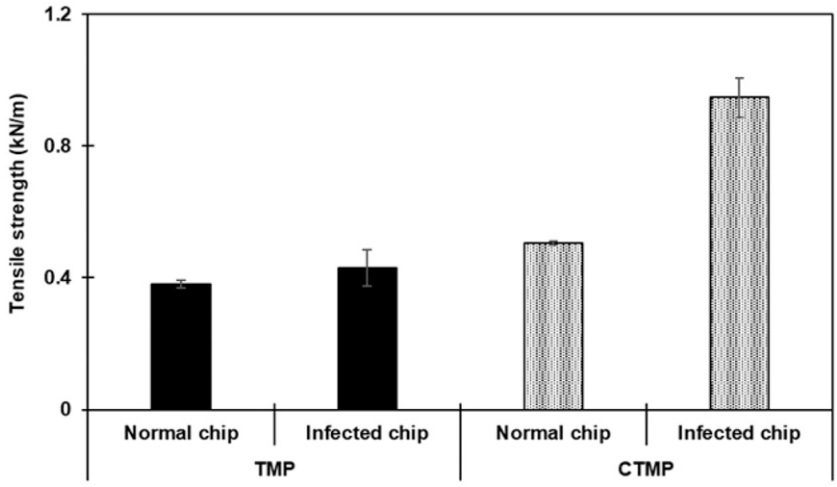

Figure 8. Tensile Strength of thermomechanical pulp (TMP) and chemithermomechanical pulp (CTMP) manufactured from the normal chip and the infected chip.

the infected chips showed 87.1% and 10.3% higher tensile and tear strengths, respectively, than CTMP made with the normal chips. It was considered that the infected chips could induce more fiber-to-fiber bonding because they had longer fiber lengths than the normal chips even after mechanical treatment such as refining.

Unlike other mechanical pulps, TMP requires higher refining energy but can produce pulp with longer fiber lengths and fewer shives and fines, resulting in paper with higher strength. Although this depends on the type of wood species used as raw material, it was greatly encouraging that the pine nematode-infected chips used in this study showed higher tensile and tear strength in TMP and CTMP compared with normal pine chips.

Optical Properties

Table 2 shows the brightness and opacity of TMP and CTMP manufactured from the two different raw materials. There was little difference in the

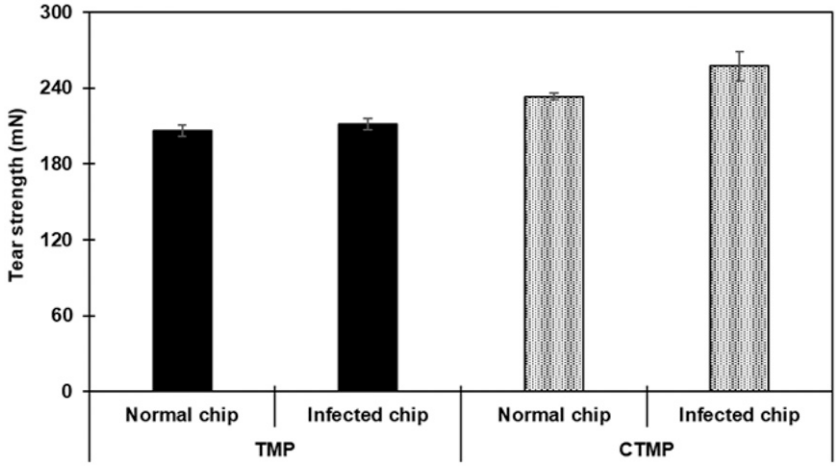

Figure 9. Tear Strength of thermomechanical pulp (TMP) and chemithermomechanical pulp (CTMP) manufactured from the normal chip and the infected chip.

Table 2. Optical properties of TMP and CTMP manufactured from infected pine tree.

	Raw material	Brightness (%)	Opacity (%)
TMP	Wood chip	34.48 ± 0.09	99.46 ± 0.09
	Damaged tree	34.49 ± 0.28	98.95 ± 0.22
CTMP	Wood chip	27.41 ± 0.09	98.96 ± 0.17
	Damaged tree	28.76 ± 0.30	98.09 ± 0.49

CTMP, chemithermomechanical pulp; TMP, thermomechanical pulp.

whiteness and opacity of TMP and CTMP prepared from the infected and the normal chips, respectively. Factors affecting the optical properties of mechanical pulp are very diverse. It is known that these properties are greatly influenced by the qualities of the raw materials, pulping, refining, and chemical treatment eg bleaching (Nam et al 2015b). In particular, the content of lignin and extract and the ratio of heartwood have a great influence on the brightness of mechanical pulp (Mishra 1990) However, the infected chips had slightly less lignin and extract content than the normal chips, but there was no remarkable difference in the brightness of TMP and CTMP.

CONCLUSIONS

After TMP and CTMP were prepared from wilt-nematode-infected pine chips and normal pine chips, their pulping properties were compared. The infected chips had lower amounts of lignin and extractives than the normal chips, leading to the refining energy saving. The fiber lengths of TMP and CTMP prepared under the same conditions were longer and there were fewer fines in the infected chips, and the shives content was also lower in the infected chips. TMP and CTMP prepared from the infected pine chips showed fewer pitch contents than those from the normal chips. Strength properties of the TMP and CTMP showed better values in the infected chips than in the normal chips, and there were no remarkable differences in optical properties.

ACKNOWLEDGMENTS

This work was supported by Program for Forest Convergence Professional Manpower Promotion, funded by Korea Forest Service in 2020 (FTIS Grant No. 2020186A00-2022-AA02) and Jeonju Paper Co. Ltd.

REFERENCES

Chen Y, Zhou X, Guo K, Chen SN, Su X (2021) Transcriptomic insights into the effects of CytCo, a novel nematotoxic protein, on the pine wood nematode *Bursaphelenchus xylophilus*. BMC Genomics 22(1):1-10.

Donald PA, Stamps WT, Linit MJ, Todd TC (2016) Pine wilt disease. The American Phytopathological Society, MN. https://www.apsnet.org/edcenter/disandpath/nematode/pdlessons/Pages/PineWilt.aspx (14 September 2021).

Eriksson I, Haglind I, Lidbrandt O, Salmon L (1991) Fiber swelling favoured by lignin softening. Wood Sci Technol 25:135-144.

Fiber lab (2013) Mechanical pulping. TMP/CTMP, Vancouver, Canada. http://www.fibrelab.ubc.ca/files/2013/01/Topic-3.3-Mechanical-Pulping-TMP-CTMP.pdf (14 September 2021).

Guéra N, Schoelkopf J, Gane PA, Rauatmaa I (2005) Comparing colloidal pitch adsorption on different talcs. Nord Pulp Paper Res J 20(2):156-163.

Hoekstra PM, McNeel TE, Proulx GP (2009) New methods for analysis of extractives and application in control of pitch, 2009 TAPPI Engineering. Pulping & Environmental Conference.

Ikegami M, Jenkins TA (2018) Estimate global risks of a forest disease under current and future climates using species distribution model and simple thermal model–Pine wilt disease as a model case. For Ecol Mgmt 409:343-352.

Illikainen M (2008) Mechanisms of thermomechanical pulp refining. Acta Universitatis Ouluensis. Series C, Technica 38.

Kim E-A (2015) Recycling rate 37%, 18% higher than the previous year. Environmental Law Newspaper, Seoul, Korea. http://www.ecolaw.co.kr/news/articleView.html?idxno=60377 (14 September 2021).

Lee J-Y, Kim C-H, Kwon S, Yim H-T, Kim J-H (2016a) Study for improving wood chip softening for CTMP. J Korea TAPPI 48(6):81-88.

Lee J-Y, Kim C-H, Nam H-G, Park H-H, Kwon S, Park D-H (2016b) Characteristics of thermomechanical pulps made of Russian spruce and larix, and Myanmar bamboo. J Korean Wood Sci Technol 44(1):135-146.

Lee J-Y, Kwon S, Lee M-S, Seo J-M, Lee J-S, Kim C-H (2016c) Study for prevention of photo yellowing occurring at TMP. J Korea TAPPI 48(4):24-31.

Lee S-H (2021) Pine wilt disease. Korea Forest Service, Daejeon, Korea. https://www.forest.go.kr/kfsweb/kfi/kfs/cms/cmsView.do?mn=NKFS_02_02_02_01_03&cmsId=FC_001186 (14 September 2021).

Mishra AK (1990) Effect of refining on the brightness of softwood CTMP and TMP pulps. MS thesis, Western Michigan University, Kalamazoo, MI. 8 pp.

Moon D-Y (2007) Recycling methods for damaged and suspected pine wilt disease. Korean Patent 10-2009-0011397.

Mota MM, Vieira P (2008) Pine wilt disease: A worldwide threat to forest ecosystems. Springer, Heidelberg, Germany. pp. 1-3.

Nam H-G, Kim C-H, Lee J-Y, Park H-H, Kwon S (2015a) Optimization technology of thermomechanical pulp made from *Pinus densiflora* (II)—Quantification of pitch contents in TMP. J Korea TAPPI 47(5):33-42.

Nam H-G, Kim C-H, Lee J-Y, Park H-H, Kwon S, Cho H-S, Lee G-S (2015b) Optimization technology of thermomechanical pulp made from *Pinus densiflora* (I)—Effect of temperature and NaOH at presteaming and refining. J Korea TAPPI 47(1):35-44.

Nordström B, Hermansson L (2018) Effect of softwood kraft fiber coarseness on formation and strength efficiency in twin-wire roll forming. Nord Pulp Paper Res J 33(2):237-245.

Pulmac International (2020) White paper: Measuring shives to increase communication paper making productivity. Pulmac Systems International Inc., VT. https://pulmac.com/wp-content/uploads/2014/05/Shive-white-paper-mech-pulp.pdf (14 September 2021).

Rajotte E (2017) Pine wilt disease. Penn State Extension, PA. https://extension.psu.edu/pine-wilt-disease (14 September 2021).

Sundholm J (1999) Papermaking science and technology Book 5—Mechanical pulping. Fapet Oy, Helsinki, Finland. pp. 16-21.

World Wildlife Fund (2021) Pulp and paper. Washington, DC. https://www.worldwildlife.org/industries/pulp-and-paper (14 September 2021).

PERCEPTION AND EVALUATION OF (MODIFIED) WOOD BY OLDER ADULTS FROM SLOVENIA AND NORWAY[1]

*D. Lipovac**

Assistant Researcher
Human Health in the Built Environment and Department of Technology
InnoRenew CoE and Andrej Marušič Institute
University of Primorska
Livade 6, 6310 Izola, Slovenia
E-mail: dean.lipovac@innorenew.eu

S. Wie

PhD Student
E-mail: solvi.wie@nmbu.no

A. Q. Nyrud

Professor
Faculty of Environmental Science and Natural Resource Management
Norwegian University of Life Sciences Elizabeth Stephansens vei 15, 1430 Ås, Norway
E-mail: anders.qvale.nyrud@nmbu.no

M. D. Burnard†

Assistant Professor
Human Health in the Built Environment and Department of Technology
InnoRenew CoE and Andrej Marušič Institute
University of Primorska
Livade 6, 6310 Izola, Slovenia
E-mail: mike.burnard@innorenew.eu

(Received October 2021)

Abstract. Many building users prefer wood over other building materials, but it is unclear how modified wood is perceived compared with unmodified wood. Additionally, it is unclear which material properties play a role in the general preference for wood, how tactile and tactile–visual perceptions of materials affect user preference for wood, and whether human preference for wood is consistent across countries and cultures with different wood use practices. One hundred older adults from Slovenia and Norway rated and ranked wooden materials (ie handrails) made of either unmodified or modified wood and a stainless steel control sample. The materials were rated on a semantic differential scale (capturing sensory and affective attributes) by each participant twice: first, while only touching the materials and then while simultaneously touching and seeing the materials. Finally, each participant ranked the handrails in order of preference. Wooden handrails were generally more preferred than the steel sample. Preference ratings and rankings of modified wood were comparable to those of unmodified wood. Results were relatively consistent across both countries. Materials rated as liked were perceived as somewhat less cold, less damp, more usual, less artificial, more expensive, and less unpleasant. The ratings were fairly consistent between the tactile and tactile–visual tasks. In some indoor applications, certain types of modified wood could be used in place of unmodified wood while meeting human aesthetical preferences. Specific visual and tactile properties can predict material preference and could be considered in the material design phase. The tactile experience is important in overall material perception and should not be overlooked. These findings seem to be stable across countries with different wood use practices.

Keywords: Material preference, wood modification, elderly, handrails.

* Corresponding author
† SWST member

INTRODUCTION

People spend most of their time indoors, and indoor environments can affect their health (Redlich et al 1997; Evans 2003). Focus in interior design has shifted beyond approaches minimizing harm, such as reducing outdoor noise, to creating restorative environments that can induce positive changes in well-being (Mcsweeney et al 2015; Markevych et al 2017). In recent years, research on restorative environments has begun to focus on older adults. An overview of the topic by Roe and Roe (2018) concludes that more attention should be paid, among other things, to restoration in residential (rather than natural) environments and to sensory stimuli. According to the authors, the residential environment, where older adults spend much of their time, "arguably offers the most important context for restoration," whereas "sensory stimulation in the living environment triggers curiosity and, in turn, our motivation to move around and explore" (490).

One of the main restorative design practices is to bring elements of nature into indoor spaces, as this can improve psychological and physiological indicators of human well-being (Mcsweeney et al 2015). Comparable outcomes have been observed when people were exposed to indoor wood (Sakuragawa et al 2005; Fell 2010; Nyrud and Bringslimark 2010; Burnard and Kutnar 2015; Zhang et al 2016; Zhang et al 2017; Dematte et al 2018; Nakamura et al 2019; Burnard and Kutnar 2020; Lipovac and Burnard 2020; Lipovac et al 2020; Shen et al 2020).

According to stress reduction theory, the observed positive response to nature is mediated by human aesthetic preferences that are predominantly innate (Ulrich 1983). The theory states that the initial response to a natural setting is affective (eg appreciation, interest), and that it precedes cognitive appraisal of the scene. This response is elicited quickly by different features of the natural environment, including water and vegetation, and many such (nonthreatening) features trigger a positive response. The initial affective response, along with one's experience and culture, influences cognitive appraisal of the scene, which can alter the initial affective state. The interplay between affect and cognition culminates in motivating (adaptive) behavior or functioning. The main predictions of the stress reduction theory are supported by findings showing that people from different cultures prefer natural environments over built environments (see Ulrich 1983, for a brief overview), and the environmental preference is positively associated with restoration (van den Berg et al 2003) and perceived restorativeness of the environment (Purcell et al 2001; Han 2010). Similarly, spaces furnished with wooden materials are perceived as more natural and preferred than environments without wood (Sakuragawa et al 2005; Nyrud et al 2014; Strobel et al 2017; Dematte et al 2018). Improved indicators of well-being and higher preference ratings have also been observed when wood was experienced only through touch (Bhatta et al 2017; Ikei et al 2017a, 2017b). These findings suggest that preference ratings of environments and materials could be used as an indicator of their potential restorativeness: investigating the perception of wood may help create materials that are not only useful in construction but may also contribute to restorative environments.

Modified Wood and Human Preference

Wood is generally perceived as more natural and liked than other common building materials (Rice et al 2006; Burnard et al 2017; Ikei et al 2017b). Recently, however, a lot of attention has been given to modified wood: wood that has undergone modification process that enhances its construction-related properties (Sandberg et al 2017). As a side effect, modification processes change material properties directly available to human senses, such as color, dryness, or roughness (Esteves and Pereira 2009; Bakar et al 2013). Due to its enhancements, modified wood can be expected to become more widely used in the future, but few studies have examined how people perceive it. Existing studies reported promising results: professionals and lay users liked certain thermally and chemically modified wood samples similarly to other types of wood in multiple settings (Gamache and Espinoza 2017;

Lipovac et al 2019). However, more evidence is needed to confirm these findings in other settings and determine whether modified wood is suitable for use in restorative environments.

Wood Properties and Human Preference

To determine whether materials can be used in restorative environments, we need to explore human preferences for materials and material properties that affect these preferences, including visual and tactile qualities of wooden materials, such as color, grain patterns, and surface treatments. People evaluate materials differently when these properties change (Waka et al 2015; Kidoma et al 2017). Studying these variations could help us develop materials that are more attractive to building users.

Human preference ratings (eg "like") can be viewed as the culmination of lower-level affective attributes (eg "interesting") and physical surface perceptions (eg "rough") (Okamoto et al 2016; Kidoma et al 2017). Existing studies have identified certain properties of wood that are associated with greater preference. When people sense wood by touch, they prefer untreated wood surfaces (compared with coated surfaces) (Bhatta et al 2017; Ikei et al 2017a), and their physiological indicators of well-being tend to improve (Ikei et al 2017a). People generally prefer wood surfaces they perceive as smoother (Jonsson et al 2008; Waka et al 2015; Bhatta et al 2017), and some evidence suggests this is also true for surfaces perceived as a denser, warmer, damper, softer, and more natural (Jonsson et al 2008; Waka et al 2015). In a study in which wood samples of outdoor tabletops were visually and tactilely inspected and ranked according to preference, greater preference was associated with perceived surface dampness and with material colors that were darker and closer to red on the green–red color component (Lipovac et al 2019). Other factors additionally influence visual preference for wood: people appear to prefer shinier and less knotty surfaces as well as surfaces with homogeneous color (Nyrud et al 2008; Sande and Nyrud 2008; Høibø and Nyrud 2010; Manuel et al 2015; Waka et al 2015). As relatively few materials have been studied in few contexts, how material properties influence preferences for wooden materials remains unclear.

The Relationship between Tactile and Visual Domain in Material Evaluation

Wood treatments are usually used to improve the performance of mechanical properties or to inhibit degradation of wood, but they often also change tactile properties, such as dampness. Moreover, coatings are frequently used to improve the longevity of the wood and reduce surface roughness. Such treatments might inadvertently negatively impact the tactile experience of materials: when touching materials, people rate unmodified as more liked than coated wood (Bhatta et al 2017), and their physiological state indicates greater relaxation (Ikei et al 2017a). The importance of focusing on surface texture to enhance the tactile experience of materials has been highlighted by Bhatta et al (2017). They argued that surfaces should have qualities that are perceived as natural. The significance of tactile material properties has been further explored in studies examining the consistency of perception between tactile and visual modalities. In a study in which participants rated naturalness of materials, ratings were consistent between tactile, visual, and tactile–visual experience of wood, suggesting that the tactile experience of materials is a rich source of information that is not substantially altered by the visual information (Overvliet and Soto-Faraco 2011). The authors of the study concluded that vision and touch are equally good at predicting naturalness. It seems that the tactile domain plays an important role in general material perception and should be further explored in different contexts of wood use.

Potential Cultural Effect on Wood Perception and Evaluation

Human affinity for natural elements may be widespread, but the role of culture should not be overlooked. When people observe wood, they can struggle in separating natural from artificial materials (Overvliet and Soto-Faraco 2011), and their

knowledge about wood treatments can influence their perception of material naturalness (Rozin 2005, 2006). Perception of naturalness, in turn, can affect preference (Jonsson et al 2008). When participants from Slovenia, Norway, and Finland rated several materials on perceived naturalness, their ratings were generally consistent. However, the ratings between participants from Slovenia and the two Nordic countries diverged in certain instances where processed wood samples were rated: Nordic participants perceived these samples as less natural than Slovenian respondents (Burnard et al 2017). This divergence could stem from differences in the knowledge and familiarity with wood and wood processing between the country populations, which, in turn, could result from different practices of wood use in these countries. Wooden buildings have a rich tradition in the Nordic countries (Mayo 2015), whereas in Slovenia, relatively little wood is used for structural components of houses (Statistical Office of the Republic of Slovenia [SURS]). If perceived naturalness and general preference of materials may vary between countries, studying wood perception and evaluation in countries with different wood use practices may help us reach stronger conclusions about the (potentially) universal appeal of wooden materials.

Objectives

The objectives of this study were to investigate 1) general preference for modified wood compared with unmodified wooden materials (and a non-wood control sample), 2) the association between perceived wood properties and wood preference, and 3) the relationship between the tactile and tactile–visual domain of material perception. To extend the work of existing studies, wood samples used were brought closer to real-life context by using handrail samples instead of often used small rectangular blocks of wood. The study was conducted across two countries (Slovenia and Norway) with different practices of wood use, to explore possible cultural influences on perception and evaluation of wood. The sample of participants consisted of older adults, as they may physically interact with interior materials more often than other age groups (eg using assistive railings for walking), and, consequently, contact with pleasant materials may affect them more profoundly.

MATERIALS AND METHODS

Participants

One hundred older adults aged 60 yr or more (M = 68.46 yr, SD = 7.23; 41 women) from Slovenia and Norway participated in the study. Participants were eligible to participate if they had no health impairments that could interfere with the study protocol, such as severely impaired vision or significant cognitive impairment. Subjects were not compensated for participation. Before the testing, subjects signed an informed consent form explaining the study purpose and protocol, participants' rights, and data management practice.

Slovenia. Fifty participants (M = 71.14 yr, SD = 7.19; 27 women) were from Slovenia. Thirty-four of them were recruited and tested in an activity center for older adults (city of Koper), which is visited predominantly by retired people. The remaining 16 participants, who were tested at their homes, were recruited through the social network of the first author and through snowball sampling.

Norway. Fifty participants (M = 65.78 yr, SD = 6.27; 14 women) were from Norway. Eight of them were recruited and tested in various places (eg coffee shop, mall, library) in the city of

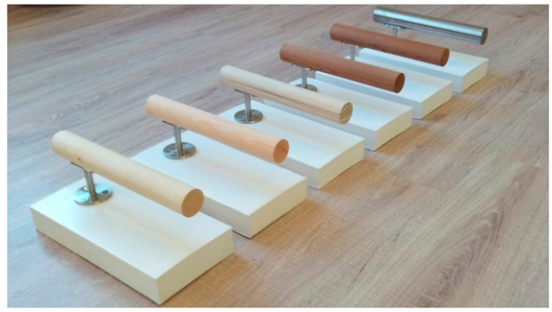

Figure 1. Handrail samples (from left to right: unmodified spruce, unmodified pine, acetylated radiata pine, thermally modified pine, thermally modified spruce, stainless steel).

Kristiansund. The other 42 participants, who were part of the still-active faculty staff, were recruited and tested at Norwegian University of Life Sciences (city of Ås).

Handrail Samples

Six cylindrical handrail samples were prepared (Fig 1); one was made of stainless steel and five of modified or unmodified wood. Specifically, we included handrails made of unmodified spruce, unmodified pine, acetylated radiata pine, thermally modified spruce, and thermally modified pine. The thermal modification was performed using the commercial ThermoD process at 212°C and superheated steam at the Heatwood company (Hudiksvall, Sweden). The handrail samples were 42 mm in diameter and 30 cm long. Each sample was mounted on a wooden base measuring approximately 30 cm × 15 cm × 5 cm, which was covered with white foil.

Semantic Differential Scale

Based on the previous work examining material perception in general (Guest et al 2011; Baumgartner et al 2013; Datta 2016; Okamoto et al 2016; Kidoma et al 2017) and wood perception in particular (Overvliet and Soto-Faraco 2011; Waka et al 2015; Kanaya et al 2016; Bhatta et al 2017), we selected sensory and affective descriptors that we considered relevant in the assessment of the materials used in this study. To each selected descriptor, we added a polar opposite descriptor. Altogether, we ended up with 11-word pairs, which captured tactile sensory properties (ie rough—smooth, warm—cold, dry—damp, soft—hard), affective attributes (ie unusual—usual, natural—artificial, cheap—expensive, pleasant—unpleasant, dislike—like), and visual sensory properties (ie dark—light, shiny—matte). The latter two-word pairs were used only in the part of the study in which participants could visually inspect the materials. Subjects responded to each word pair based on a five-point scale that consisted of the adverbs "considerably (eg rough)," "somewhat (eg rough)," "in the middle," "somewhat (eg smooth)," and "considerably (eg smooth)." The order *between* the presented word pairs was kept constant throughout the study; the word pairs followed each other in the same order as presented in this section. The order of descriptors *within each* word pair was also constant and followed the order presented in this paragraph. Note that to minimize possible effects of order within word pairs, the position of descriptors (ie left or right in the word pair) with positive and negative valence alternates among word pairs (eg the first word pair contains "rough" with negative valence on the left, the second word pair contains "cold" with negative valence on the right, etc.). The resulting scale was translated into Slovenian (Table S1) and Norwegian (Table S2). For simplicity, the remainder of this article presents only the item from the right-hand side of the scale (eg smooth) instead of the entire word pair (eg rough—smooth) when referring to the scale items.

Testing Procedure

The study consisted of three tasks. In the first task, participants could touch (but not see) the materials: they were instructed to keep their eyes closed during the test. Based on their tactile experience of materials, participants provided a response on a five-point semantic differential scale that was read to them. Responses were immediately entered into a computerized version of the scale. After completing the tactile task, participants proceeded to the second part of the study: tactile–visual task. This task was identical to the tactile task, except that the subjects could both touch and see the materials. Materials were presented to each participant in randomized order; however, for each participant, the order from the tactile task was repeated in the tactile–visual task, to allow for a better comparison of results on the two tasks. The third part of the study consisted of the ranking task. Participants were presented with all the materials at once to inspect them tactilely and visually. They were asked to rank the materials from most to least preferred by placing cards with numbers from one (most preferred) to six (least preferred). In total, the study session lasted approximately 30 min per participant. All sessions were conducted first in Slovenia and later in Norway.

Statistical Analysis

The data were processed and analyzed in R 4.0.2 (Team R Core 2021) using R Studio 1.3.959 (R Studio Team 2021) with the packages dplyr (Wickham et al 2020), ggplot2 (Wickham et al 2019), rstatix (Kassambara 2020), and rcompanion (Mangiafico 2019). Data from the entire sample of 100 participants were available and analyzed in all results presented below. There were no missing values, as the responses from subjects were entered directly into a computerized tool, which did not allow progressing without receiving a response.

We begin the analysis by examining the general preference of materials. We first calculate means and 95% confidence intervals (CI) for the scores on the item "like" for each material, separately for the tactile and tactile–visual tasks. We then test for differences between these scores with pairwise t-tests. The ranking task results present median ranks and bootstrapped percentile CI, and we test for differences between the ranks with pairwise Wilcoxon tests. For all tasks (tactile task, tactile–visual task, and ranking task), we first analyze results from the entire group of participants, continue with the analysis of results within each country, and conclude with the comparison of results between the countries. Note that in between-country comparisons, scores for each material are only compared with the scores of the same material, in contrast with overall and within-country comparisons, where scores for each material are compared with scores of all other materials.

The second section examines the association between the scores on the "like" item and the remaining items from the semantic differential scale. We calculate Kendall rank correlation coefficients between scores on the item "like" and scores on the other rating items, separately for the tactile and tactile–visual tasks.

The third and final section examines the relationship between the tactile and tactile–visual task scores: we first compare the scores between the tactile and tactile–visual tasks on all rating items (except "matte" and "light," which were not included in both tasks) across all materials and continue with computing Kendall rank correlation coefficients between the scores of both tasks.

In cases where multiple significance tests were used in the analysis (ie pairwise comparisons and significance tests of correlation coefficients), p values were adjusted with the Holm–Bonferroni method.

Data, data analysis R code, and supplementary tables are available in an open-access repository (Lipovac et al 2021).

RESULTS

In the following sections, we first present results on the preference of materials: scores on the item "like" from the semantic differential scale (for both tactile and tactile–visual tasks) and the ranks from the ranking task. We continue by presenting the association between scores on the item "like" and the remaining rating items. Finally, we present the relationship between the item scores on the tactile task and the tactile–visual task.

Preference of Materials

The scores on the item "like" from the tactile and tactile–visual tasks and the ranks from the ranking task are presented in Table 1. In both the tactile and tactile–visual tasks, all five wooden materials were on average rated similarly, as somewhat or considerably liked, whereas the stainless steel sample was on average rated as "in the middle" of the dislike–like item. Pairwise comparisons of scores between materials are presented in Tables S3 and S4. In both tasks, all wooden materials were rated statistically significantly higher than the stainless steel (median differences from 0.90 to 1.27, in all cases $p < 0.001$). In contrast, we did not detect statistically significant differences between ratings of wooden materials.

The results (Fig 2 and Tables S5 and S6) and pairwise comparisons (Tables S7 and S8) *within* each country show that the ungrouped scores mirror the overall results. In each country, wooden materials tend to be similarly liked and more liked than the steel sample in both the tactile and tactile–visual tasks. Some exceptions

Table 1. Mean scores on the item "like" from the tactile and tactile–visual tasks with 95% confidence intervals and median ranks from the ranking task with bootstrapped percentile 95% confidence intervals.

Material	Tactile task ("like" mean score)	Tactile–visual task ("like" mean score)	Ranking task (median rank)
Steel	3.01 [2.74, 3.28]	3.03 [2.75, 3.31]	6.0 [5.0, 6.0]
Spruce (thermally modified)	4.28 [4.10, 4.46]	4.02 [3.82, 4.21]	2.5 [2.0, 3.0]
Spruce (unmodified)	4.03 [3.81, 4.25]	3.93 [3.70, 4.17]	4.0 [4.0, 5.0]
Pine (thermally modified)	4.26 [4.08, 4.44]	3.97 [3.76, 4.18]	3.0 [3.0, 4.0]
Pine (acetylated)	4.20 [4.03, 4.37]	3.97 [3.76, 4.18]	3.0 [3.0, 3.5]
Pine (unmodified)	4.25 [4.06, 4.44]	4.12 [3.93, 4.31]	3.0 [3.0, 4.0]

were observed in the Slovenian sample. In the tactile task, Slovenian participants gave lower preference ratings to unmodified spruce compared with acetylated pine (mean difference = 0.52 [95% CI 0.19, 0.85], $p = 0.026$) and thermally modified pine (mean difference = 0.48 [95% CI 0.18, 0.79], $p = 0.027$). In the visual–tactile task, only unmodified pine (mean difference = 0.84 [95% CI 0.37, 1.31], $p = 0.012$) and acetylated pine (mean difference = 0.80 [95% CI 0.30, 1.30], $p = 0.035$) had statistically significantly higher preference scores than the steel sample.

Some differences were observed when the scores on the "like" item were compared *between* the countries (Fig 2 and Tables S9 and S10). In both tasks, Slovenian respondents gave acetylated pine (tactile task: mean difference = 0.48 [95% CI 0.14, 0.82], $p = 0.006$; tactile–visual task: mean difference = 0.78 [95% CI 0.39, 1.17], $p < 0.001$) and steel (tactile task: mean difference = 0.94 [95% CI 0.43, 1.46], $p < 0.001$; tactile–visual task: mean difference = 1.06 [95% CI 0.53, 1.59], $p < 0.001$) somewhat higher preference ratings than their Norwegian counterparts. Additionally, unmodified pine (mean difference = 0.56 [95% CI 0.19, 0.93], $p = 0.003$) and thermally treated spruce (mean difference = 0.40 [95% CI 0.02, 0.79], $p = 0.042$) received higher preference ratings in the tactile–visual task by Slovenian participants.

In the ranking task, thermally modified spruce was on average ranked the highest, followed by the three pine samples with the same median rank and the unmodified spruce with the lowest median rank among the wooden samples. Stainless steel was on average ranked the lowest among all materials. Pairwise comparisons (Table S11) show that all wooden materials except unmodified spruce were ranked statistically significantly higher than the steel sample (median differences

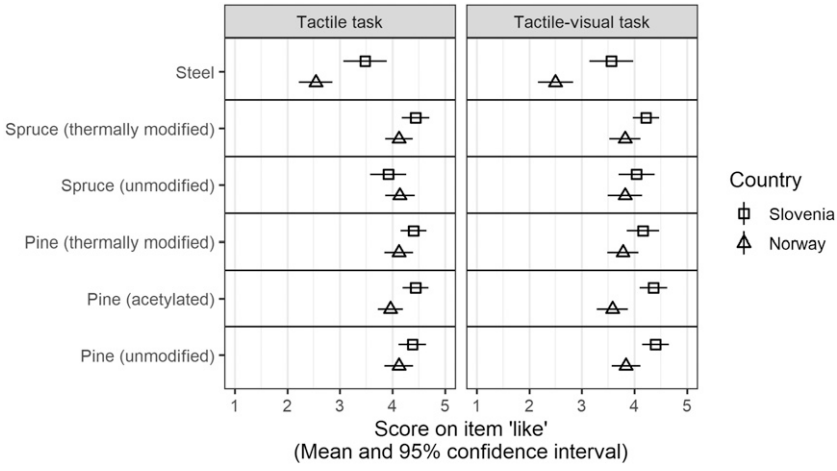

Figure 2. Scores on the item "like" split by countries.

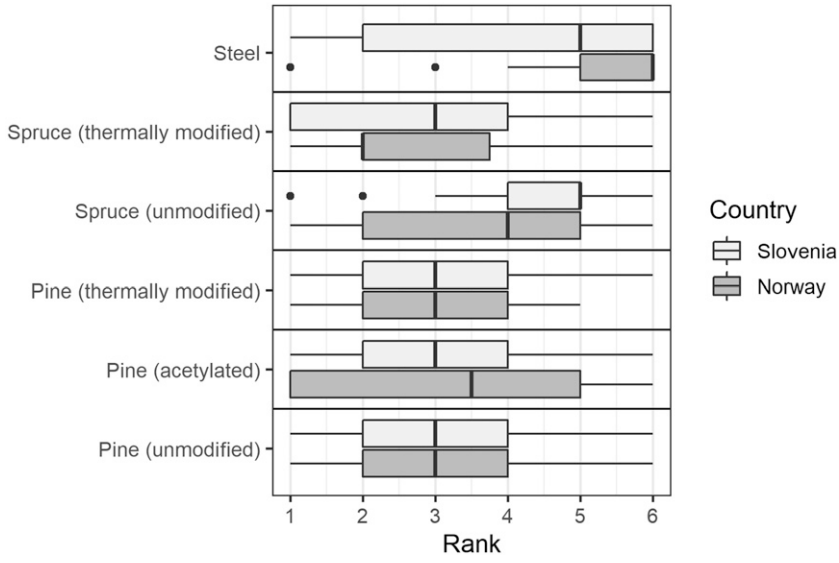

Figure 3. Ranks of materials split by countries.

from 1.5 to 2.0, in all cases $p < 0.001$). Specific differences were also detected between wooden samples: unmodified spruce was on average ranked lower than the other four wooden materials (median differences from 1.0 to 1.5, in all cases $p < 0.05$).

In general, similar results were observed in the ranks *within* each country (Fig 3, Table 2, Tables S12 and S13), with some exceptions: Slovenian participants gave unmodified spruce lower ranks compared with all wooden materials except thermally modified pine (median differences from 1.5 to 2.0, in all cases $p < 0.01$), and only thermally modified spruce received higher ranks than the steel sample (median difference = 1.5 [95% CI 0.5, 2.5], = p = 0.029). Comparisons *between* the countries (Fig 3) revealed differences in the ranking of two materials: compared with Norwegian respondents, Slovenian participants on average assigned higher ranks to steel (median difference = 0.0 [95% CI 0.0, 1.0]; $p = 0.014$) and lower ranks to spruce (median difference = 1 [95% CI 0.0, 2.0]; $p = 0.003$).

Rating Items Associated with the Preference of Materials

Table 3 presents Kendall rank correlation coefficients between the scores on the item "like" and the remaining items for the tactile and visual–tactile task. Correlation coefficients are similar across both

Table 2. Ranks of mean and median ranks of each material for both countries.

Material	Rank of mean rank—Slovenia	Rank of median rank—Slovenia	Rank of mean rank—Norway	Rank of median rank—Norway
Steel	5	5.5	6	6.0
Spruce (thermally modified)	1	2.5	1	1.0
Spruce (unmodified)	6	5.5	5	5.0
Pine (thermally modified)	4	2.5	2	2.5
Pine (acetylated)	2	2.5	4	4.0
Pine (unmodified)	3	2.5	3	2.5

The values in the table were obtained by first computing mean and median ranks for each material (separately for each country) and then assigning ranks to these mean and median ranks.

Table 3. The association between the scores on the item "like" and the remaining rating items for the tactile and tactile–visual tasks—Kendall rank correlation coefficients.

Item	Tactile task	Tactile–visual task
Smooth	−0.02	0.03
Cold	−0.37***	−0.36***
Damp	−0.24***	−0.25***
Hard	−0.04	0.00
Usual	0.33***	0.27***
Artificial	−0.43***	−0.36***
Expensive	0.07	0.11**
Unpleasant	−0.73***	−0.61***
Light	—	0.03
Matte	—	0.24***

** $p < 0.01$, *** $p < 0.001$. p-values are adjusted with the Holm–Bonferroni method.

tasks. In both tasks, materials rated as liked were perceived as somewhat less cold, less damp, more usual, less artificial, more expensive, and less unpleasant. The statistically significant positive correlation between scores on the items "like" and "hard" was found only in the tactile task. We did not detect statistically significant associations between the "like" item scores and the scores from the two items included only in the visual–tactile task (ie "light" and "matte"). The correlation coefficients are generally small to medium; the only exception is the negative correlation coefficient between the scores on the items "like" and "unpleasant," which is larger.

The Relationship between Tactile and Tactile–Visual Task Scores

The comparison of scores between the tactile and tactile–visual tasks on all items (except "matte" and "light" that were included only in one task) for all materials is presented in Fig 4 and Table S14. In general, the ratings are fairly consistent between the two tasks. Some discrepancies are noticeable for the items "usual" and "expensive."

Kendall rank correlation coefficients were calculated for scores on each item between the tactile and tactile–visual tasks (Table 4). Correlation coefficients are moderately high for the items "artificial," "unpleasant," "damp," and "like," and the three items capturing tactile sensory properties (ie "cold," "smooth," "hard"), and somewhat lower for the items "usual" and "expensive."

DISCUSSION

Preference of Materials

The results on the preference of materials show that wooden materials were generally similarly liked and more liked than the steel sample in both the tactile and tactile–visual tasks. This observation is mirrored in the results of the ranking task, in which wooden materials were on average ranked higher than the steel sample. These results are in line with existing studies, which have observed that wood is generally favored over other common building materials (Rice et al 2006; Ikei et al 2017b). The results of this study thus extend previous findings by showing that wood may be preferred over at least some other everyday materials, even when materials are presented in a form that more closely resembles the real-world context (ie presented as handrail samples instead of typically used small rectangular blocks of wood).

Preference ratings and rankings were fairly similar across the participants from Slovenia and Norway. The results *within* each country reflected the overall pattern: the wooden materials were generally rated and ranked similarly, while they were preferred over the steel sample. This pattern was clearly reflected in the results of the Norwegian participants, whereas some deviations occurred in the results of the Slovenian subjects. The Slovenians preferred unmodified spruce somewhat less than some other wooden materials. Although they still generally preferred the steel sample the least, their preference scores varied more than the Norwegian scores. This discrepancy between the countries could stem from cultural differences: clearer distinction in preference between the wooden materials and the steel sample observed among the Norwegians could have resulted from different general attitudes toward wood or steel. Nevertheless, even though the results from Slovenia and Norway varied, it should be highlighted that they are generally very similar.

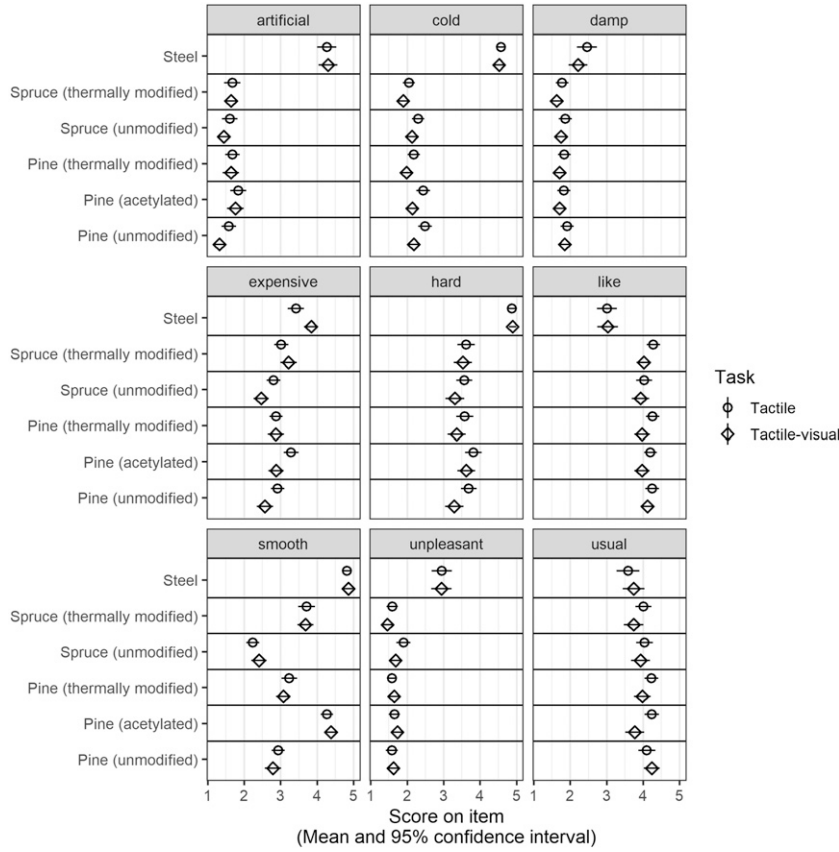

Figure 4. Scores on scale items split by tasks.

Comparison of the results *between* the countries showed that Slovenians, compared with Norwegians, gave higher absolute preference ratings (item "like") to the steel sample and certain wooden samples in both the tactile and tactile–visual tasks. This observation, however, is probably less informative than comparing the within-country results between countries. First, subtle language differences in the scales used in the two countries could have influenced absolute values of the preference scores. Second, lower absolute scores sometimes observed among the Norwegians could have resulted from the slight damage that the materials sustained in the second part of the study conducted in Norway. Comparing the countries on the ranking task, which is not influenced by the abovementioned issues, reveals the same pattern observed in the within-country analysis: Slovenians generally preferred steel more and unmodified spruce less than the Norwegians.

Analysis of the preference scores within wooden materials revealed that modified wood samples

Table 4. The association between the rating item scores on the tactile and tactile–visual tasks—Kendall rank correlation coefficients.

Item	Like	Smooth	Cold	Damp	Hard	Usual	Artificial	Expensive	Unpleasant
Kendall rank correlation coefficients	0.50***	0.60***	0.60***	0.52***	0.62***	0.33***	0.55***	0.37***	0.56***

*** $p < 0.001$. p-values are adjusted with the Holm–Bonferroni method.

were rated and ranked comparably to unmodified wood. The only wooden sample that was ranked somewhat lower than the others was unmodified (ie unmodified spruce). These observations contrast with the observations that treated materials are less preferred than the original, unmodified samples (Ikei et al 2017a). This suggests that modified wood exhibits tactile and visual properties that are, in terms of human preference, comparable to those of unmodified wood and different to those of wood that has been treated otherwise (eg with coating). Splitting these results by country showed similar results: wooden samples, regardless of their treatment, generally received similar preference scores within each country, suggesting that potential cultural influences might not influence the perception and evaluation of modified wood samples.

Association between Material Properties and Preference

Many perceived material properties were associated with a preference for wooden materials in both the tactile and tactile–visual tasks. Materials rated as liked were also rated as somewhat less cold, less damp, more usual, less artificial, less unpleasant, and, only in the tactile–visual task, more expensive and more matte. The observed associations between material properties and preference tend to be minor, which suggests that additional visual and tactile properties, beyond those examined in this study, are important in predicting material preference. Perceived material smoothness, hardness, and color lightness were not associated with preference scores.

The observed results are partially consistent with findings from existing studies. In line with the observations of Waka et al (2015), we observed that materials with higher preference ratings had been perceived as warmer. This suggests that perceived warmth might be associated with preference relatively independently of the context in which the wood samples are presented. In contrast to the findings of Waka et al (2015), who observed that preferred materials were perceived as a damper, we observed they were perceived as dryer. This discrepancy could have resulted from the way the materials had been presented: in handrails, dampness could be associated with (unwanted) slipperiness.

The perceived color lightness of materials was not associated with their preference scores. This observation contrasts with the study that found darker wooden materials had been preferred for an outdoor tabletop (Lipovac et al 2019), suggesting that the relationship between wood lightness and human preference may depend on the context of wood use. Similarly, our results contrast with the observations of Waka et al (2015), who found shinier samples were more preferred, whereas we observed that participants preferred matte materials. This discrepancy could be explained by differences in materials tested in the two studies. Waka et al (2015) examined only samples of wood, many of which likely varied in surface shininess. Our study, on the other hand, included wood samples with relatively uniform shininess levels, so the observed association—shinier materials being less preferred—might have been driven primarily by the presence of the (shiny) steel sample, which was generally the least preferred material. This could also explain why we have not detected the association between perceived smoothness and material preference, which is typically observed in other studies (Jonsson et al 2008; Waka et al 2015; Bhatta et al 2017): the ratings of the stainless steel sample, which was perceived as smooth but less liked, might have steered the association between perceived smoothness and preference toward the opposite direction than typically observed within wood samples. We found no relationship between perceived material hardness and material preference, possibly because the scores on the item "hard" did not vary sufficiently among the tested materials.

We observed that materials perceived as more natural tended to be preferred, similar to what has been observed in other studies (Rice et al 2006; Jonsson et al 2008; Ikei et al 2017b). Such studies, however, typically compared different types of materials instead of mostly different *wooden* materials. Our study thus extends these findings

and shows that perception of naturalness may be an important predictor of preference even within the same material (ie wood). Two other items that predicted preference in our study and that we had not identified in other studies assessing the perception of wood, were "usual" and "expensive." Materials perceived as more expensive and more usual were generally rated as more liked. Possibly, perceived expensiveness can reflect the perception of overall material quality, which in turn may be inferred from the pleasantness of the tactile and visual material properties. However, the steel sample was generally perceived as the most expensive material, although it was generally less liked than the wooden samples. This suggests there is a more complex mechanism behind the association between perceived expensiveness and preference of materials.

We observed that people preferred materials with which they were more familiar (ie materials rated higher on the item "usual"). It is possible that preferred materials are more widespread in everyday life, increasing the chances that people will become familiar with them. The association between perceived usualness and preference is particularly interesting in this study, which includes several samples of modified wood that are currently rarely used in real life; so, the participants have probably had few opportunities to come into contact with them. This suggests that modified wood samples exhibit certain visual and tactile properties that are perceived similarly to properties of more common wooden materials.

Association between Tactile and Tactile–Visual Task Scores

Comparison of the results between the tactile and tactile–visual tasks showed that the scores of the two tasks correlate with each other. The highest correlation coefficients between the two tasks were observed in the rating items predominantly assessed by touch: "smooth," "cold," "damp," and "hard." This is unsurprising as the visual modality is not expected to substantially influence the perception of these properties. Somewhat weaker correlations were observed in the affective attributes "usual" and "expensive," suggesting that the perception of these properties changes to a greater extent when people can inspect materials visually. Interestingly, the correlations on the items "artificial," "unpleasant," and "like" were relatively high, comparable to the correlations observed in the items assessing tactile sensory properties, suggesting that the tactile experience importantly influences the perception of naturalness and preference of materials. This finding is consistent with the results of previous studies that reached similar conclusions: tactile domain is important in overall material perception (Overvliet and Soto-Faraco 2011; Waka et al 2015; Bhatta et al 2017). The results of this study extend previous findings by demonstrating the importance of the tactile domain even when assessed materials are brought closer to a real-world context.

LIMITATIONS AND RECOMMENDATIONS FOR FUTURE STUDIES

Due to transportation, the handrail samples were slightly damaged in the tests conducted in Norway, which might have led to some differences in scores that occurred between the countries. Other differences between the countries could have resulted from the demographic characteristics of the participants: most Slovenian subjects were retired individuals with different backgrounds. In contrast, most Norwegian subjects were still-active academic staff. The samples of the two countries additionally differed on gender: women represented 54% of the Slovenian sample but only 28% of the Norwegian participants. For these reasons, it should not be assumed that identified differences between the countries in material perception are due to differences in culture, until the findings are confirmed by future studies. Another limitation stems from the limited variety of selected wooden samples: we used only two types of modification processes despite using three modified wood samples. The findings of this study could be extended by testing additional materials treated with different modification processes and including additional rating items that could further identify and clarify the role of material properties influencing the perception of materials. Testing materials that are similar in all

but one property (eg varying only on roughness) would better reveal the role of specific material properties in overall material preference. Future studies could also explore the perception of wooden materials in different furnishings, such as chairs and desks. More generally, the field of study would benefit from a theory explaining how and why specific material properties relate to preference of materials.

CONCLUSIONS

The results of this study confirm and extend previous findings showing that wooden materials tend to be more liked than other common materials—in our case, more than steel. The results also suggest that older adults prefer modified wood samples similarly to unmodified wooden materials. The findings are consistent across Slovenia and Norway, suggesting that different practices of wood use in these two countries do not significantly influence the perception of wooden materials. Preference of materials is associated with certain perceived material properties, and tactile experience has a significant role in the overall perception of materials. Altogether, the results suggest that wood, either unmodified or modified, may be a promising addition to restorative indoor environments for older adults.

ACKNOWLEDGMENTS

The authors gratefully acknowledge the European Commission for funding the InnoRenew CoE project (Grant Agreement 739574) under the Horizon2020 Widespread-Teaming program, the Republic of Slovenia (Investment funding of the Republic of Slovenia and the European Union of the European Regional Development Fund), and COST (European Cooperation in Science and Technology) for funding the travel to Norway through the COST Action CA16226.

REFERENCES

Bakar BFA, Hiziroglu S, Tahir PM (2013) Properties of some thermally modified wood species. Mat Des 43(January):348-355. doi: 10.1016/j.matdes.2012.06.054.

Baumgartner E, Wiebel CB, Gegenfurtner KR (2013) Visual and haptic representations of material properties. Multisens Res 26(5):429-455. doi: 10.1163/22134808-00002429.

Bhatta SR, Tiippana K, Vahtikari K, Hughes M, Kyttä M (2017) Sensory and emotional perception of wooden surfaces through fingertip touch. Front Psychol 8:1-12. doi: 10.3389/fpsyg.2017.00367.

Burnard MD, Kutnar A (2015) Wood and human stress in the built indoor environment: A review. Wood Sci Technol 49(5):969-986. doi: 10.1007/s00226-015-0747-3.

Burnard MD, Kutnar A (2020) Human stress responses in office-like environments with wood furniture. Build Res Inform 48(3):316-330. doi: 10.1080/09613218.2019.1660609.

Burnard MD, Nyrud AQ, Bysheim K, Kutnar A, Vahtikari K, Hughes M (2017) Building material naturalness: Perceptions from Finland, Norway and Slovenia. Indoor Built Environ 26(1):92-107. doi: 10.1177/1420326X15605162.

Datta BC (2016) Emotive materials: Towards a shared language of the meaning of materials. 200 pp. http://hdl.handle.net/1721.1/107574.

Demattè ML, Zucco GM, Roncato S, Gatto P, Paulon E, Cavalli R, Zanetti M (2018) New insights into the psychological dimension of wood–human interaction. Eur J Wood Wood Prod 76(4):1093-1100. doi: 10.1007/s00107-018-1315-y.

Esteves BM, Pereira HM (2009) Wood modification by heat treatment: A review. BioResources 4(1):370-404. doi: 10.15376/biores.4.1.370-404.

Evans GW (2003) The built environment and mental health. J Urban Health 80(4):536-555. doi: 10.1093/jurban/jtg063.

Fell DR (2010) Restorative properties of wood in the built indoor environment. PhD thesis, The University of British Columbia, Vancouver. 132 pp. doi: 10.14288/1.0071305.

Fujisaki W, Tokita M, Kariya K (2015) Perception of the material properties of wood based on vision, audition, and touch. Vision Res 109(PB):185-200. doi: 10.1016/j.visres.2014.11.020.

Gamache LS, Espinoza OA (2017) "Professional consumer perceptions of thermally-modified wood. https://conservancy.umn.edu/bitstream/handle/11299/188802/Gamache_umn_0130M_18091.pdf?sequence=1&isAllowed=y.

Guest S, Dessirier JM, Mehrabyan A, Mcglone F, Essick G, Gescheider G, Fontana A, Xiong R, Ackerley R, Blot K (2011) The development and validation of sensory and emotional scales of touch perception. Attention, Perception & Psychophysics 73(2):531-550. doi: 10.3758/s13414-010-0037-y.

Han K-T (2010) An exploration of relationships among the responses to natural scenes. Environ Behav 42(2):243-270. doi: 10.1177/0013916509333875.

Høibø O, Nyrud AQ (2010) Consumer perception of wood surfaces: The relationship between stated preferences and visual homogeneity. J Wood Sci 56(4):276-283. doi: 10.1007/s10086-009-1104-7.

Ikei H, Song C, Miyazaki Y (2017a) Physiological effects of touching coated wood. Int J Environ Res Public Health 14(7):1-14. doi: 10.3390/ijerph14070773.

Ikei H, Song C, Miyazaki Y (2017b) Physiological effects of touching wood. Int J Environ Res Public Health 14 (7):1-14. doi: 10.3390/ijerph14070801.

Rice J, Kozak RA, Meitner MJ, Cohen DH (2006) Appearance wood products and psychological well-being. Wood Fiber Sci 38(4):644-659.

Jonsson O, Lindberg S, Roos A, Hugosson M, Lindström M (2008) Consumer perceptions and preferences on solid wood, wood-based panels, and composites: A repertory grid study. Wood Fiber Sci 40(4):663-678.

Kanaya S, Kariya K, Fujisaki W (2016) Cross-modal correspondence among vision, audition, and touch in natural objects: An investigation of the perceptual properties of wood. Perception 45(10):1099-1114. doi: 10.1177/0301006616652018.

Kassambara A (2020) Rstatix: Pipe-friendly framework for basic statistical tests. R Package Version 0.7.0. https://cran.r-project.org/package=rstatix.

Kidoma K, Okamoto S, Nagano H, Yamada Y (2017) Graphical modeling method of texture-related affective and perceptual responses. International Journal of Affective Engineering 16(1):27-36. doi: 10.5057/ijae.IJAE-D-16-00009.

Lipovac D, Burnard MD (2020) Effects of visual exposure to wood on human affective states, physiological arousal and cognitive performance: A systematic review of randomized trials. Indoor Built Environ 0(0):1-21. doi: 10.1177/1420326X20927437.

Lipovac D, Burnard MD, Sandak A, Sandak J (2019) Wood protection techniques and natural weathering: Their effect on aesthetics and preference of people. *In* Proc IRG Annual Meeting. Quebec City, Quebec, Canada: The International Research Group on Wood Protection.

Lipovac D, Podrekar N, Burnard MD, Šarabon N (2020) Effect of desk materials on affective states and cognitive performance. J Wood Sci 66(December):1-12. doi: 10.1186/s10086-020-01890-3.

Lipovac D, Wie S, Nyrud AQ, Burnard MD (2021). Perception and evaluation of (modified) wood by older adults from Slovenia and Norway (Datasets, R analysis code, and supplementary tables) [Data set]. Zenodo. doi: 10.5281/zenodo.5793185.

Mangiafico S (2019) Rcompanion: Functions to support extension education program evaluation. R Package Version 2.3.25. https://cran.r-project.org/package=rcompanion.

Manuel A, Leonhart R, Broman O, Becker G (2015) Consumers' perceptions and preference profiles for wood surfaces tested with pairwise comparison in Germany. Ann For Sci 72(6):741-751, doi: 10.1007/s13595-014-0452-7.

Markevych I, Schoierer J, Hartig T, Chudnovsky A, Hystad P, Dzhambov AM, de Vries S, Triguero-Mas M, Brauer M, Nieuwenhuijsen MJ, Lupp G, Richardson EA, Astell-Burt T, Dimitrova D, Feng X, Sadeh M, Standl M, Heinrich J, Fuertes E (2017) Exploring pathways linking greenspace to health: Theoretical and methodological guidance. Environ Res 158(October): 301-317. doi: 10.1016/j.envres.2017.06.028.

Mayo J (2015) Solid wood. New York, NY: Routledge. doi: 10.4324/9781315742892.

Mcsweeney J, Rainham D, Johnson SA, Sherry SB, Singleton J (2015) Indoor Nature Exposure (INE): A health-promotion framework. Health Promot Int 30(1): 126-139. doi: 10.1093/heapro/dau081.

Nakamura M, Ikei H, Miyazaki Y (2019) Physiological effects of visual stimulation with full-scale wall images composed of vertically and horizontally arranged wooden elements. J Wood Sci 65(1):1-11. doi: 10.1186/s10086-019-1834-0.

Nyrud AQ, Bringslimark T (2010) Is interior wood use psychologically beneficial? A review of psychological responses toward wood. Wood Fiber Sci 42(2):202-218.

Nyrud AQ, Bringslimark T, Bysheim K (2014) Benefits from wood interior in a hospital room: A preference study. Archit Sci Rev 57(2):125-131. doi: 10.1080/00038628.2013.816933.

Nyrud AQ, Roos A, Rødbotten M (2008) Product attributes affecting consumer preference for residential deck materials. Can J For Res 38(6):1385-1396. doi: 10.1139/X07-188.

Okamoto S, Nagano H, Kidoma K, Yamada Y (2016) Specification of individuality in causal relationships among texture-related attributes, emotions, and preferences. Int J Affect Eng 15(1):1-9. doi: 10.5057/ijae.IJAE-D-15-00018.

Overvliet KE, Soto-Faraco S (2011) I can't believe this isn't wood! An investigation in the perception of naturalness. Acta Psychol (Amst) 136(1):95-111. doi: 10.1016/j.actpsy.2010.10.007.

Purcell T, Peron E, Berto R (2001) Why do preferences differ between scene types? Environ Behav 33(1):93-106. doi: 10.1177/00139160121972882.

Redlich CA, Sparer J, Cullen MR (1997) Sick-building syndrome. Lancet 349:1013-1016. doi: 10.1016/S0140-6736(96)07220-0.

Roe J, Roe A (2018) Restorative environments and promoting physical activity among older people. Pages 485-505 *in* The palgrave handbook of ageing and physical activity promotion. Nyman SR, Barker A, Haines T, Horton K, Musselwhite C, Peeters G, Victor CR, Wolff JK, eds. Cham, Switzerland: Springer International Publishing. doi: 10.1007/978-3-319-71291-8_24.

Rozin P (2006) Naturalness judgments by lay Americans: Process dominates content in judgments of food or

water acceptability and naturalness. Judgm Decis Mak J 1(2):91-97.

Rozin P (2005) The meaning of 'natural': Process more important than content. Psychol Sci 16(8):652-658. doi: 10.1111/j.1467-9280.2005.01589.x.

R Studio Team (2021) RStudio: Integrated development environment for R. Boston, MA: RStudio. http://www.rstudio.com/.

Sakuragawa S, Miyazaki Y, Kaneko T, Makita T (2005) Influence of wood wall panels on physiological and psychological responses. J Wood Sci 51(2):136-140. doi: 10.1007/s10086-004-0643-1.

Sandberg D, Kutnar A, Mantanis G (2017) Wood modification technologies—A review. Forest - Biogeosciences and Forestry 10(6):895-908. doi: 10.3832/ifor2380-010.

Sande JB, Nyrud AQ (2008) Consumer preferences for wood surfaces—A latent variable approach. Pages 195-215 *in* Bergseng E, Delbeck G, Hoen HF, eds. Proc biennial meeting of the scandinavian society of forest economics. Scandinavian Forest Economics, Ås, Norway.

Shen J, Zhang X, Lian Z (2020) Impact of wooden versus nonwooden interior designs on office workers' cognitive performance. Percept Mot Skills 127(1):36-51. doi: 10.1177/0031512519876395.

Statistical Office of the Republic of Slovenia [SURS] (2020) Buildings with dwellings by type of building, number of storeys, material of construction and type of roofing, and dwellings by type of building and number of storeys, statistical regions, Slovenia, Census 2002. Accessed 20 April 2020. https://pxweb.stat.si/SiStatData/pxweb/sl/Data/Data/05W2409S.px/.

Strobel K, Nyrud AQ, Bysheim K (2017) Interior wood use: Linking user perceptions to physical properties. Scand J Fr Res 32(8):1-9. doi: 10.1080/02827581.2017.1287299.

Team R Core (2021) R: A language and environment for statistical computing. Vienna, Austria: R Foundation for Statistical Computing. https://www.r-project.org/.

Ulrich RS (1983) Aesthetic and affective response to natural environment. Pages 85-125 *in* Altman I, Wohlwill JF, eds. Behavior and the natural environment: Advances in theory & research. New York, NY: Springer Science + Business Media. doi: 10.1007/978-1-4613-3539-9.

van den Berg AE, Koole SL, and van der Wulp NY (2003) Environmental preference and restoration: (How) are they related? J Environ Psychol 23(2):135-146. doi: 10.1016/S0272-4944(02)00111-1.

Wickham H, Chang W, Henry L, Pedersen TL, Takahashi K, Wilke C, Woo K, Yutani H (2019) Ggplot2: Create elegant data visualisations using the grammar of graphics. R Package Version 3.3.2. https://cran.r-project.org/package=ggplot2.

Wickham H, François R, Henry L, Müller K (2020) Dplyr: A grammar of data manipulation. R Package Version 1.0.6. https://cran.r-project.org/package=dplyr.

Zhang X, Lian Z, Ding Q (2016) Investigation variance in human psychological responses to wooden indoor environments. Build Environ 109:58-67. doi: 10.1016/j.buildenv.2016.09.014.

Zhang X, Lian Z, Wu Y (2017) Human physiological responses to wooden indoor environment. Physiol Behav 174:27-34. doi: 10.1016/j.physbeh.2017.02.043.

EMPIRICAL MODELS FOR PREDICTION COMPRESSION STRENGTH OF PAPERBOARD CARTON[1]

Yuriy Pyr'yev
Professor
Department of Printing Technologies
Faculty of Mechanical and Industrial Engineering
Warsaw University of Technology
Konwiktorska 2, 00-217 Warsaw, Poland
E-mail: yuriy.pyryev@pw.edu.pl

*Edmundas Kibirkštis**
Professor
E-mail: edmundas.kibirkstis@ktu.lt

Laura Gegeckienė
Lecturer
E-mail: laura.gegeckiene@ktu.lt

Kęstutis Vaitasius
Associate Professor
E-mail: kestutis.vaitasius@ktu.lt

Ingrida Venytė
Lecturer
Department of Production Engineering
Faculty of Mechanical Engineering and Design
Kaunas University of Technology
Studentų 56, 51424 Kaunas, Lithuania
E-mail: ingrida.venyte@ktu.lt

(Received October 2021)

Abstract. When designing packaging in the shape of a rectangular parallelepiped from various paperboard materials, it is important to determine their resistance to vertical compression force, which should be less than the maximum compression force. This is especially relevant when the products packed in these boxes are stacked during transport or storage. The developed empirical models make it possible to more optimally/more accurately determine the critical vertical compressive force of these packages. The purpose of this work is to create an semi-empirical model of the maximum compressive force of a paperboard box (carton) based on the corrected formulas of the maximum compressive force of the McKee corrugated cardboard box (taking into account the height) of the box and allowing to optimize its parameters. The accuracy of the developed semi-empirical models is presented by comparing the results of theoretical and experimental studies. It should be noted that the determination of the maximum compression force of the box is a contact problem of the nonlinear theory of elasticity and plasticity for structures whose elements are made of an anisotropic material. On this basis, semi-empirical models of three and one parameters were developed, which also estimated the values of experimental studies previously performed by other authors. One mathematical model also estimates the height of the box, which is not determined by the McKee formula. For the experiments, we used cartons of different geometric parameters and made from different types of paperboards. During the experiment, the boxes were compressed with vertical force until the packages collapsed. The results of the compared theoretical and experimental studies show the suitability of the proposed

* Corresponding author

mathematical models for calculating the critical compressive force of packages, since the obtained mean absolute percentage error (MAPE) is within the acceptable limits. Taking into account the small discrepancy between the obtained experimental and theoretical research results, the proposed method for calculating the vertical maximum compressive force of the rectangular parallelepiped package is suitable for use. The methodology for calculating the carton compressive strength of such packages presented in this paper will be extended in the future for additional testing to verify the model with carton size and design variations.

Keywords: Paperboard, cartons, compression, strength, critical force, empirical model McKee.

INTRODUCTION

In these days the most important question in the packaging industry is—What should be the modern packaging? First of all, naturally, it should be environmentally friendly and completely harmless. Moreover, the packaging must be sufficiently strong, lightweight, reliable, and the manufacture of it should be cheap. All these criteria apply together to one type of material—paperboard. The wide range of applications, from the packaging of industrial goods to food, makes the future possible to continue using paperboard in the packaging industry.

Paperboard cartons are mainly used for light products. Paperboard cartons are used in food, cosmetics, clothing, and many other industries. This type of packaging may be glued or folded. Paperboard packaging gives wide advertising opportunities. The ability to apply any print design makes it one of the most commonly used marketing tools.

Packaging plays a pivotal role in the distribution and transportation of goods, which means that it must comply with all major requirements, both in terms of aesthetics and durability standards (RDC-Environment and Pira International 2003).

The most popular paperboard packaging type is cartons in the shape of a rectangular parallelepiped.

Models for the prediction of the maximum force the top-to-bottom compressive of folding cartons may be divided into analytical and numerical based on the finite element analysis (Beldie et al 2001; Garbowski and Przybyszewski 2015). In their turn, analytical models (mathematical formulae indicating relations between the value in question and parameters of the model) may be divided into empirical (Pyryev et al 2016), semi-empirical (McKee et al 1963; Coffin 2015) and "exact" within the scope of the assumptions (eg linearity of the model) made (Grangård and Kubát 1969; Pyryev et al 2019). "Exact" models for a maximum compression force does not require any experimental data. Models for different carton designs will also be different (Ristinmaa et al 2012). Models for the prediction of maximum compression force differ according to the material used to manufacture the boxes. More research has been done for corrugated cardboard and fewer for paperboards (Pyryev et al 2016, 2019; Kibirkštis et al 2007).

In 1963, McKee et al (1963) developed and published a mathematical equation to determine the compressive strength of a three-ply cardboard box, which is still in use today.

$$F_{\max} = aP_m^b(\sqrt{D_{CD}D_{MD}})^{1-b}P^{2b-1} \qquad (1)$$

Based on his research, McKee came to the conclusion that the dominant parameter affecting the properties of a box compressed from above and below by force F, as in the case of box storage, is the edge crush strength of corrugated cardboard in the cross direction (CD), which he defined as the parameter P_m and parameters describing the bending stiffness of a cardboard box in two directions D_{CD} and D_{MD}. McKee also used the parameter P, meaning the perimeter of the box, a and b constants defined experimentally. The ratio of height H to the circumference P must be $>1{:}7$ » 0.143. Let us assume that the direction of the force F coincides with the x-axis.

Mathematical models can take very divergent paths to try to achieve the goal. Little (1943) identified the main factors influencing box strength by analogy to column failure: box size, inherent material strength, and material stiffness.

One of the earliest practical formulations for estimating box compression strength (*BCT*) using

these parameters was developed by Kellicutt and Landt (1958). Then, McKee et al published in 1963 likely the most popular industry method of box compression estimation and the one used among the most publicly available software programs.

Most packaging engineers are familiar with the McKee equation, typically in one of its numerical forms:

$$BCT = 2.028 \times ECT^{0.746} (\text{RMSBending})^{0.254} \text{Perimeter}^{0.492}, \quad (2)$$

$$BCT = 5.87 \times ECT (\text{Caliper} \times \text{Perimeter})^{1/2}. \quad (3)$$

The structure of these equations highlights the importance of different material parameters on box performance. The edge crush strength (*ECT*) of the combined board, has the largest role in estimating box strength. Measuring *ECT* attempts to quantify the inherent material strength of the complex corrugated board structure, and researchers (Frank 2014) have taken many approaches over the years to assess this material property of the combined board. Batelka and Smith (1993) expanded the original McKee box compression model (1) to include all box dimensions in their formula.

Two of the criteria proposed by Urbanik and Frank (2006) appear to lead to compression strength predictions in accordance with a large set of experimental results. The second approach considers that the buckling mode *m*, which yields the lowest critical buckling load for the side panel, has to be applied to both panels.

The carton board is an orthotropic material (Edholm 1998). This is because, during its manufacture, the majority of the fibers orient themselves in a direction, known as the machine direction (MD). The direction perpendicular to this is known as the CD. Furthermore, the properties of the board in the thickness direction (ZD) differ from those of MD and CD because of its laminar construction. A big effort of research has been taken to investigate the mechanical properties of the carton board (Sirkett et al 2006).

A simplified version of the McKee formula was fitted to the data set by Popil (2016) and the resulting equation improves the prediction average error.

Urbanik and Saliklis (2003) applied finite element analysis to observe the buckling phenomena in corrugated boxes.

Interesting studies carried out in the work by Gong et al (2020), where the effects of indentation shape on the compressive strength of corrugated cartons are studied by experiments and finite element analysis. A crippling analysis method has been utilized to estimate the compression strength of paperboard boxes in work (Linvill 2015). Two types of tests are required to characterize the crippling strength of material: compression tests of panels with one edge free and compression tests of panels with no edges.

The purpose of this work is to create an semi-empirical model of the maximum compressive force of a paperboard box (carton) based on the modified formulas (Batelka et al 1993) of the maximum compressive force of the McKee corrugated cardboard box, taking into account the height of the box and allowing to optimize of its parameters.

EXPERIMENTAL DATA AND MATERIALS

Six different types of paperboard packaging constructions were used for the creation of the engineering calculation procedure in relation to the maximum compression force. The paper proposes models to predict the top-to-bottom compressive strength of folding cartons. In the work, the experiment consisted of determining the compression data of 72 cartons ($i = 1, \ldots, 72$), (Fig 1[a]): six different geometrical parameter cartons and six different types of paperboard compressed in the CD, (Fig 1[b]), and six in the MD, (Fig 1[c]).

The number of repetitions of the tests for each of the 72 cartons is six. The geometrical parameters of the packaging are listed in the caption under Fig 2.

The simplified scheme for a compression stand and the view of packaging samples are both shown in Figs 1-2. Packaging of such sizes is

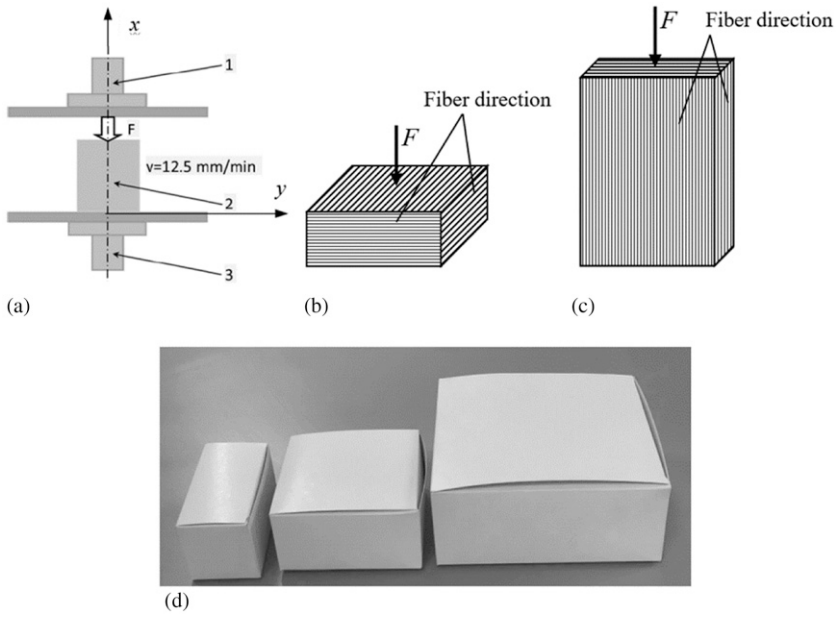

Figure 1. Compression testing scheme for a package under the action of vertical force F, N: (a) principal scheme, (b) compression testing scheme in cross direction (CD), (c) compression testing scheme in the machine direction (MD), (d) illustration the three different packages A60.20.00.03 classified according to ECMA considered in this study: 1—moving base support (v = 12.5 mm/min); 2—package under compression; 3—fixed base support.

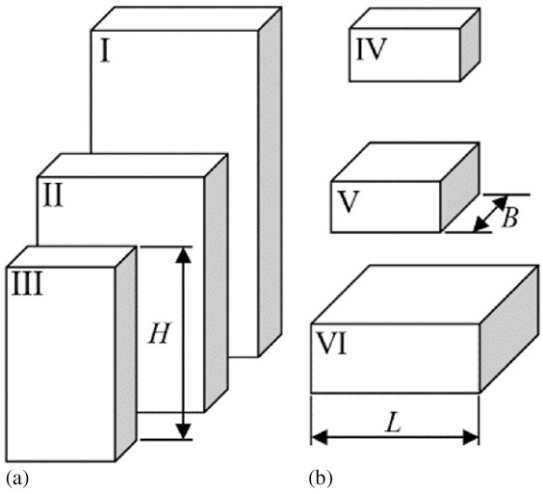

Figure 2. The packaging specimen's geometrical parameters: (a) carton size I: H = 230 mm, L = 118 mm, B = 48 mm; carton size II: H = 165 mm, L = 118 mm, B = 48 mm; carton size III: H = 137 mm, L = 77 mm, B = 37 mm; (c) carton size IV: H = 37 mm, L = 77 mm, B = 37 mm; carton size V: H = 37 mm, L = 77 mm, B = 77 mm; carton size VI: H = 48 mm, L = 118 mm, B = 118 mm.

widely used in Lithuania for packing products such as, for example, grain products (rice, buckwheat, etc.), which are prepacked into a separate carton for cooking (Kibirkštis et al 2007). The choice of this type of packaging specimen was determined by their wide-ranging usage for packing food products. For cartons with dimensions in Fig 2(a) (i = 1, . . ., 36), some of the experimental data carton strength and the short span compression strength, the bending stiffness of the paperboards was previously presented by the authors in earlier papers (Kibirkštis et al 2007; Pyryev et al 2016). Experimental data for paperboard package compression tests were obtained in standard atmosphere for conditioning and testing according to ISO 187:1990 requirements. The low cartons were also investigated for additional analysis (Fig 2[b]). Note that this paper presents new experimental data for 36 cartons (Fig 2[b]) (i = 37, . . ., 72) that have not been published before. The experiments for the low cartons in Fig 2(b) were carried out for the same type of paperboards as for the cartons in Fig 2(a).

When testing its compression strength, the carton is placed between two parallel rigid plates and is compressed at a constant rate of deformation of 12.5 mm/min in accordance with ISO 12048 recommendations. For the measurements were used: sensor—DBBMTOL-500 N, serial number AP34282. Load measurement accuracy: ±0.5% indicated load from 2% to 100% capacity, extended range. Position measurement accuracy ±0.01% of reading or 0.001 mm, whichever is greater. Speed accuracy ±0.005% of set speed. The maximum force of load that the sample can support is called the compression force F_{exp} (experimental value).

The main characteristics of the cartons are bending stiffness D and compressive strength SCT.

Figure 2 shows the sample cartons. For cartons I parameter $\lambda = P/H = 1.44$, for cartons II parameter $\lambda = 2.01$, for cartons III parameter $\lambda = 1.66$, for cartons IV parameter $\lambda = 6.17$, for cartons V parameter $\lambda = 8.33$, for cartons VI parameter $\lambda = 9.80$, where $P = 2\ (L + B)$ is the perimeter of rectangular plate $L \times B$.

With consideration to the potential conditions involved in storage, transportation, and maintenance, the packages were made of different paperboard types:

- Soft MC Mirabell paperboard (WLC) or (GD2)—Recycled coated white lined chipboard
- Kromopak paperboard (FBB) or (GC2)—Folding boxboard
- Korsnas Carry (SUB) or (GN4)—Solid unbleached board
- Korsnas Light (SUB) or (GN4)—Solid unbleached board

The boxes were made according to No A60.20. 00.03 PackDesign 2000 Standard Libraries for European Carton Makers Association (ECMA).

The technical characteristics provided by the manufacturers of these paperboards are listed in Table 1. MD—the direction in the board where the fibers are arranged in the direction of machine casting during the board manufacturing process. CD—the direction perpendicular to the MD. In the carton, it is most common to have the MD parallel to the vertical axis (for several reasons—primarily the reliability of opening on high-speed machinery), but to compare the experimental and theoretical results in both directions (MD) and (CD) need to be explored.

The findings from the proposed calculation procedures were later compared with the findings from experimental compression tests (see Table 2 (column 5), $i = 1, \ldots, 36$), which were analyzed in the paper (Kibirkštis et al 2007) for cartons from Fig 2(a).

Based on the work of Ristinmaa et al (2012) in this work, the proposed semi-empirical models have been tested on independent experimental data to predict the critical compressive force of a carton.

MODELING THE COMPRESSIVE STRENGTH

Formula McKee (1),[1] which takes into account the compressive force, is a two-parameter one. In addition, Eq 1 does not take into account the height of the box. It is anticipated that the height of the box may affect its strength. This assumption leads to a three-parameter formula. For the sake of simplicity, we will further reduce it to a one-parameter form, which will contribute to a simplified design of packages. For the above transformations, we will further use an empirical analysis of the obtained experimental data.

The Structural Formula of Maximum Compression Force

It should be noted that the determination of the maximum compression force of the carton is a contact problem of the nonlinear theory of elasticity and plasticity for a structure whose elements are made of an anisotropic material. The contact load on the side panels of the carton and the area of plasticity are unknown quantities. The solution to such a problem can be obtained only using numerical methods or a semiempirical approach.

A model can be devised based on the empirical results for structures that fail through combined compression and bending with the dimensionless

Table 1. A comparison of paperboard technical characteristics (Kibirkštis et al 2007).

				D = Bending stiffness		*SCT* = Compressive strength	
				L&W[a], (5°), (mNm)		(kN/m)	
		Grammage ISO 536	Thickness ISO 534	ISO 5628		ISO 9895	
	Type of paperboard	(g/m^2)	(μm)	*MD*[b]	*CD*[c]	*MD*[2]	*CD*[3]
1	MC Mirabell (WLC)	400	565	60.9	24.4	12.7	8.5
2	MC Mirabell (WLC)	320	435	31.8	13.3	9.8	7.4
3	Kromopak (FBB)	300	430	34.3	14.3	9.2	6.8
4	Kromopak (FBB)	275	395	29.0	12.0	8.6	6.2
5	Korsnas Carry (SUB)	400	585	113.0	55.3	11.2	8.4
6	Korsnas Light (SUB)	290	420	41.9	21.2	8.5	6.1

[a] L&W device-measured moment needed for bending the sample material to an angle of 5°.
[b] *MD*—machine direction.
[c] *CD*—cross machine direction.

form for the maximum force $F_{\max}$ (calculated value) as:

$$\frac{F_{\max}}{F_{cr}} = a\left(\frac{SCT_x P}{F_{cr}}\right)^b \tag{4}$$

$F_{\max}$ = maximum compression force [N] (vertical maximum force in x directions); $P = 2(L+B)$ is the perimeter of the rectangular plate $L \times B$ [m]; H = height of the carton [m]; SCT_x = compressive strength in x directions of the board using a short-span compressive tester [N/m]; F_{cr} is the critical buckling load (coefficient of similarity) [N]; a, b = constant parameters defined on the basis of experimental data.

The choice of the power-law dependence of $F_{\max}$ on SCT_x and on the height of the carton H, on the one hand, is due to the analysis of the experimental data obtained, and on the other hand, the power-law dependence of the critical compression force of the corners on SCT_x by the formula presented in the article (Pyryev et al 2019). Therefore, the $F_{\max}$ becomes:

$$F_{\max} = a(SCT_x)^b (F_{cr})^{1-b} P^b \tag{5}$$

We also assume that the critical compressive force F_{cr} is proportional to the sum of the box-critical compressive forces discussed in the article (Pyryev et al 2019) regarding four plates of the same height H:

$$F_{cr} \sim \frac{\sqrt{D_x D_y}}{P}\left(\frac{P}{H}\right)^d \tag{6}$$

where D_x, D_y = flexural rigidity in x and y directions [Nm], H = height of the carton [m], d = constant parameter, e.g. for low boxes H/L<<1, H/B<<1 (with all edges simply supported) parameter $d = 2$, for tall boxes H/L>>1, H/B >>1 parameter $d = 0$. This paper suggests building a theoretical model for a maximum compressive force of the carton as shown as follows:

$$F_{\max} = a(SCT_x)^b \left(\sqrt{D_x D_y}\right)^{1-b} P^{2b-1}\left(\frac{P}{H}\right)^c \tag{7}$$

a, b, c = constant parameters defined on the basis of experimental data, c = d(1−b). A similar approach was used in the article (Coffin 2015) for corrugated box.

The expression (7) can be written as follows:

$$\tilde{y} = b_0 + b_1 x_1 + b_2 x_2 \tag{8}$$

where

$$\tilde{y} = \ln\frac{F_{\max} P}{\sqrt{D_x D_y}},\ b_0 = \ln(a), b_1 = b, b_2 = c$$
$$x_1 = \ln\left(\frac{SCT_x P^2}{\sqrt{D_x D_y}}\right), x_2 = \ln\left(\frac{P}{H}\right)$$

Knowing the constant coefficients b_0, b_1, b_2 in Eq 8, you can write down a, b, c values in Eq 7:

$$a = e^{b_0}, b = b_1, c = b_2 \tag{9}$$

Table 2. Experimental data for paperboard package compression tests a prediction of the maximum compression force and their errors; for cases (17) $a = 15.2$, $b = 0.490$, and $c = 0.0329$; for case (19) $a = 15.8$, $b = 0.48$, and $c = 0.241$; for case (20) $a = 13.9$, $b = 0.45$, and $c = 0.247$; for cases (1) $a = 14.4$, $b = 0.499$, and $c = 0$; for cases (21) $a = 14.4$, $b = 0.5$, and $c = 0$.

Experiment number i=1, … 72	The box design type Figure 2	Type of paperboard, No.	Load direction	F_{exp}, (N)[b]	F_{max}, (N) based on Equation				100 ε_i, % based on equation			
					(17)	(19)/(20)	(1)	(21)	(17)	(19)/(20)	(1)	(21)
1	I	1	MD	329 ± 11	305	295	316	318	7.29	10.4	4.10	3.25[a]
2	I	1	CD	235 ± 6	251	244	258	260	6.63	3.68[a]	9.88	10.8
3	I	2	MD	191 ± 5	195	188	202	204	2.07	1.81[a]	5.95	6.92
4	I	2	CD	164 ± 5	170	164	176	177	3.60	0.05[a]	7.25	8.21
5	II	1	MD	320 ± 6	308	320	316	318	3.64	0.15[a]	1.40	0.53
6	II	1	CD	253 ± 3	253	264	258	260	0.13[a]	4.33	2.06	2.92
7	II	2	MD	211 ± 2	197	203	202	204	6.59	3.71	4.09	3.21[a]
8	II	2	CD	167 ± 3	172	178	176	177	2.86[a]	6.44	5.33	6.27
9	III	1	MD	267 ± 12	309	311	316	318	15.7[a]	16.4	18.3	19.2
10	III	1	CD	230 ± 8	254	257	258	260	10.3[a]	11.6	12.4	13.2
11	III	2	MD	210 ± 7	197	198	203	204	5.99	5.87	3.57	2.75[a]
12	III	2	CD	161 ± 4	172	173	176	177	6.86[a]	7.42	9.33	10.2
13	I	3	MD	184 ± 3	196	189	203	205	6.68	2.82[a]	10.6	11.6
14	I	3	CD	165 ± 2	169	164	175	177	2.60	0.69[a]	6.06	6.99
15	I	4	MD	162 ± 3	174	167	181	182	7.40	3.37[a]	11.5	12.5
16	I	4	CD	132 ± 8	148	143	153	155	12.3	8.58[a]	16.2	17.2
17	II	3	MD	196 ± 3	198	205	203	205	1.25[a]	4.57	3.83	4.77
18	II	3	CD	184 ± 3	171	178	175	177	6.98	3.52[a]	4.89	4.06
19	II	4	MD	177 ± 2	176	181	181	182	0.62[a]	2.49	2.01	2.94
20	II	4	CD	150 ± 1	150	155	153	155	0.09[a]	3.51	2.24	3.14
21	III	3	MD	196 ± 2	199	199	204	205	1.42[a]	1.74	3.90	4.77
22	III	3	CD	167 ± 4	171	173	175	177	2.66[a]	3.42	4.87	5.71
23	III	4	MD	186 ± 4	176	177	181	182	5.27	5.11	2.86	2.04[a]
24	III	4	CD	142 ± 1	150	151	153	155	5.71[a]	6.35	8.07	8.95
25	I	5	MD	447 ± 2	414	405	425	428	7.42	9.43	5.00	4.24[a]
26	I	5	CD	366 ± 3	359	353	368	371	1.79	3.53	0.51[a]	1.28
27	II	5	MD	456 ± 3	418	439	425	428	8.25	3.82[a]	6.88	6.13
28	II	5	CD	370 ± 5	363	383	368	371	1.78	3.38	0.58	0.19[a]
29	III	5	MD	395 ± 6	419	427	425	428	6.09[a]	8.03	7.58	8.36
30	III	5	CD	360 ± 5	364	372	368	371	1.11[a]	3.37	2.26	2.97
31	I	6	MD	198 ± 7	220	213	227	229	11.0	7.53[a]	14.6	15.6
32	I	6	CD	195 ± 6	187	182	192	194	4.2	6.46	1.35	0.53[a]
33	II	6	MD	246 ± 9	222	231	227	229	9.69	6.24[a]	7.73	6.92
34	II	6	CD	224 ± 8	189	197	192	194	15.7	12.0[a]	14.1	13.4
35	III	6	MD	263 ± 7	223	224	227	229	15.4	14.7	13.6	12.9[a]
36	III	6	CD	219 ± 9	191	192	193	194	12.6	12.5	12.1	11.4[a]
37	IV	1	MD	272 ± 7	322	309	316	318	18.6	13.7[a]	16.1	17.0
38	IV	1	CD	239 ± 8	265	258	258	260	10.9	7.78[a]	8.12	8.95
39	V	1	MD	312 ± 7	324	324	316	318	3.73	3.88	1.14[a]	2.02
40	V	1	CD	268 ± 6	266	270	258	260	0.79	0.76[a]	3.64	2.84
41	VI	1	MD	324 ± 5	323	325	315	318	0.46	0.29[a]	2.69	1.76
42	VI	1	CD	238 ± 5	265	271	258	260	11.3	13.7	8.42[a]	9.41
43	IV	2	MD	217 ± 4	206	195	203	204	5.02[a]	10.1	6.68	5.89
44	IV	2	CD	168 ± 5	180	172	176	177	6.92	2.21[a]	4.78	5.63
45	V	2	MD	215 ± 6	207	205	202	204	3.79[a]	4.88	5.86	5.01
46	V	2	CD	172 ± 7	180	180	176	177	4.81	4.65	2.28[a]	3.18
47	VI	2	MD	198 ± 8	206	205	202	204	4.11	3.55	2.13[a]	3.14

(*continued*)

Table 2. Experimental data for paperboard package compression tests a prediction of the maximum compression force and their errors; for cases (17) $a = 15.2$, $b = 0.490$, and $c = 0.0329$; for case (19) $a = 15.8$, $b = 0.48$, and $c = 0.241$; for case (20) $a = 13.9$, $b = 0.45$, and $c = 0.247$; for cases (1) $a = 14.4$, $b = 0.499$, and $c = 0$; for cases (21) $a = 14.4$, $b = 0.5$, and $c = 0$. (cont.)

Experiment number $i=1,\ldots 72$	The box design type Figure 2	Type of paperboard, No.	Load direction	F_{exp}, (N)[b]	F_{max}, (N) based on Equation				100 ε_i, % based on equation			
					(17)	(19)/(20)	(1)	(21)	(17)	(19)/(20)	(1)	(21)
48	VI	2	CD	167 ± 9	180	180	176	177	7.58	8.05	5.25[a]	6.27
49	IV	3	MD	185 ± 4	208	197	204	205	12.2	6.70[a]	10.1	11.0
50	IV	3	CD	153 ± 8	179	172	175	177	17.0	12.4[a]	14.5	15.4
51	V	3	MD	207 ± 1	208	207	204	205	0.62	0.04[a]	1.68	0.80
52	V	3	CD	197 ± 2	180	180	175	177	8.82	8.45[a]	11.2	10.4
53	VI	3	MD	231 ± 9	208	207	203	205	10.2[a]	10.2	12.0	11.1
54	VI	3	CD	218 ± 9	179	181	175	177	17.9	17.1[a]	19.8	19.0
55	IV	4	MD	174 ± 5	184	174	181	182	5.72	0.19[a]	3.84	4.72
56	IV	4	CD	148 ± 7	157	150	153	155	5.90	1.51[a]	3.69	4.53
57	V	4	MD	192 ± 1	185	183	181	182	3.85[a]	4.82	5.95	5.10
58	V	4	CD	161 ± 2	157	157	153	155	2.30[a]	2.19	4.74	3.91
59	VI	4	MD	171 ± 1	184	183	180	182	7.59	7.13	5.51[a]	6.55
60	VI	4	CD	145 ± 2	157	158	153	155	8.10	8.88	5.69[a]	6.70
61	IV	5	MD	428 ± 7	438	432	425	428	2.22	0.94	0.71	0.01[a]
62	IV	5	CD	397 ± 5	380	379	368	371	4.27[a]	4.52	7.27	6.63
63	V	5	MD	437 ± 8	439	453	425	428	0.48[a]	3.63	2.81	2.05
64	V	5	CD	352 ± 7	381	397	368	371	8.36	12.9	4.52[a]	5.31
65	VI	5	MD	483 ± 9	438	454	424	428	9.40	6.00[a]	12.1	11.4
66	VI	5	CD	402 ± 5	380	398	368	371	5.45	0.91[a]	8.56	7.79
67	IV	6	MD	253 ± 4	232	224	227	229	8.17[a]	11.5	10.2	9.50
68	IV	6	CD	218 ± 5	197	193	193	194	9.40[a]	11.9	11.7	11.0
69	V	6	MD	245 ± 5	233	235	227	229	4.83	4.21	7.34	6.54
70	V	6	CD	221 ± 8	198	202	192	194	10.3	8.68[a]	13.0	12.2
71	VI	6	MD	219 ± 7	232	235	227	229	6.10	7.43	3.58[a]	4.55
72	VI	6	CD	211 ± 7	198	202	192	194	6.39	4.11[a]	8.90	8.07
mean [%]									6.57	5.82[a]/6.38	6.99	7.11

CD, cross machine direction; MD, machine direction.

[a] Denotes the lowest value in the row.

[b] $F_{exp} \pm \sigma$—measured values from carton compression test with standard deviation.

Calculation of Coefficients of Multiple Linear Regression

Let us present the measurement data and the coefficients of the model in a matrix form:

$$\mathbf{y} = \begin{bmatrix} y_1 \\ \vdots \\ y_n \end{bmatrix}, \mathbf{X} = \begin{bmatrix} 1 & x_{1,1} & x_{1,2} \\ \vdots & \vdots & \vdots \\ 1 & x_{n,1} & x_{n,2} \end{bmatrix}, \mathbf{b} = \begin{bmatrix} b_0 \\ b_1 \\ b_2 \end{bmatrix},$$
$$\mathbf{e} = \begin{bmatrix} e_1 \\ \vdots \\ e_n \end{bmatrix}, \tilde{\mathbf{y}} = \mathbf{Xb}, n = 72, \quad (10)$$

where $\mathbf{y}$ is the measurement vector-column for measuring the compression force, $y_i = \ln(F^i_{exp} P^i / \sqrt{D^i_x D^i_y})$ (observed values of the dependent variable); $\mathbf{X}$—dimension matrix $n \times (m+1)$, m = 2, in which the i-th row $i = 1, 2, \ldots, n$ represents the i-th observation of the vector of independent variable values x_1, x_2 values corresponding to the variables at given free term b_0; $\mathbf{b}$—vector-column of dimension m+1 parameters of multiple regression equation; $\mathbf{e}$—vector-column of dimension n of deviations $e_i = y_i - \tilde{y}_i$ where y_i depends on $\tilde{\mathbf{y}}_i$ obtained from the regression equation:

$$\tilde{y}_i = b_0 + b_1 x_{i,1} + b_2 x_{i,2}, i = 1, 2, \ldots, n, \tilde{\mathbf{y}} = \mathbf{Xb} \quad (11)$$

The matrix form of the relation is:

$$\mathbf{e} = \mathbf{y} - \mathbf{Xb} \tag{12}$$

According to the least squares method:

$$\sum_{i=1}^{n} e_i^2 = \mathbf{e}^T\mathbf{e} = (\mathbf{y}-\mathbf{Xb})^T(\mathbf{y}-\mathbf{Xb}) \rightarrow min, \tag{13}$$

where $\mathbf{e}^T = (e_1, \ldots, e_n)$, ie the superscript T means a transpose matrix. It may be shown that the previous condition is fulfilled if the vector-column of coefficient **b** can be obtained by the following formula:

$$\mathbf{b} = (\mathbf{X}^T\mathbf{X})^{-1}\mathbf{X}^T\mathbf{y} \tag{14}$$

where $\mathbf{X}^T$ is a matrix transposed to matrix **X**, and $(\mathbf{X}^T\,\mathbf{X})^{-1}$ is a matrix inverse to $(\mathbf{X}^T\,\mathbf{X})$. The relation is valid for equations of regression with a random number m of explanatory variables.

The model of multiple regression is evaluated by using the determination coefficient R^2, R is the multiple coefficient of correlation between the dependent variable and the explanatory parameters:

$$R^2 = 1 - \frac{\sum_{i=1}^{n}(y_i - \tilde{y}_i)^2}{\sum_{i=1}^{n}(y_i - \bar{y})^2} \tag{15}$$

where the average value of the dependent variable

$$\bar{y} = \frac{1}{n}\sum_{i=1}^{n} y_i \tag{16}$$

The model is based on experiments with different mechanical and geometrical dimensions of packages (72 different cartons). The model will also be valid for cartons with other parameters, which are within the parameter range studied in the present paper.

RESULTS AND DISCUSSION

To calculate the maximum compression force, Eq 7, it is necessary to know the geometrical P, H, and physical SCT_x, D_x, D_y parameters of the sidewalls of the carton. Manufacturers produce a paperboard with the bending stiffness levels shown in Table 1. As mentioned previously, the index x corresponds to the direction of the acting compression force. Direction y is perpendicular to the direction of the acting compression force. Parameters D_x, D_y correspond to S^x_{DIN}, S^y_{DIN}.

The experimental findings and the parameters of the cartons under testing are presented in Table 2. The experimentally obtained values for the maximum force of compression $F_{\exp}$ are shown in column 5 of Table 2. For example, for the first experiment (i = 1) obtained: mean carton compression strength, 329 N, maximum, 344 N, minimum, 315 N, standard deviation, 11 N, coefficient of variation, 3.29%. The experimental data contains measurement uncertainty and individual replicate variability. The samples will not be perfect or consistent (folding/gluing, etc.), the board will have local variability (±5% in thickness, approximately = ±15% in stiffness).

The analysis of the data presented in Table 2 allows us to determine the range of nondimensional parameters: $SCT_x/SCT_y \in [1.0; 2.08]$; D_x/D_y Î [0.52; 9.42]; $B/H \in [0.2; 2.5]$; $L/H \in [0.51; 8{,}6]$; $\lambda = P/H \in [1.44; 9.80]$; $\ln [F_{\exp}\, P\, (D_xD_y)^{-0.5}] \in [6.95; 8.50]$; $\ln[SCT{\cdot}P^2(D_xD_y)^{-0.5}] \in [8.62;11.6]$.

In our case, n = 72. Having the findings of the experiment, we can evaluate the coefficients of linear regression Eq 11 by using the least squares method: $b_0 = 2.722$, $b_1 = 0.490$, $b_2 = 0.0329$.

The multiple coefficient of correlation (Eq 15) between the dependent variable and the explanatory parameters is equal to $R = 0.975$.

In accord with Eq 9, the following constant values are found: $a = 15.2$, $b = 0.490$, $c = 0.0329$.

Finally, the following mathematical model was developed upon the basis of the experimental findings:

$$F_{\max} = 15.2 \cdot SCT_x^{0.49}\left(\sqrt{D_xD_y}\right)^{0.51} P^{-0.020}(P/H)^{0.0329} \qquad R^2 = 0.950. \tag{17}$$

By entering the data from Table 2 into Eq 17, we calculated the values of the critical compression force (Table 2, column 6).

The average deviation of the calculated values $F^i_{\max}$ from the experimental data $F^i_{\exp}$, $i = 1, \ldots, 72$, as determined by the following formula:

$$MAPE = \frac{100}{n}\sum_{i=1}^{n}\varepsilon_i, \varepsilon_i = \frac{|F^i_{\exp} - F^i_{\max}|}{F^i_{\exp}} \quad (18)$$

turned out to be *MAPE* (mean absolute percentage error) = 6.57%.

A comparison of the predicted forces (Table 2, column 6) and the experimental failure forces (Table 2, column 5) is shown in Fig 3, revealing a close correlation. The line $F_{\max} = F_{\exp}$ represents the calculated maximum forces (Eq 17), and the lines indicated +20% and −20% show the region with the absolute value of the relative error $\varepsilon_i < 0.2$ and includes no <80% of the obtained values.

As can be seen from the work (Pyryev et al 2019), the critical value of the parameter λ can be $\lambda^* = 4(D_y/D_x)^{1/4}$. For six types of paperboards (Table 1), the parameter $\lambda^* \in [3.18; 5.03]$. The parameter λ for the cartons shown in Fig 2(b) is <5.03. We find semi-empirical formulas for the critical compressive strength of the carton based on the results for cartons from Fig 2(a) ($\lambda \leqslant \lambda^*$) and for cartons from Fig 2(b) ($\lambda \geqslant \lambda^*$).

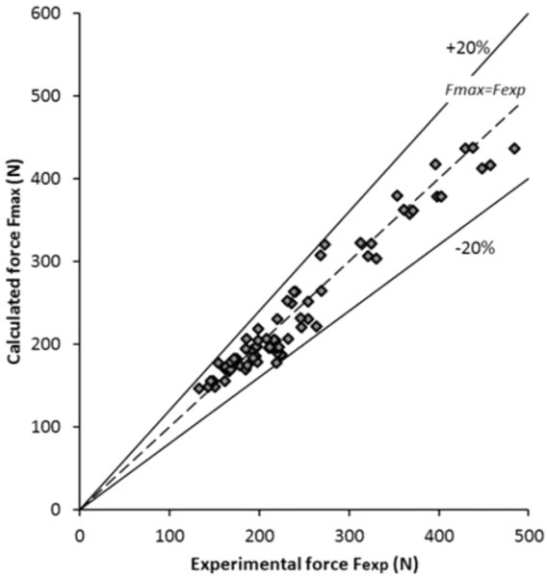

Figure 3. A prediction of the maximum compression force $F_{\max}$ (Eq 17) for the packaging compared with experimental data $F_{\exp}$.

$$F_{\max} = 15.8 \cdot SCT_x^{0.48}\left(\sqrt{D_xD_y}\right)^{0.52}P^{-0.04}(P/H)^{0.241}$$
$$\lambda<\lambda^*, R^2 = 0.954, MAPE = 5.82\%. \quad (19)$$

$$F_{\max} = 13.9 \cdot SCT_x^{0.45}\left(\sqrt{D_xD_y}\right)^{0.55}P^{-0.1}(P/H)^{0.247}$$
$$\lambda>\lambda^*, R^2 = 0.954, MAPE = 6.38\%. \quad (20)$$

A prediction of the maximum compression force $F_{\max}$ is shown in column 7 of Table 2 according to Eqs 19 and 20 for $\lambda \leqslant \lambda^*$ (experiments 1-36) and $\lambda \geqslant \lambda^*$ (experiments 37-72), respectively. The absolute value of the relative errors $100\cdot\varepsilon_i$ are shown in column 11 of Table 2.

The small value of the parameter c in Eq 17 allows the empirical formula to be written in the form(1), where $a = 14.4$, $b = 0.499$, $R^2 = 0.946$, $MAPE = 6.99\%$.

A prediction of the maximum compression force $F_{\max}$ according to McKee's Eq 1 is shown in column 8 of Table 2. Errors for force $F_{\max}$ are shown in column 12 of Table 2.

Given that the empirical formula $b \approx 0.5$ can be found in the following form:

$$F_{\max} = a \cdot SCT_x^{0.5}(\sqrt{D_xD_y})^{0.5} \quad (21)$$

where the parameter a is calculated from the experimental data:

$$a = \frac{\sum_{i=1}^{72} F^i_{\exp}\left(SCT^i_x\sqrt{D^i_xD^i_y}\right)^{0.5}}{\sum_{i=1}^{72} SCT^i_x\sqrt{D^i_xD^i_y}} \quad (22)$$

According to the data (Table 2), the parameter a in Eq 22 is $a = 14.4$, $R^2 = 0.947$, $MAPE = 7.11\%$. Error's $100\cdot_i$ (%) for force $F_{\max}$ are shown in column 12 of Table 2.

Figure 4 shows the *MAPE* (%) of the calculated values $F^i_{\max}$ from the experimental data $F^i_{\exp}$, $i = 1, \ldots, 72$ based on Eqs 17, 19, 20, 1, and 21, as well as the maximum absolute value of the

relative error $100{\cdot}\varepsilon_i$. Based on Eqs 17, 1, and 21, the maximum values are calculated by the formula $\max_{i=1,\ldots72}\{100{\cdot}_i\}$, based on Eq 19—by the formula $\max_{i=1,\ldots36}\{100{\cdot}_i\}$, and based on Eq 20—according to the formula $\max_{i=37,\ldots72}\{100{\cdot}_i\}$.

This work presented 72 experiments and the empirical formulas obtained on the basis of them, which show that the accuracy of the prediction, although slightly, increases when the height of the carton is taken into account. McKee Eq 1 according to Fig 4 gives the mean error MAPE = 6.99%, and Eqs 17, 19, and 20, which estimate the height of the carton, give lower values MAPE = 6.57%, MAPE = 5.81%, and MAPE = 6.39%, respectively.

Note that the analysis of the obtained results $F_{\max}$ based on Eqs 17, 19, 20, 21, and 1 and their errors shows that the obtained model based on McKee's Eq 1 gives the best prediction (asterisk for the lowest error) for only 10 experiments: 26, 39, 42, 46, 47, 48, 59, 60, 64, and 71. Only experiment 26 (I 6 CD) was carried out for a tall drawer (drawer design type I) and with the maximum board thickness (type 6 carton), load direction CD. The remaining nine experiments were carried out on low cartons V and VI.

Simplified model (21) gives the best estimate of the maximum compressive force compared with Eqs 17, 19, 20, and 1 for 10 experiments: 1, 7, 11, 23, 25, 28, 32, 35, 36, and 61. Experiment 61 (IV 5 MD) was carried out on a low carton and with the largest cardboard thickness, and the remaining nine experiments were carried out with high cartons I, II, and III. Only for the two experiments 35 (III 6 MD) and 36 (III 6 CD), the relative errors $(100 \cdot \varepsilon_i)$ using Eq 21 are more than 10%, and for the rest of the experiments the relative errors using Eq 21 are $<5\%$.

The testing of the proposed semi-empirical prediction models for the maximum compressive force of a cardboard box was carried out on the experimental results of Ristinmaa et al.[8] Experimental results are presented for three different materials and for four different box sizes and for two different types A1111 (i = 1, . . . 16) and A6020 (i = 17, . . .20) according to the ECMA classification (Table 3, columns 1-3). The bending resistance values BR_{MD}, BR_{CD} (mN), (ISO 2493) and SCT_{MD}, and SCT_{CD} (mN/m) are presented in Table 3, column 3.

A comparison of the predicted forces (Table 3, column 5) and the experimental failure forces (Table 3, column 4) is shown in Fig 5, revealing a close correlation.

Moreover, a comparison of the predicted loads (Table 3, columns 5-7) and the experimental failure loads (Table 3, column 4) is shown in Table 3,

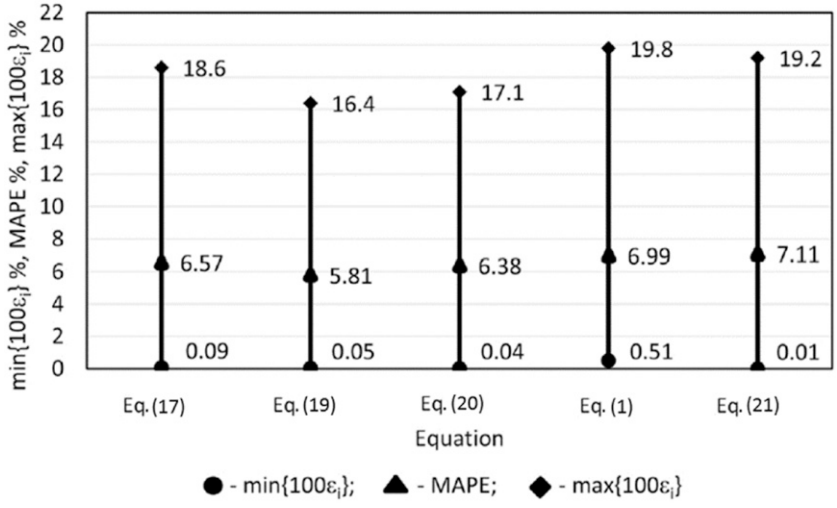

Figure 4. $\min\{100{\cdot}_i\}$ (%), *MAPE* (%), and $\max\{100{\cdot}_i\}$ (%) based on Eqs 17, 19, 20, 1, and 21.

Table 3. Experimental data of paperboard package compression tests (Ristinmaa et al 2012) a prediction of the maximum compression force and their errors.

Experiment number	Material	Dimensions, mm		Technical characteristics of paperboard (Ristinmaa et al 2012)				F_{exp} (N) (Ristinmaa et al 2012)	F_{max} (N)			100 ε_i, %		
		L = 150 mm		BR, (mN); SCT, (kN/m)					Based on Equation			Based on Equation		
		H	B	BR_x	BR_y	SCT_x	SCT_y		(17)	(1)	(21)	(17)	(1)	(21)
1	Mtrl-4	200	40	165	382	4.70	6.80	162	160	164	162	1.23	1.23	0.00
2	Mtrl-4	200	40	382	165	6.80	4.70	169	191	197	195	13.0	16.6	15.4
3	Mtrl-5	200	40	317	682	6.60	8.30	238	258	264	262	8.40	10.9	10.1
4	Mtrl-5	200	40	682	317	8.30	6.60	285	289	296	293	1.40	3.86	2.81
5	Mtrl-6	50	50	293	400	6.07	7.02	241	222	217	215	7.88	9.96	10.8
6	Mtrl-6	50	50	400	293	7.02	6.07	240	238	234	231	0.83	2.50	3.75
7	Mtrl-7	100	50	879	1340	7.81	8.74	409	452	439	435	10.5	7.33	6.36
8	Mtrl-7	100	50	1340	879	8.74	7.81	450	478	464	460	6.22	3.11	2.22
9	Mtrl-6	100	50	293	400	6.07	7.02	257	217	217	215	15.6	15.6	16.3
10	Mtrl-6	100	50	400	293	7.02	6.07	257	233	234	231	9.34	8.95	10.1
11	Mtrl-7	100	50	879	1340	7.81	8.74	422	442	439	435	4.74	4.03	3.08
12	Mtrl-7	100	50	1340	879	8.74	7.81	467	467	464	460	0.00	0.64	1.50
13	Mtrl-6	250	50	293	400	6.07	7.02	247	210	217	215	15.0	12.1	13.0
14	Mtrl-6	250	50	400	293	7.02	6.07	260	226	234	231	13.1	10.0	11.1
15	Mtrl-7	250	50	879	1340	7.81	8.74	441	429	439	434	2.72	0.45	1.59
16	Mtrl-7	250	50	1340	879	8.74	7.81	475	453	464	460	4.63	2.32	3.16
17	Mtrl-4	200	40	382	165	6.80	4.70	181	191	197	195	5.52	8.84	7.73
18	Mtrl-4	200	40	165	382	4.70	6.80	148	160	164	162	8.11	10.8	9.46
19	Mtrl-5	200	40	682	317	8.30	6.60	318	289	296	293	9.12	6.92	7.86
20	Mtrl-5	200	40	317	682	6.60	8.30	238	258	264	262	8.40	10.9	10.1
mean [%]												7.29	7.35	7.32

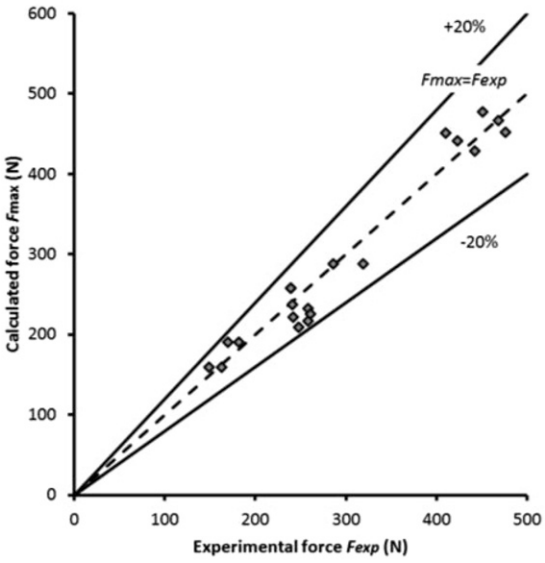

Figure 5. A prediction of the maximum compression force F_{max} (Eq 17) for the packaging compared with experimental data F_{exp} (Ristinmaa et al 2012).

which reveals a close correlation; the average error is 7.29% (based on Eq 17), 7.35% (based on Eq 1), 7.32% (based on Eq 21), respectively (Table 3, columns 8-10). In the absence of values of bending stiffness, it was taken the dependence $\sqrt{D_{MD}D_{CD}} = 0.103\sqrt{BR_{MD}BR_{CD}}$.

Note that different models give similar results. This means that common elements (or highly correlated elements) dominate their results. The dominant factor leading to this model similarity is the combination of compressive and flexural stiffnesses $SCT_x^{0.5}S^{0.5}$, where S = geometric mean of MD and CD bending stiffness $\sqrt{D_{MD}D_{CD}}$. Such a combination of stiffness is found in works of Grangård and Kubát (1969) and Pyryev et al (2019).

CONCLUSIONS

1. Formula McKee (1) has two parameters. Developed three-parameter theoretical models (17), (19), (20), and one-parameter model (21) of the maximum compression force were proposed and analyzed, describing the compression of paperboard packaging.
2. Table 3 shows, it does not any of the equations give significantly improved results over McKee (1). One would expect that with more parameters one would get a better fit, but it is not as if the fit got extremely better.
3. For the experimental data presented in the paper, we get $MAPE = 6.57\%$ (model (17)).
4. The comparison between theoretical (17) and experimental testing has shown sufficient accuracy in terms of the results.
5. For cartons with the parameter $\lambda \leqslant \lambda^*$, it is better to use Eq 19, $MAPE = 5.82\%$ for predicting the compressive strength, and for $\lambda \geqslant \lambda^*$ Eq 20, $MAPE = 6.38\%$.
6. The semi-empirical Eq 21 for predicting the compression force of the carton $MAPE = 7.11\%$ is noteworthy. The formula has a simple shape and does not depend on the geometric parameters of the carton, including the height of the carton H. As a first approximation, new Equation (24) is to be used.
7. Based on McKee's Eq 1 and experimental data, a model was obtained for which $MAPE = 6.99\%$.
8. Analyzing the obtained models, we can state that the semi-empirical model (19) for $\lambda \leqslant \lambda^*$, and (20) for $\lambda \geqslant \lambda^*$ have the best *MAPE* value; then the semi-empirical model (17), then the semi-empirical model (1), the worst *MAPE* value is model (21). However, the latter model allows you to perform calculations on a calculator (Fig 4).
9. The proposed models (17), (1), and (21) have been successfully tested on 20 independent experimental data (Ristinmaa et al 2012) the average error is 7.29% (based on Eq 17), 7.35% (based on Eq 1), 7.32% (based on Eq 21).
10. The considered theoretical model (17) allows us to predict the height of the carton if the expected load F_{cr} is set on it.

$$H = \left(\frac{15.2 \cdot SCT_x^{0.49} \left(\sqrt{D_x D_y} \right)^{0.51} P^{0.0129}}{F_{\max}} \right)^{30.4} \quad (23)$$

11. If the geometric parameters and the expected force F_{max} of the carton are

indicated, we can choose cardboard with a predicted compressive strength SCT_x according to (21).

$$SCT_x = \frac{F_{\max}^2}{14.39^2\sqrt{D_x D_y}} \tag{24}$$

12. The developed simplified semi-empirical models allow to optimize the design of rectangular parallelepiped packaging with sufficient accuracy.

ACKNOWLEDGMENTS

The work has been supported by the European Union in the framework of the European Social Fund through the Warsaw University of Technology Development Programme.

REFERENCES

Batelka JJ, Smith CN (1993) Package Compression Model. Project 3746. Final Report to the Containerboard and Kraft Paper Group of the American Forest and Paper Association.

Beldie L, Sandberg G, Sandberg L (2001) Paperboard packages exposed to static loads—Finite element modelling and experiments. Packag Technol Sci 14(4):171-178.

Coffin DW (2015) Some observations towards improved predictive models for box compression strength. Tappi 14(8):537-545.

Edholm B (1998) Bending stiffness loss of paperboard at conversion—predicting the bending ability of paperboard. Packag Technol Sci 11(3):131-140.

RDC-Environment and Pira International (2003) Evaluation of costs and benefits for the achievement of reuse and recycling targets for the different packaging materials in the frame of the packaging and packaging waste directive 94/62/EC: Final Consolidated Report. 131 pp. Annexes 1-13, 211 pp.+ 59 pages of tables and diagrams.

Frank B (2014) Corrugated box compression—A literature survey. Packag Technol Sci 27(2):105-128.

Garbowski T, Przybyszewski G (2015) The sensitivity analysis of critical force in box compression test. Przeglad Papierniczy 71(5):275-280.

Gong G, Liu Y, Fan B, Sun D (2020) Deformation and compressive strength of corrugated cartons under different indentation shapes: Experimental and simulation study. Packag Technol Sci 33(6):215-226.

Grangård H, Kubát J (1969) Some aspects of the compressive strength of cartons. Sven Papperstidn 72(15): 466-473.

Kellicutt KQ, Landt EF (1958) Basic Design Data for the Use of Fiberboard in Shipping Containers. United States Department of Agriculture Forest Service in cooperation with the University of Wisconsin. Report No. 1911. Forest Production Laboratory, Madison, WI.

Kibirkštis E, Lebedys A, Kabelkaitė A, Havenko S (2007) Experimental study of paperboard package resistance to compression. Mechanika 63(1):27-33.

Linvill E (2015) Box compression strength: A crippling approach. Packag Technol Sci 28(12):1027-1037.

Little JR (1943) A theory of box compressive resistance in relation to the structural properties of corrugated paperboard. Paper Trade J 116(24):275-278.

McKee RC, Gander JW, Wachuta JR (1963) Compression strength formula for corrugated board. Paperboard Packaging 48(8):149-159.

Popil D (2016) The Box Compression for Copy Paper Boxes-Applying McKee's Formula. Presented at Tappi Corbotec Meeting, Orlando, FL, October 17. View project: 1-9.

Pyryev Y, Kibirkštis E, Miliūnas V, Sidaravičius J (2016) Engineering calculation procedure of critical compressive force of paperboard packages. Przeglad Papierniczy 72(6):374-381.

Pyryev Y, Zwierzyński T, Kibirkštis E, Gegeckienė L, Vaitasius K (2019) Model to predict the top-to-bottom compressive strength of folding cartons. Nord Pulp Paper Res J 34(1):117-127.

Ristinmaa M, Ottosen NS, Korin C (2012) Analytical prediction of package collapse loads—basic considerations. Nord Pulp Paper Res J 27(4):806-813.

Sirkett DM, Hicks BJ, Berry C, Mullineux G, Medland AJ (2006) Simulating the behaviour of folded cartons during complex packing operations. Proc Inst Mech Eng, C J Mech Eng Sci 220(12):1797-1811.

Urbanik TJ, Frank B (2006) Box compression analysis of worldwide data spanning 46 years. Wood Fiber Sci 38(3): 399-416.

Urbanik TJ, Saliklis EP (2003) Finite element corroboration of buckling phenomena observed in corrugated boxes. Wood Fiber Sci 35(3):322-333.

CALL FOR APPLICATIONS

The Society of Wood Science and Technology invites applications for Editor, *Wood and Fiber Science* (W&FS). The Editor provides overall management and coordination with the publisher of the quarterly Journal.

The initial term for this position begins June 1, 2022. The Editor will be appointed for a 3-year term and will overlap with the current Editor for 6 months.

In general, the Editor should excel in leadership and organizational skills, have a national and international reputation in the field, and possess academic credentials similar to a full professor. The Editor receives an honorarium of $8500 per year.

Overview: The Editor is the principal architect of the scientific content of W&FS. The Editor is an active scientist, well-known, and well-regarded in his/her discipline. The Editor must be active in soliciting the best science from top scientists. Working with the Editorial Board members, the Editor is the arbiter of W&FS content.

DUTIES

- Acting as an Ambassador: The Editor is the public voice of W&FS and exercises that voice through appearances on behalf of the Journal, through Editorials in the Journal, and through interactions with scientists and the public. The Editor actively promotes and solicits high-quality manuscripts.
- Leading Editorial Process: The Editor reviews submitted articles for appropriate content for W&FS, required format and overall acceptability of research content.
  - Assigns appropriate articles to Assistant Editor, as appropriate
  - Sends submitted articles to reviewers, obtains comments and returns to authors with reviewers' recommendations
  - Sends accepted articles to publisher for copyediting and formatting
  - Communicates with authors during all steps of procedures, including invoice details
  - Publishes issue quarterly in January, April, July, and October
  - Compiles Proceedings for SWST Annual Meeting
  - Maintains the DOI spreadsheet with each new issue published and makes sure the DOI number is placed on article before publication
- Working with Executive Board: The Editor serves on the Executive Board; serves as an ex-officio member of the Marra Award Committee and cooperates in evaluation of papers for consideration; and processes and writes copy for publication of the Marra Award and other SWST awards in W&FS.

MINIMUM/REQUIRED QUALIFICATIONS

- Past or current researcher in the field of Wood Science
- Experience with scientific journals through publishing, editing, or managing
- Knowledgeable about all fields of Wood Science
- Excellent organization skills
- Demonstrated computer literacy

Time Commitment: The anticipated commitment is 10 to 15 h/wk with intense activity during compilation of Annual Proceedings and during publishing of issues.

Start Date: June 1, 2022 to overlap with existing Editor for last two issues of 2022.

To Apply: Provide a detailed cover letter explaining your skills and experiences to meet the required qualifications, along with your CV to Vicki Herian at vicki@swst.org.

For further information, contact current Editor, Susan LeVan-Green at sue.levangreen@gmail.com or 608-235-8667.

Editor, Wood and Fiber Science Society of Wood Science and Technology
Applications Due April 1, 2022

Wood and Fiber Science, 54(1), 2022, p. 74
https://doi.org/10.22382/wfs-2022-07

EDITORIAL AND PUBLICATION POLICY

Wood and Fiber Science as the official publication of the Society of Wood Science and Technology publishes papers with both professional and technical content. Original papers of professional concern, or based on research of international interest dealing with the science, processing, and manufacture of wood and composite products of wood or wood fiber origin will be considered.

All manuscripts are to be written in US English, the text should be proofread by a native speaker of English prior to submission. Any manuscript submitted must be unpublished work not being offered for publication elsewhere.

Papers will be reviewed by referees selected by the editor and will be published in approximately the order in which the final version is received. Research papers will be judged on the basis of their contribution of original data, rigor of analysis, and interpretations of results; in the case of reviews, on their relevancy and completeness.

As of January 1, 2022, Wood and Fiber Science will be an online only, Open Access journal. There will be no print copies. Color photos/graphics will be offered at no additional cost to authors. The Open Access fee will be $1800/article for SWST members and $2000/article for nonmembers. The previous five years of articles are still copyright protected (accept those that are identified as Open Access) and can be accessed through member subscriptions. Once a previous article has reached its 5th anniversary date since publication, it becomes Open Access.

Technical Notes

Authors are invited to submit Technical Notes to the Journal. A Technical Note is a concise description of a new research finding, development, procedure, or device. The length should be **no more than two printed pages** in WFS, which would be five pages or less of double-spaced text (TNR12) with normal margins on 8.5 x 11 paper, including space for figures and tables. In order to meet the limitation on space, figures and tables should be minimized, as should be the introduction, literature review and references. The Journal will attempt to expedite the review and publication process. As with research papers, Technical Notes must be original and go through a similar double-blind, peer review process.

On-line Access to *Wood and Fiber Science* Back Issues

SWST is providing readers with a means of searching all articles in *Wood and Fiber Science* from 1968 to present Articles from 1968 to 2017 are available to anyone, but in order to see 2017 to 2021 articles you must have an SWST membership or subscription. SWST members and subscribers have full search capability and can download PDF versions of the papers If you do not have a membership or subscription, you will not be able to view the full-text pdf.

Visit the SWST website at http://www.swst.org and go to Wood & Fiber Science Online. Click on either SWST Member Publication access (SWST members) or Subscriber Publication access (Institution Access). All must login with their email and password on the HYPERLINK "http://www.swst.org" www.swst.org site, or use their ip authentication if they have a site license.

As an added benefit to our current subscribers, you can now access the electronic version of every printed article along with exciting enhancements that include:

- IP authentication for institutions (only with site license)
- Enhanced search capabilities
- Email alerting of new issues
- Custom links to your favorite titles

(ISSN 0735-6161)
CODEN WOOFAJ

WOOD AND FIBER SCIENCE

JOURNAL OF THE SOCIETY OF WOOD SCIENCE AND TECHNOLOGY

VOLUME 54 JANUARY 2022 NUMBER 1

CONTENTS

Articles

Volume 54, Number 1 WOOD AND FIBER SCIENCE January 2022